THE UNIVERSITY
of EDINBURGH

This thesis has been submitted in fulfilment of the requirements for a postgraduate degree (e.g. PhD, MPhil, DClinPsychol) at the University of Edinburgh. Please note the following terms and conditions of use:

This work is protected by copyright and other intellectual property rights, which are retained by the thesis author, unless otherwise stated.
A copy can be downloaded for personal non-commercial research or study, without prior permission or charge.
This thesis cannot be reproduced or quoted extensively from without first obtaining permission in writing from the author.
The content must not be changed in any way or sold commercially in any format or medium without the formal permission of the author.
When referring to this work, full bibliographic details including the author, title, awarding institution and date of the thesis must be given.

The relevance of aldehydes in understanding gene-drug interactions and cancer subpopulations

Andrea Coates

PhD Genetics and Molecular Medicine

The University of Edinburgh

2019

Declaration

I declare that this thesis was composed by myself, the work submitted is my own, with contribution from others clearly indicated in the text and that this work has not been submitted for any other degree or professional qualification.

Andrea Coates
August 2019

Abstract

Aldehyde dehydrogenase (ALDH) enzymes are key for the metabolism and detoxification of aldehydes and biosynthesis of molecules critical for cellular function. ALDHs are highly expressed in stem cells and are considered reliable experimental markers of cancer initiating cells. ALDHs are key enzymes for the bioactivation of 5-nitrofurans (5-NFNs) but downstream effects of this interaction on ALDH-mediated metabolic pathways have not been characterised. 5-NFN compounds have anti-bacterial and anti-trypanosome activity driven by bacterial- and parasite-specific nitroreductases. Despite recommendation of the 5-NFN compound, nifurtimox as a World Health Organisation essential medicine, this compound produces a multitude of side effects in humans, similar to those resulting from exposure to disulfiram, a known ALDH inhibitor. The 5-NFNs, nifurtimox and nifuroxazide are both promising candidates for repurposing as neuroblastoma and melanoma anti-cancer therapeutics, respectively. Results chapter 1 of this thesis explored the hypothesis that 5-NFNs are competitive substrates for mammalian ALDH enzymes in vivo and that this interaction drives the side-effects of 5-NFNs. Recombinant enzymes, murine liver extracts, precision cut liver slices and *in vivo* models were utilised to explore the effects of 5-NFNs in the liver, that highly expresses ALDH enzymes. The 5-NFNs are found to act as competitive substrates for the dehydrogenase and esterase activities of acetaldehyde-detoxifying ALDH enzymes and differentially inhibit

ALDH activity in mammalian liver. Additionally, the human hepatoma cell line, HepG2 was discovered to be sensitive to 5-NFNs and the addition of ALDH substrates alters sensitivity to 5-NFNs. A study to determine the effect of 5-NFN treatment on ALDH metabolic pathways indicates that circulating levels of acetaldehyde are increased in the blood of ethanol- and nitrofuran-treated *Aldh1b1*$^{-/-}$ mice. Acetaldehyde is a DNA-damaging agent and carcinogen that cells are exposed to from endogenous and exogenous sources: However, quantitation of acetaldehyde levels in plasma presents technical difficulties. With the aim of initiating set up of a short-chain aldehyde detection method that could be applied to the quantification of aldehydes in blood and cell lysates, results chapter 2 describes the development of acetaldehyde derivatisation methods coupled with comparison of Orbitrap high-resolution and triple Quadrupole mass spectrometry detection of aldehyde derivatives. Given that ALDH1A3 is expressed in cancer initiating cells and the 5-NFN, nifuroxazide targets ALDHhigh populations, the effect of ALDH1A3 expression in ALDHhigh cells in relation to the long-chain aldehyde, and main ALDH1A3 substrate, retinaldehyde was explored. Results chapter 3 explores consequences of ALDH1A3 expression through transcriptomic analysis. To investigate the importance of ALDH1A3 activity on gene expression regulation in melanoma, transcriptomes of ALDHhigh, ALDHlow and ALDH1A3null melanoma populations were compared. Comparison of ALDHhigh- and ALDHlow-expressing A375 melanoma cell populations revealed a MITFlow-neural crest stem cell-(NCSC) high transcriptional signature that is driven through retinoic acid receptor (RXRG) signalling. This signature is differentially expressed in the ALDHhigh population compared to ALDHlow and is associated with minimal residual disease in melanoma; this highlights a therapeutic opportunity for developing an anti-cancer strategy that is specific to melanoma minimal residual disease

by targeting ALDHhigh populations with nifuroxazide and inhibitors of retinaldehyde/retinoic acid metabolism. Collectively, understanding the ALDH:5-NFN enzyme-drug interaction and its downstream consequences on aldehyde-metabolising pathways informs about the mechanisms of 5-NFN-induced side effects but also has potential to be exploited for chemotherapeutic targeting of the ALDH-expressing minimal residual disease population in melanoma. This highlights ALDH as an important drug target in terms of 5-NFN-induced side effects and as a therapeutically useful target for cancer therapy.

Lay Summary

Every day, our bodies are exposed to chemical molecules that can be beneficial or detrimental to our health. One group of molecules that can have good and bad effects on the cells in our body are aldehydes. Aldehydes are small molecules that our bodies can produce on their own but are also present in the environment. Acetaldehyde is one type of aldehyde that is produced by our own bodies during normal metabolism but is found at high concentrations in alcohol and in air pollution. Aldehydes are very small and reactive which means they can bind to DNA and proteins within cells, where they can cause damage and cause cells to die. To prevent acetaldehyde from reaching high concentrations within our bodies, our liver expresses high levels of a protein called ALDH. This protein converts acetaldehyde to acetic acid. Acetic acid is otherwise known as vinegar, it is non-toxic to cells which means that protein and DNA damage does not occur. This is great news for the majority of people but 8% of people worldwide have a form of the ALDH gene called ALDH2*2. This gene codes for a less functional protein which converts acetaldehyde to acetic acid much slower or not at all. This means that when cells become exposed to acetaldehyde, it is not detoxified and levels of it rise in cells, causing cells to die. With my research I have discovered that a class of drugs called 5-nitrofurans prevent the ALDH protein from breaking down acetaldehyde. This is bad news for people with the ALDH2*2 form of the gene because they are already unable to breakdown acetaldehyde fast enough to

prevent damage. Levels of acetaldehyde rise in the blood when cells are exposed to alcohol and 5-nitrofurans at the same time and so I set up a scientific method to robustly measure the amount of different aldehydes that are in blood. Alcohol and 5-nitrofurans cause levels of acetaldehyde to rise in normal mice, but this effect is enhanced when the ALDH1B1 protein is removed in mice. This means that people who are undergoing treatment with 5-nitrofurans might suffer the damaging effects of acetaldehyde when they drink alcohol. 5-nitrofuran drugs can be used to kill cancer cells that have high levels of ALDH enzyme. I wanted to discover why ALDH enzymes are expressed in cancer cells, what the differences were between cancer cells that had lots of ALDH protein and cancer cells that did not, and what would happen to the genetic instructions inside the cell if ALDH was removed. I discovered that ALDH and the molecule it generates, called retinaldehyde are responsible for maintaining skin cancer cells in a state that is resistance to chemotherapy. These results mean that we now have a better understanding of how aldehydes can be altered within our bodies with 5-nitrofurans and how this might be the reason why 5-nitrofurans have damaging effects on both healthy and cancerous cells.

Acknowledgements

I am fortunate to have carried out my PhD at the MRC Human Genetics Unit, Institute of Genetics and Molecular Medicine in the laboratory of Prof. E. Elizabeth Patton. I would like to thank Liz for taking me on as a PhD student and for providing me a generous opportunity with the freedom to explore different avenues during my research. I am appreciative of the discussions and enthusiasm, especially with optimisations! I am also grateful for the theatre, book and scientific paper recommendations as well as the yearly celebrations at the Kingdom!

Thank you to my co-workers in the Patton group for their support, providing feedback and for the endless supply of treats (even the durian)! A special thanks to Marija for contributing to this project. Many thanks to the MRC for funding my science and to the ERC and L'Oreal Melanoma Research Alliance for laboratory funding that meant I could work with such a diverse research group.

Thank you to those at the IGMM and wider scientific community who have generously provided reagents, expertise and advice for my experiments; Dr. Luke Boulter (MRC HGU) for all of your help and welcoming me to your laboratory in the early days; Prof. Mark Arends (CRUK Edinburgh) for the aldehyde and ALDH discussions and for generously sharing your mouse resources; Dr. Ian Adams (MRC HGU) for your advice and useful critique of the work. Thank you to Luke, Mark and Ian for the time and effort you have

put into serving as committee members during my PhD. Thank you to Dr. Andy Finch (CRUK Edinburgh), Dr. Natalie Homer (Edinburgh Clinical Research Facility) and Dr. Jimi Wills (CRUK Edinburgh) who were instrumental in the running of the mass spectrometry studies; Prof. KJ Patel and laboratory (MRC LMB) for conference discussions and the ALDH2 mouse line; Prof. James Chen, Dr. Zhiping Feng (Stanford) and Dr. Matt Nowicki (Edinburgh EPPF) for supplying ALDH proteins; Richard Clarke (WTCRF) and Dr. Graeme Grimes (IGMM) for sequencing and bioinformatic assistance; Lizzie Freyer for FACS-expertise and the BVS team especially Scott Noble, Gary Waugh and Julie Thompson. Thanks to all of the HGU technical support teams for enabling our research and to Jim McQueenie for delivering reagents and anecdotes.

To my fellow IGMM PhD students who have become great friends over the past four years; Lana, Fiona, Issy, David, Nick, Dan and Toby. You have all made this time a lot more fun and a lot less stressful than it could have been! Jeanette, thank you for being a wonderful mentor and friend.

Finally, to my loved ones for being a wonderful bunch of people. You have all given me more support and advice than was necessary. Thank you Nas for having endless confidence in my abilities and always rooting for me. Rajan, Laura and James, thanks for staying close despite the distance. Thanks to the Ross clan, Kenny, Morag, Graham and Fern for all of the dinner and game invites and for making me feel at home in Scotland. Most of all thank you to Mum, Dad, Grandma and Grandad for all of your unwavering encouragement, for supporting my education and for giving me plenty to laugh and smile about. Craig, thanks for enduring science chat every day and for all of your support while researching and writing this thesis.

List of Abbreviations and Symbols

4-NP	4-nitrophenol
4-NPA	4-nitrophenyl acetate
5-NFN	5-nitrofuran
AA	acetaldehyde
AA-DNPH	acetaldehyde-2,4-DNPH
ALDH	aldehyde dehydrogenase
amu	atomic mass unit
BAAA	BODIPY™-aminoacetaldehyde
BAAA-DA	BODIPY™-aminoacetaldehyde diethyl acetal
bp	base pair
cDNA	complementary deoxyribonucleic acid
CE	collision energy
coA	coenzyme A
cps	counts per second
cts	counts
CXP	cell exit potential

DEAB	diethylamino-benzaldehyde
DEG	differentially expressed gene
DIMATE	dimethyl ampal thiolester
DNPH	2,4-dinitrophenylhydrazine
ds	double stranded
ECACC	European Collection of Authenticated Cell Cultures
ESI	electrospray ionisation
FA-DNPH	formaldehyde-2,4-DNPH
FACS	fluorescence activated cell sorting
FDR	false discovery rate
GAPDH	glyceraldehyde-3-phosphate dehydrogenase
GSEA	gene set enrichment analysis
HPLC-MS	high-performance liquid chromatography
HSA	highest single agent
kb	kilobase
LC	liquid chromatography
LC-MS/MS	liquid chromatography tandem mass spectrometry

MeCN	acetonitrile
min	minutes
mRNA	messenger ribonucleic acid
MS	mass spectrometry
m/z	mass-to-charge ratio
NAD^+	nicotinamide adenine dinucleotide (oxidised)
NADH	nicotinamide adenine dinucleotide (reduced)
$NADP^+$	nicotinamide adenine dinucleotide phosphate (oxidised)
NADPH	nicotinamide adenine dinucleotide phosphate (reduced)
NCSC	neural crest stem cell
NAZ	nifuroxazide
NES	normalised enrichment score
NFX	nifurtimox
NFN1	nitrofuran-1
NTR	nitroreductase
OD	optical density
PA-DNPH	propionaldehyde-2,4-DNPH
PCR	polymerase chain reaction
PF	pass-filter

RA	retinoic acid
RAR	retinoic acid receptor
RXR	retinoid X receptor
RXRG	retinoid X receptor gamma
RARE	retinoic acid response element
rpm	revolutions per minute
RNA	ribonucleic acid
ROS	reactive oxygen species
RT	room temperature
SNP	single nucleotide polymorphism
SPE	solid phase extraction
TCGA	The Cancer Genome Atlas
UPLC	Ultra Performance Liquid Chromatography
UV-Vis	ultraviolet-visible spectroscopy

Contents

List of Tables

List of Figures

Chapter 1

Introduction

1.1 Aldehyde Dehydrogenases and Aldehyde Metabolism

Aldehyde metabolism is dependent on the activities of the Aldehyde Dehydrogenase (ALDH) enzyme superfamily (EC 1.2.1.3; systematic name: aldehyde:NAD(P)$^+$ oxidoreductase). The nineteen enzymes that constitute this family are known for their capacity to metabolise aldehydes that are relevant to both physiology and pathophysiology. Although a diverse enzyme class, ALDHs have been highly conserved throughout evolution, highlighting the importance of ALDH and particularly aldehyde metabolism in maintaining cellular function.

1.1.1 Substrates

ALDH enzymes share common catalytic activities but each ALDH isoform demonstrates distinct substrate specificities (Table 1.1). The number of molecules that have been identified as substrates of enzymes in this class is considerable and so it is unsurprising that ALDHs have diverse functions in maintaining cellular states (Marchitti et al., 2008). Aldehydes comprise the largest class of substrates for the ALDH enzymes. Pathophysiologically, the metabolism of aldehydes by ALDH dehydrogenase activity is of central importance to detoxification processes. Historically, the focus of aldehyde biology has been largely directed toward these detoxification functions of ALDH enzymes. However, recent developments and improved tools for tracing of aldehydes, aldehyde precursors and the biological adducts that aldehydes produce including probe-based imaging and mass spectrometric techniques have uncovered a new field of interest in aldehyde biology, providing new ways to research long-standing questions such as the origin and detoxification of DNA damage and functional importance of ALDH

expression particularly in cancer.

As ALDH enzymes differ in their relative specificity for aldehyde substrates, some ALDHs are involved preferentially in mediating the pathophysiological effects of aldehydes, whereas others are required to generate physiologically important endogenous cell signalling molecules from aldehyde precursors (Marchitti et al., 2008). There is some degree of overlap between these two seemingly opposing functions and most ALDHs catalyse metabolism of several substrates, exposure to which can be modulated on a tissue-specific level.

The dehydrogenase activity of ALDH is well-described and endogenous aldehyde substrates have been identified but ALDH enzymes also possess an esterase function (Sidhu and Blair, 1975; Blackwell et al., 1983). ALDH1 and ALDH2 isoforms have been shown to catalyse ester hydrolysis of 4-nitrophenyl acetate (4-NPA) to 4-nitrophenol (4-NP) (Morgan and Hurley, 2015). Although there are currently no discovered endogenous or xenobiotic ester substrates of ALDH enzymes *in vivo*, ALDHs are involved in xenobiotic metabolism and a nitroglycerin reductase function of ALDHs is exemplified by the ALDH-dependent bioactivation of nitroglycerin to NO and other nitrates (Chen et al., 2002; Beretta et al., 2008; D'Souza et al., 2011).

Table 1.1: Key Substrates of ALDH Enzymes

Substrate	**ALDH**	K_m (μM)	**Reference**
Acetaldehyde	ALDH2	0.2	Klyosov et al. (1996) and Klyosov (1996)
	ALDH2	3.2	Stagos et al. (2010)
	ALDH1B1	55	Stagos et al. (2010)
	ALDH1A1	180	Klyosov et al. (1996)
	ALDH8A1	10240	Lin and Napoli (2000)
	ALDH9A1	-	
All-*trans* Retinaldehyde	ALDH1A1	11.6	Gagnon et al. (2003)
		26.8	Jackson et al. (2015)
	ALDH1A2	0.66	Gagnon et al. (2002)
	ALDH1A3	0.2	Graham et al. (2006)
	ALDH8A1	-	Lin and Napoli (2000)
9-*cis* Retinaldehyde	ALDH1A1	3.59	Gagnon et al. (2003)
	ALDH1A2	2.25	Gagnon et al. (2002)
	ALDH1A3	-	
	ALDH8A1	3.15	Lin and Napoli (2000)
13-*cis* Retinaldehyde	ALDH1A2	0.62	Gagnon et al. (2002)

Enzymes highlighted in green are the major ALDH isoform involved in metabolism of each substrate. Information from sources Marchitti et al. (2008); Singh et al. (2015); Wang et al. (2009) and as designated in the table.

1.1.2 Acetaldehyde Sources

Cellular acetaldehyde originates from endogenous and exogenous sources. Sources of acetaldehyde are plentiful in the environment: Alongside other aldehydes, acetaldehyde is produced upon hydrocarbon combustion in vehicle motors and cigarette smoke and is a component of industrial dyes, plastics and rubber. Bacteria in the oral cavity and gut produce acetaldehyde through pyruvate decarboxylase catalysis of pyruvate to acetaldehyde (Chandra Raj et al., 2001). In addition to effects of microbiotic metabolism, it is claimed that endogenous acetaldehyde can arise in cells through catabolism of alanine and the degradation of deoxyribose PO_4 (Tacconi et al., 2017) but evidence for this in mammalian systems is lacking. Acetaldehyde burden in cells is also affected by dietary factors. Consumption of foods, particularly those that are fermented, is a key route of exposure to acetaldehyde. The most well-documented form of exposure to acetaldehyde arises through ethanol metabolism. Ethanol is metabolised predominantly in the liver to acetaldehyde through the action of the highly expressed enzymes alcohol dehydrogenase (ADH) and Cytochrome P450 2E1 (CYP2E1).

1.1.3 Acetaldehyde Metabolism

1.1.3.1 ALDHs as Mediators of Acetaldehyde Metabolism

Acetaldehyde, CH_3CHO is a major substrate of ALDH2 and ALDH1B1 enzymes (Table 1.1, Figure 1.2). These isozymes are located in the mitochondria and have a high affinity for aliphatic aldehydes including acetaldehyde (K_m = 0.2 μM, 55 μM) and propionaldehyde (K_m = 0.095 μM, 14 μM) (Stewart et al., 1995; Stagos et al., 2010; Klyosov, 1996). The specificity of these ALDHs toward their substrates is determined by the residues that line the hydrophobic tunnel of each ALDH subunit (Koppaka et al., 2012). At the base of this hydrophobic tunnel is the enzyme active site, which is positioned opposite to the cofactor binding site. The base of the tunnel is located in proximity to the linker region. This linker (or oligomerisation) region enables dimerisation of each monomeric subunit. Two homodimers are consequently assembled into the tetrameric (dimer of dimers), which is the catalytically active form of the enzyme, containing four active sites, one per monomer (Figure 1.1). Both ALDH1B1 and ALDH2 function as homotetrameric enzymes (Rodriguez-Zavala and Weiner, 2002; Lutfullah et al., 2011). The active site of acetaldehyde-metabolising ALDHs binds a single aldehyde molecule and the cofactor nicotinamide adenine dinucleotide (NAD^+) or nicotinamide adenine dinucleotide phosphate ($NADP^+$) in their oxidised states. NAD^+ is a cofactor for ALDH1B1 and ALDH2 enzymes whereas $NADP^+$ serve only as a cofactor for the ALDH1B1 isoform.

All of these functional regions; coenzyme binding domain, catalytic domain and linker domain have a high degree of structural homology between ALDHs, despite differences in their substrate preference. The capacity of ALDH1B1 and ALDH2 to catalyse oxidation is afforded by possession of the amino acid, cysteine at position 302 (Cys302) (Figure 1.1). The Cys302 residue is

completely conserved in all catalytically active members of the ALDH family alongside asparagine at position 169 (Asn169) (Perozich et al., 2008; Hempel et al., 1999). The Cys302 residue is critical for nucleophilic attack of acetaldehyde, which is responsible for forming a covalent enzyme-substrate intermediate. Performing classical site-directed mutagenesis experiments on the ALDH active site residues enabled dissection of the functional amino acid residues for activity. By mutating the cysteine amino acid residue to alanine (C302A), a tetrameric enzyme was generated that maintained NAD^+-binding but lacked dehydrogenase and esterase activity (Farres et al., 1995). Replacement of Cys302 for Ser302 (C302S) led to a reduction in the enzymatic rate of ALDH2. This is because the hydroxyl group of serine is a weaker nucleophile than the sulfanyl group of cysteine. This confirmed that Cys302 was an essential amino acid for ALDH activity.

1.1.4 Aldehyde Detoxification

Short-chain aldehydes that include formaldehyde and acetaldehyde are DNA- and protein-damaging agents which present a toxic metabolic challenge to the cell that must be eliminated or repaired. Elimination of aldehydes occurs through degradation or inactivation of aldehydes (Tier I protection), predominantly by ALDH enzymes. Substrates of ALDH1B1 and ALDH2 enzymes that are directly relevant to this project are highlighted in Table 1.2.

Table 1.2: Biological Aldehyde Substrates of ALDH1B1 and ALDH2

Aldehyde	**Systematic Name**	**Synonyms**
Formaldehyde	Methanal	Formalin
		Formol
		Oxomethane
Acetaldehyde	Ethanal	
Propionaldeyhde	Propanal	

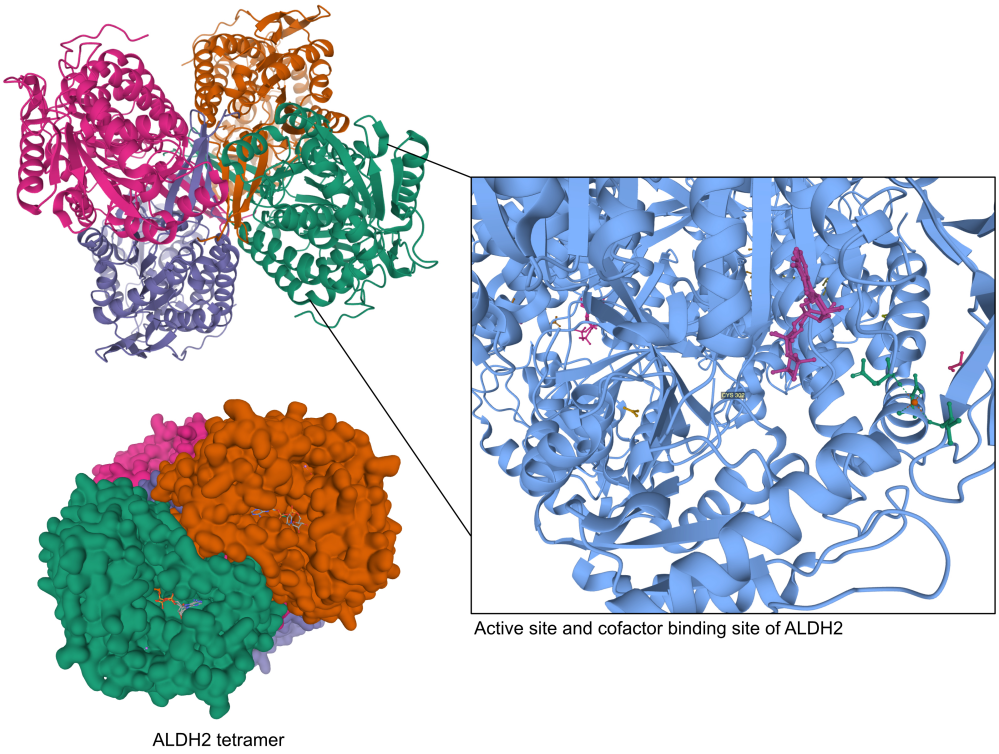

Figure 1.1: **Tetrameric Structure of ALDH2**

Structure of the human mitochondrial aldehyde dehydrogenase complexed with cofactor NAD^+. Individual subunits are coloured differently. Ribbon view and Gaussian surface representation to show ALDH2 monomeric subunits. Gaussian surface representation demonstrates the presence of the hydrophobic tunnel in ALDH2 subunits and bound position of the cofactor. Expanded ribbon view of the base of the hydrophobic tunnel of an ALDH2 monomer highlights that the active site cysteine residue, Cys302 (labelled CYS 302) is positioned opposite to the NAD^+ cofactor binding domain. Bound NAD^+ is highlighted on the ribbon structure in purple. This figure was producted using the RSCB Protein Databank (PDB) and crystal structure data from Larson et al. (2007).

1.1.4.1 Acetaldehyde Fate and Consequences of Acetaldehyde Exposure

The major site of acetaldehyde detoxification is the liver. In cells with competent acetaldehyde-metabolising ALDH enzymes, acetaldehyde is detoxified by oxidation to acetic acid (Figure 1.2). Free acetic acid dissociates at cellular pH 7.4 to acetate anions and protons. Acetate enters the mitochondria where it undergoes rapid assimilation alongside coenzyme A (CoA) into acetyl coenzyme A (acetyl-CoA) via ligation of acetyl-CoA and acetate (Figure 1.3). The resulting acetyl-CoA is a key metabolic intermediate that can be used for oxidation through the tricarboxylic acid cycle and is central to many metabolic reactions (Shi and Tu, 2015; Pietrocola et al., 2015).

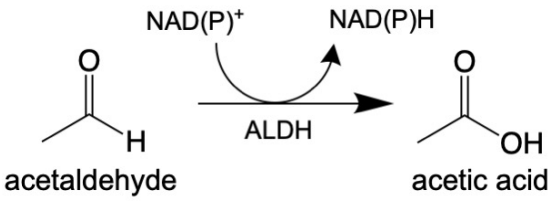

Figure 1.2: **Oxidation of Acetaldehyde by Aldehyde Dehydrogenase Enzymes**
ALDH isozymes ALDH1B1 and ALDH2 catalyse irreversible oxidation of the acetaldehyde carbonyl to its respective carboxylic acid, acetic acid. Oxidation of acetaldhyde is coupled to reduction of the cofactor NAD^+ (for ALDH2 and ALDH1B1) or $NADP^+$ (for ALDH1B1) and generates NADH or NADPH as a reaction product.

Figure 1.3: **Acetaldehyde Metabolic Pathway**

Ethanol is metabolised through alcohol dehydrogenase (ADH) enzymes predominantly in the liver to acetaldehyde. Aldehyde dehyrogenase catalyses the oxidation of acetaldehyde to acetic acid, which dissociates to acetate. Acetate enters the mitochondria where it is ligated to CoA by acetyl-CoA synthetase and acyl-CoA synthetase 2. Acetate can also be utilised as a source of acetyl groups for acetyl-modifications including histone and protein acetylation.

1.1.5 Retinaldehyde Metabolism

1.1.5.1 ALDHs as Mediators of Retinaldehyde Metabolism

Retinaldehyde is a major substrate of ALDH1A1, ALDH1A2 and ALDH1A3 isozymes (RALDH1, RALDH2, RALDH3) (Yoshida et al., 1992). Retinaldehyde is biosynthesised in the cell by the reversible action of retinol dehydrogenases (RDH) on retinol (vitamin A). ALDH1A1, 1A2 (Zhao et al., 1996; Wang et al., 1996) 1A3 and 8A1 enzymes catalyse the irreversible cytosolic oxidation of retinaldehyde to retinoic acid (RA) (Figure 1.4). Oxidation of retinaldehyde yields the retinoic acid (RA) isomers, all-*trans*-RA (ATRA), 9-*cis*-RA and 13-*cis*-RA. ALDH1A1 has high affinity for all-*trans*- and 9-*cis*-retinal, whereas ALDH1A3 has a high affinity for all-*trans*-retinal (Table 1.1).

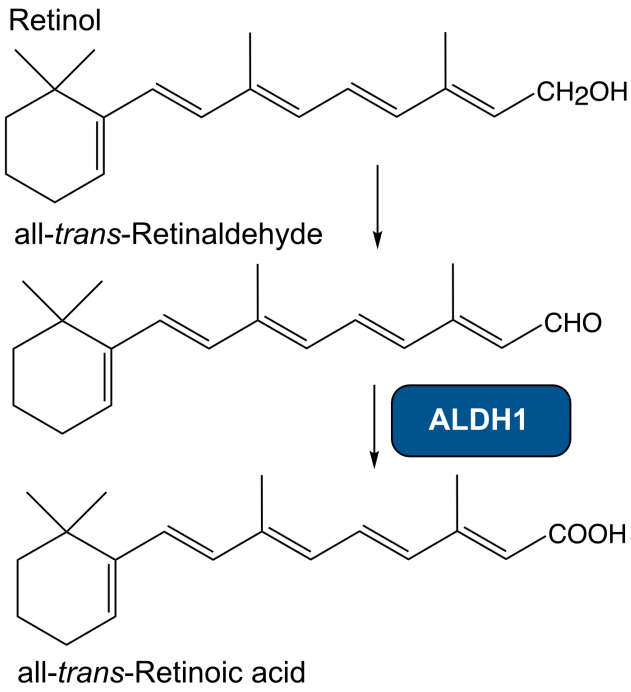

Figure 1.4: **Retinaldehyde Metabolic Pathway**
Retinol is metabolised through retinol dehydrogenase (RDH) enzymes to retinaldehyde. Retinaldehyde is oxidised to retinoic acid by the action of the ALDH1 subfamily of ALDH enzymes. All-*trans*-retinaldehyde has the lowest K_m for the ALDH1A3 isoform.

1.1.5.2 Downstream Effects of Retinoic Acid

Retinoic acid isomers differ in their biological potency; of all three isomers, ATRA exerts the most potent and experimentally-defined cellular effects. RA binds to two familes of receptors, nuclear retinoic acid receptors (RAR) and retinod X receptors (RXR). Both of these classes have α, β, γ isoforms. Binding of the heterodimerised forms of these receptors to the retinoic acid response element (RARE) drives transcriptional activation and expression of RA target genes. Retinoic acid signalling is key during times of enhanced transcriptional activation and control, including embryonic development and adult differentiation during tissue repair and thus tissue-specific expression and activity of ALDH is essential for governing these processes (Duester et al., 2003).

1.2 ALDHs in Disease

1.2.1 Biological Reactivity of Aldehydes

The electrophilic nature of aldehydes contributes to their high degree of reactivity with environmental and biological matter. This reactivity of aldehydes is provided by their characteristic formyl functional group (CHO). The carbonyl group provides aldehydes (R-CHO) with an electrophilic carbon that reacts readily with nucleophilic sites in DNA and proteins, leading to aldehyde adduct formation.

A notable DNA adduct arising from acetaldehyde exposure is N^2-ethylidene-2′-deoxyguanosine (N^2-Et-dG). It is the most abundant DNA adduct resulting from ethanol and acetaldehyde exposure that has been discovered so far (Wang et al., 2006; Matsuda et al., 2007). Despite ethanol exposure being a desirable candidate for the identification of biomarkers for human cancer, liver disease and alcoholism, investigation of mutational spectra of acetaldehyde exposure have lagged behind investigations of similar xenobiotics such as aflatoxin B_1, for which characteristic mutational spectra have been elucidated (Chawanthayatham et al., 2017). Although biomarker discovery for acetaldehyde-specific DNA and protein adducts is in its infancy, there has been much research on more general adducts such as those arising from ethanol treatment. These DNA and protein adducts arising from aldehyde or ethanol exposure can be reversible and irreversible (Sonohara et al., 2019) but ultimately, their detoxification through mechanisms that remove acetaldehyde (tier I) and those that repair acetaldehyde-induced damage (tier II) is essential for maintenance of cell homeostasis and viability.

1.2.2 Acetaldehyde Metabolism Underpins Disease Pathogenesis

Aldehyde metabolism underpins many complex disease pathologies and cell signalling pathways. In the past, aldehyde metabolism by ALDH has been noted for its contribution to alcohol toxicity and related disease (Ambroziak and Pietruszko, 1993; Amir, 1978; Horton, 1970). More recently, the field of aldehyde metabolism has been expanded to include increasingly complicated metabolic networks including DNA demethylation, methylation cycles and one carbon metabolism (Bae et al., 2017; Burgos-Barragan et al., 2017). This recent research has mostly focused on the involvement of other short chain aldehydes, including formaldehyde, in metabolic networks. Although similar studies of acetaldehyde exist, isotopic labelling of acetaldehyde is rarely employed (Shukla et al., 2007; Chen et al., 2018). Key recent studies of aldehyde biology have demonstrated that expression of ALDH2 and ALDH1B1 is protective against ethanol and acetaldehyde-induced DNA damage (Amanuma et al., 2015; Garaycoechea et al., 2018), which is particularly relevant for alcohol-induced cancers and liver disease (Müller et al., 2016, 2018).

1.2.2.1 Human ALDH Polymorphisms Demonstrate the Necessity of Aldehyde Metabolism

The most significant reporter of ALDH2 function exists in the genome of 8% of the World's population (Brooks et al., 2009). A single nucleotide polymorphism (SNP) in the *ALDH2* gene (*ALDH2*2*) is the most frequently identified single nucleotide variant. The *ALDH2*2* allele arises from a single point mutation of guanine to adenine. This mutation gives rise to an amino acid substitution at position 487 of the ALDH2 protein of glutamate to lysine

(E487K, or E504K when including the mitochondrial targeting sequence) in the ALDH2 monomer (Yoshida et al., 1984; Steinmetz et al., 1997) (Figure 1.5). The ALDH2*2 monomer exerts a dominant negative effect when present in the ALDH2 tetramer. Incorporation of only one defective ALDH2*2 subunit in the overall ALDH2 tetramer depletes the enzymatic activity of the ALDH2 enzyme by 52%, whereas homozygotes for *ALDH2*2* have closer to 1 - 4% of the wild-type *ALDH2*1* activity (Weiner et al., 2001). This means that heterozygosity for *ALDH2*2* is enough to significantly hamper cellular oxidation of acetaldehyde to acetate. Although the *ALDH2*2* polymorphism is the most common SNP, suggesting there is a possible evolutionary advantage of possessing the mutated allele, the SNP has been linked to various pathogeneses and has revealed fundamental consequences of defective aldehyde detoxification. The most famous example of this is demonstrated by *ALDH2*2* carriers who have a heavy intolerance to ethanol consumption. Deficiency of ALDH2 acetaldehyde-metabolising capacity manifests with facial flushing, headaches, nausea, dizziness, and cardiac palpitations following alcohol consumption. The inability of *ALDH2*2* individuals to metabolise ethanol is thought to underpin the enhanced risk *ALDH2*2* carriers have of developing digestive tract cancers (Chang et al., 2017; Matsumoto et al., 2016).

1.2.2.2 Mouse Models Used for the Study of Aldehyde Metabolism

Mouse genetic mutants harbouring *Aldh2*-deficiency have been heavily utilised as models of *ALDH2*2* genetics. Pathogenic effects of ALDH mutations are not limited to oncogenesis and span many organ systems. Exposure of *Aldh2* wild-type status mice to acetaldehyde led to a preconditioning, upregulation of ALDH2 and subsequent protection against cardiac ischaemia-reperfusion injury. Conversely, the same treatment of

*Aldh2*2* mice, with diminished ALDH2 activity, abolished the cardioprotective effects of acetaldehyde and ethanol (Ueta et al., 2018). In some cases, defective acetaldehyde metabolism is advantageous: For instance, in enhancing sensitivity to chemotherapy, where *Aldh2*2* mice exhibit enhanced reactive oxygen species (ROS) production in response to cisplatin (Kim et al., 2017).

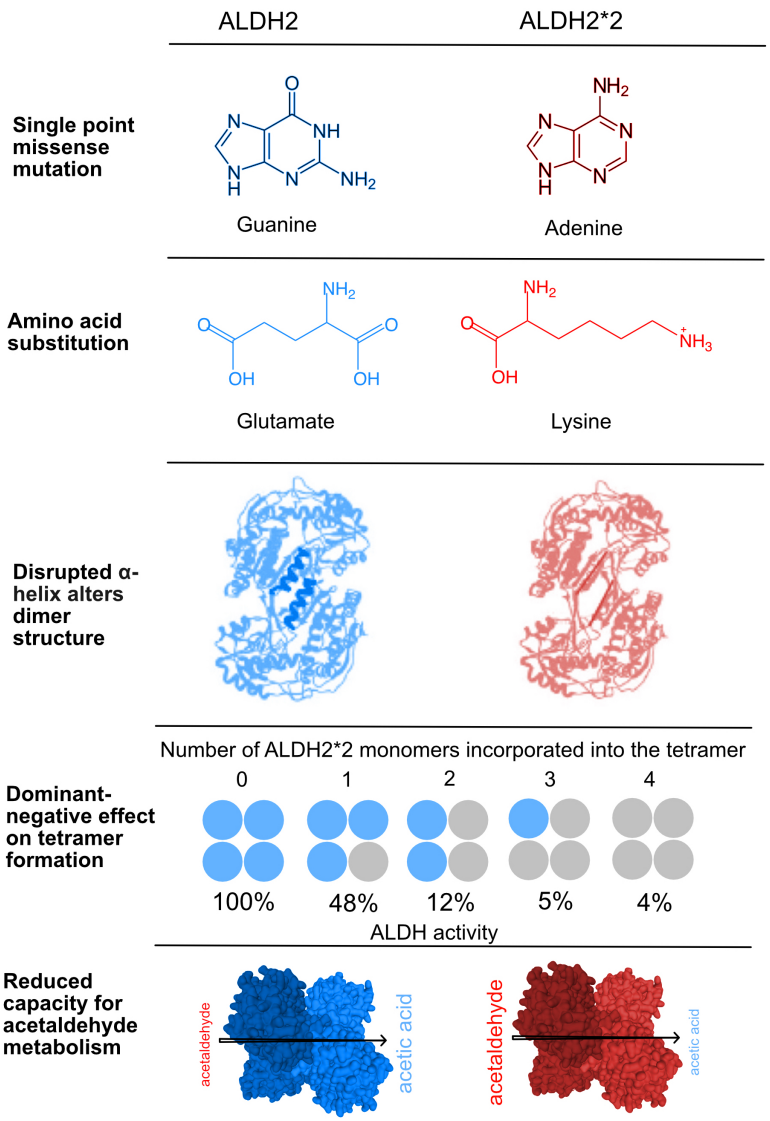

Figure 1.5: **Possession of the ALDH2*2 Variant Disrupts ALDH2 Tetramer Activity**

The *ALDH2*2* allele results from a single point substitution of guanine to adenine and a substitution in the amino acid sequence from glutamate to lysine which disrupts the dimerisation domain of ALDH2 and prevents proper assembly of the ALDH2 tetramer. ALDH2*2 monomers exhibit a dominant negative effect on ALDH activity and prevent the oxidation of acetaldehyde to acetic acid. Image based on figure from Gross et al. (2015).

1.2.3 ALDHs as Markers of Tumour-Initiating Cells

1.2.3.1 Basis of the ALDEFLUOR™ Assay

ALDH enzymes are widely used experimental markers of tumour-initiating cells. The ALDEFLUOR™ assay has been instrumental in the use of ALDH as a marker of bonafide stem cells and tumour-initiating cells and its usefulness was first demonstrated through isolation of ALDH-expressing haematopoietic stem cells (Storms et al., 1999). The assay relies upon metabolism of the fluorescent ALDEFLUOR™ reagent, BODIPY-aminoacetaldehyde (BAAA) to a negatively charged and membrane-impermeable BODIPY-aminoacetate conjugate (Figure 1.5). This causes the metabolised reagent to accumulate within the cytosol and generate a fluorescent signal that can be used to analyse and isolate cell populations with flow cytometry. The ALDH inhibitor 4-(Diethylamino)benzaldehyde (DEAB) is used as a negative control in the ALDEFLUOR™ assay. Although the mechanism of ALDH inhibition has not been established for this compound, the low rate of turnover of the DEAB benzyl aldehyde group to benzoate means that it essentially functions as a competitive inhibitor (Morgan et al., 2015).

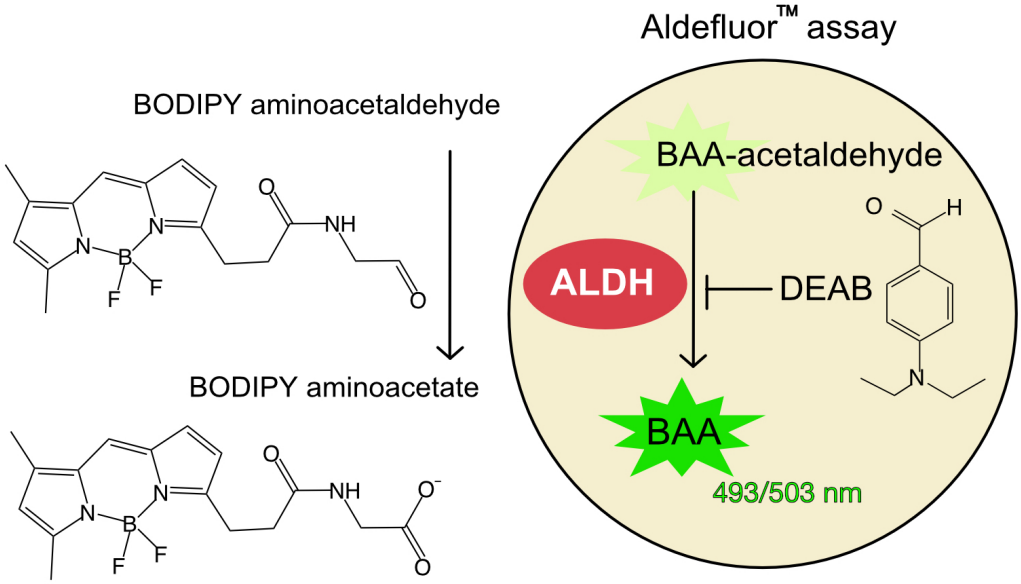

Figure 1.6: **ALDEFLUOR™ Assay for Monitoring Cellular ALDH Activity** Cells uptake the fluorescent BODIPY-aminoacetaldehyde substrate. In cells that express ALDH isoforms which are capable of BODIPY aminoacetaldehyde (BAAA) metabolism, BODIPY-AAA is converted to the negatively charged BODIPY aminoacetacetate. This conjugate is membrane impermeable and therefore is retained in the cells which express ALDH, generating a fluorescent read-out of ALDH activity.

1.2.3.2 Tumour-Initiating Cells

Tumour-initiating cells were first described in leukaemia (Lapidot et al., 1994). Given the lineage-orientated nature of the haematopoietic system, extrapolation from this established developmental model gave rise to the hierarchical model of tumour initiation and development. This model proposes that tumours harbour a subpopulation of cells which are capable of self-renewal and differentiation and that these cells are responsible for tumour initiation and progression. This cancer subpopulation is thought to be resistant to conventional chemotherapies, as a result of upregulated drug-resistance genes or lower levels of cellular proliferation. ALDH was first identified as a marker of a subpopulation of tumour-initiating cells in breast cancer and leukaemia and since has been vastly used as a marker to delineate tumour populations that coincide with drug resistance (Ginestier et al., 2007; Cheung et al., 2007).

1.2.3.3 ALDEFLUOR™ as a Reporter of ALDH Activity in Tumour Initiating Cells

Although ALDH1A1, ALDH1A2, ALDH1A3 and ALDH2 activity have been shown to underlie ALDEFLUOR™-induced fluorescence in stem cells and tumour-initiating cells, the contribution of individual ALDH isoforms to turnover of ALDEFLUOR™ BAAA reagent in cells is unknown. The substrate specificity of each ALDH isoform toward BAAA has not been reported but a recent overexpression screen of the 19 human ALDH isoforms in kidney and breast cancer immortalised cell lines alongside respective catalytic mutants reinforced the notion of tissue-specific ALDEFLUOR™ activity, describing nine isoforms which underlie BAAA turnover in these cell types (Zhou et al., 2019).

1.2.4 ALDH in Melanoma

The functional importance of expression of ALDH1 enzymes in chemoresistance is attributed to their role in retinoic acid synthesis. Retinoic acid synthetic pathways have been widely explored as opportunities for the modulation of drug tolerance. Retinoic acid has been used as a treatment strategy to enhance the anticancer effects of many drugs but the mechanism of how retinoic acid induces these effects is not understood.

Although exact models of cancer cell dynamics and tumour evolution are subject of dispute, enrichment of ALDH enzymes at tumour sites during radiotherapy and chemotherapy has been reported and targeting these cellular subpopulations can overcome drug resistance (Duan et al., 2016). Recently, Sarvi et al. (2018) and Pérez-Alea et al. (2017) independently demonstrated that ALDH1A3 is upregulated in melanoma subpopulations and that these populations are sensitive to the ALDH inhibitors, nifuroxazide and dimethylthioampal (DIMATE). Pérez-Alea et al. (2017) attributed cytotoxicity of DIMATE in ALDH1 populations to elevations in ROS and subsequent generation of peroxidation markers, 4-Hydroxynonenal (4-HNE) and Malondialdehyde (MDA). Sarvi et al. (2018) propose a two-hit mechanism of nifuroxazide toxicity, the first through bioactivation of nifuroxazide to ROS and the second through direct inhibition of ALDH1A3. Neither study addressed the potential for accumulation of aldehydes and dysfunctional retinoic acid signalling in the cytotoxic effects resulting from ALDH1A3 inhibition.

1.2.5 Modifiers of ALDH Function

Given that isoforms in the ALDH family are important for detoxification or generation of biologically important molecules and are upregulated or dysfunctional in disease, they are attractive targets for the development of ALDH isozyme-selective inhibitors and activators (Koppaka et al., 2012). The natural product, Daidzin has antidipsotropic effects and is a selective, reversible inhibitor that is specific to the ALDH2 isoform (IC_{50}, 80 nM). Daidzin inhibits ALDH function through binding to a hydrophobic cleft of the ALDH2 active site (Lowe et al., 2008). Inhibition of the ALDH2 enzyme is responsible for the antidipsotropic effects of Daidzin.

Disulfiram (tetraethylthioperoxydicarbonic diamide) is used clinically for the treatment of alcoholism, with effects upon alcohol consumption that mimic possession of the *ALDH2*2* polymorphism. Disulfiram is an irreversible, non-selective inhibitor of ALDH isoforms (Lipsky et al., 2001). Disulfiram is also a non-nucleoside DNA methyltransferase inhibitor (Lin et al., 2011). Due to its dual pharmacological effects on both ALDH and DNA methylation, the anticancer properties of Disulfiram have been widely studied (Yang et al., 2019). Disulfiram is metabolised by hepatic thiol methyltransferases to various metabolites that have the potential to carbamoylate and therefore inactivate Cys302 of the ALDH2 active site (Koppaka et al., 2012).

1.3 5-Nitrofurans

5-Nitrofuran compounds (5-NFNs) are a class of effective antiparasitic and antibiotic drugs used in human and veterinary medicine. The clinical application of 5-NFNs is broadening; some 5-NFNs have emerged as potential chemotherapeutic agents. Nifurtimox (NFX) has been repurposed in clinical trial for neuroblastoma and neuroblatoma therapy (Saulnier Sholler et al., 2006, 2009, 2011a,b). Recently, nifuroxazide has been shown in principle to provide effective therapy against minimal residual disease in melanoma (Sarvi et al., 2018).

1.3.0.1 Clinical Use of Nifurtimox in Chagas Disease

Nifurtimox is used for the treatment of human American trypanosomiasis (Chagas disease), as a second line option to benznidazole and as a combination therapy with eflornithine for second-stage human African trypanosomiasis (sleeping sickness). The causative agents of these diseases, *Trypanosoma cruzi* (*T. cruzi*) and *Trypanosoma brucei* (*T. brucei*) are present in millions of people worldwide; the most recent estimates for *T. cruzi* infection range between six and ten million people (Bonney, 2014; WHO, 2017). Twenty-five million people are at risk of Chagas disease (WHO, 2012), the disease is endemic in Latin America and migration has led to increased incidence of infection in non-endemic regions such as North America, Europe, Australia and Japan (Gascon et al., 2010). Untreated Chagas disease often results in life-long morbidity and disability which severely reduces quality of life for patients. This combined mortality and disabling effects of Chagas disease and their treatment means that they are a primary target for the World Health Organisation (WHO). Nifurtimox, is one of only two drugs used to treat Chagas disease and one of three used to treat second stage sleeping

sickness. Nifurtimox is of such importance in tackling the burden of Chagas disease that the WHO has classified it as an essential medicine (WHO, 2017).

1.3.1 Antiparasitic and Antibiotic Mechanisms of 5-Nitrofurans

Despite the use of nifurtimox against Chagas disease spanning 40 years, the mechanism of action of nifurtimox has not been elucidated in its entirety. Various mechanisms of action have been proposed, including oxidative stress induction, nitroreductase-mediated bioactivation and roles of the prostaglandin F2 synthase and cytochrome P450 reductase enzymes (Hall et al., 2011).

1.3.1.1 Nitroreductase Enzymes

As with all prodrugs, 5-NFNs require metabolism to generate pharmacologically active derivatives. Bioactivation of 5-NFNs occurs via two sequential nitroreduction reactions that yield an active hydroxylamine derivative. Reduction of the nitrofuran functional group, 5-NO_2-furan (Figure 1.7) is catalysed by nitroreductase enzymes (NTRs) and leads to generation of ROS and cell death induction (Maya et al. (2007)). The nitroreductases (NTRs) responsible for reduction of nifurtimox are commonly found in bacteria and protozoa, but are sparse in higher eukarotes. This is ideal from a drug selectivity perspective, in that nifurtimox can efficiently kill bacteria and parasites without bioactivation by potential host NTRs at sites other than the prokaryote.

In an effort to determine the selectivity of nifurtimox against *T. brucei*, Hall et al. (2011) overexpressed multiple enzymes thought to metabolise nifurtimox in *T. brucei* and monitored susceptibility to nifurtimox under these conditions.

Increasing expression levels of eukaryotic type I nitroreductase alone was enough to alter sensitivity to the drug and so NTRs were implicated with a key role in the anti-trypanosomal activity of nifurtimox (Figure 1.8). Furthermore, loss of a single copy of type I NTR in *T. cruzi* by targeted gene deletion causes cross-resistance to nitroheterocyclic drugs, including nifurtimox, without affecting the infectivity of the parasite (Wilkinson et al., 2008).

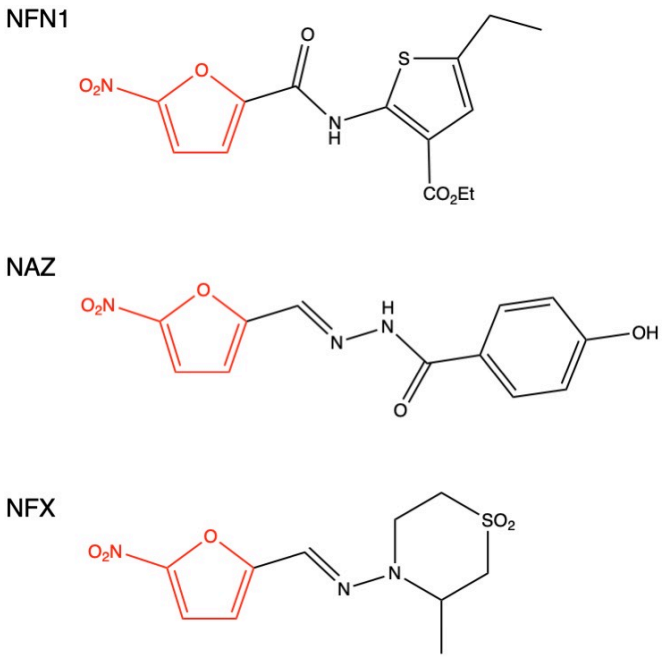

Figure 1.7: **5-Nitrofuran Compounds**

5-Nitrofurans with bioactivated groups indicated in red. The 5-nitrofuran functional group, 5-NO_2-furan is reduced by prokaryotic nitroreductase enzymes and undergoes bioactivation in zebrafish by ALDH2b. NFN1, nitrofuran-1; NAZ, nifuroxazide; NFX, nifurtimox.

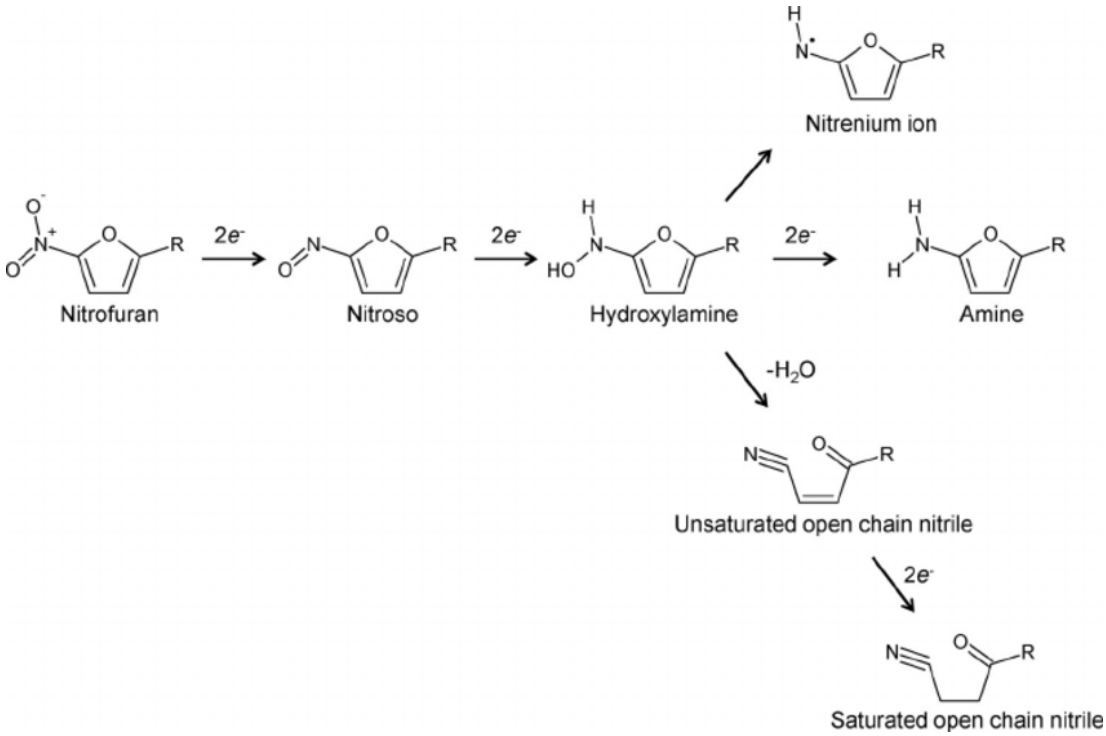

Figure 1.8: **Type I Nitroreductase Enzymes Catalyse Reduction of 5-Nitrofurans**

Type II Nitroreductases initially reduce 5-nitrofurans to a 5-NFN radical. Type I Nitroreductases catalyse reduction of the 5-NO_2-furan functional group. Nitroreduction generates a nitroso intermediate and subsequently a hydroxylamine. The hydroxylamine derivative is metabolised to form the nitrenium ion, the amine form, or unsaturated and then saturated open-chain nitriles. 5-NFN radicals can also reduce oxygen to a radical species which undergoes redox cycling with super oxide dismutase, promoting additional ROS formation. Figure from Hall et al. (2011).

1.3.2 5-Nitrofuran Off-Target Effects

Despite bioactivation of nifurtimox occuring through the action of bacterial and parasite-specific NTRs, nifurtimox causes complex adverse effects. These effects progressively worsen during the treatment course of 8-10 mg/kg for 60-90 days. The side effects of Chagas treatment with nifurtimox are often more considerable than the symptoms of Chagas disease, which manifest during the acute stage as mainly flu-like or asymptomatic (Gascon et al., 2010; WHO, 2011, 2012).

The most common nifurtimox symptoms are anorexia and weight loss, dizziness, psychic alteration, sleepiness and digestive problems including nausea, vomiting, intestinal colic and diarrhoea as well as neurological symptoms including polyneuropathy (Castro et al., 2006). These serious side effects lead to treatment cessation in a third of patients with Chagas (Castro et al., 2006). Side effects of nifurtimox can vary between populations but interestingly, these side effects are exacerbated when patients consume alcohol alongside their treatment and patients become intolerant to alcohol. This provides an intriguing hypothesis that alcohol and nifurtimox share a common molecular target.

Considering this, there is a clear, unmet need for development of a treatment strategy or refinement of therapeutic guidelines to reduce the off-target, toxic side effects of 5-NFNs. This is important not only for treatment of individual cases but to control the endemicity of Chagas disease, that like most other zoonoses, will never be fully eradicated (WHO, 2017). As of yet, such remedial treatments or drugs with lower toxicity but the same anti-trypanosomal effects have not been identified. Consequently, to refine current approaches of nifurtimox therapy and reduce the off-target side effects of 5-NFNs, understanding the mechanistic underpinnings of side effect development is essential.

1.4 Mechanisms of 5-Nitrofuran Toxicity

Multiple human enzymes capable of 5-nitrofuran reduction have been identified and are predominantly NAD(P)H quinone oxidoreductases (Morgan et al., 2015). However, whether these enzymes are relevant to 5-nitrofuran side-effects and have potential for therapeutic intervention to inhibit the off-target effects of 5-nitrofurans *in vivo* is unanswered. ALDH enzymes are a candidate target for the mediation of 5-nitrofuran adverse effects. Zebrafish ALDH2b was discovered as a target of 5-NFNs and bioactivation of NFN1 in zebrafish induced melanocytotoxic effects (Zhou et al., 2012). 5-nitrofurans are widely documented to cause DNA damage and yeast strains harbouring deletions in DNA damage repair pathways causes hypersensitivity to 5-nitrofurans (Zhou et al., 2012). The underlying DNA damaging agent(s) for this response remains to be established. A methodological means to evaluate the potential generation of DNA-damaging ALDH substrates that might underlie this interaction would support these studies.

1.5 Approaches to Quantify Aldehydes *In Vivo*

Given ever-increasing recognition of aldehydes as key cellular signalling molecules, there is a current unmet need for markers of acetaldehyde-induced damage as well as methods to quantify levels of circulating aldehydes.

1.5.1 Methods of Aldehyde Detection

Aldehydes are volatile and polar compounds that are susceptible to biochemical degradation (Table 1.3). These properties make them a problematic class of compounds to reliably quantify, particularly in biological

contexts. Large-scale detection of aldehydes and carbonyl groups in general is routinely performed in environmental chemistry. Aldehydes have a critical impact on the environment and contribute to pollution, ozone formation and photochemical smog, thus their detection in air, water and soil matrices is essential for measurement and control of air pollution. Even on large scales, such as when determining aldehyde content in ambient air, the reliability and robustness of these measurements are contentious (Herrington et al., 2007). Despite increasing recognition of aldehydes as fundamental biological molecules, there is a need for methods that accurately quantify aldehydes in biological fluids. The volatile nature of aldehydes and their capacity to degrade to carboxylic acids, causes acetaldehyde quantification in biological tissues to be a challenge. When applying large scale reactions such as those used in environmental chemistry to small scales such as quantifying relatively small differences in biological fluids that may be sufficient to have physiological implications but are under the detection threshold of current analytical methods, reactions can not be simply scaled down to the amount of compound being analysed. As a consequence, the lack of efficient means to quantify and trace aldehydes in biological systems means that understanding aldehydes as signalling and DNA-damaging molecules both *in vitro* and *in vivo* is hindered.

Aldehydes can be detected in biological samples including blood plasma and urine. Gas and liquid chromatography combined with mass spectrometry are the most common methods used for aldehyde analysis in these matrices, although enzyme-based assays are also used.

Table 1.3: Structure and Physicochemical Properties of Short-Chain Aldehydes

Property	*Aldehyde*		
	Formaldehyde	Acetaldehyde	Propionaldehyde
Linear Formula	HCHO	CH_3CHO	CH_3CH_2CHO
Molecular Weight	30.026	44.053	58.079
Monoisotopic Mass	30.026	44.026	58.042
Boiling Point	-19.5	20.2	48.8
Density	0.815	0.785	0.805

Molecular weight and monoisotopic mass reported in g/mol, boiling point reported in °C, density reported at 25°C in g/mL.

1.5.1.1 Enzyme Assays for Aldehyde Quantification

Colorimetric assays are used for the quantification of acetaldehyde in biological samples (Sung et al., 2012; Abraham et al., 2011; Müller et al., 2016; Zhang et al., 2018). These assays utilise the following reaction:

$$CH_3CHO + NAD^+ + H_2O \xrightarrow{ALDH} CH_3COOH + NADH + H^+$$

Acetaldehyde quantification with this method is based on oxidation of acetaldehyde that is catalysed by ALDH. NADH generated during the reaction reduces a formazan reagent and the product, which is proportional to the acetaldehyde concentation, is measured with UV-Vis spectrometry at 565 nm. The linear detection range for 10 μL of sample with this assay is reportedly 4 μM to 4 mM. As this assay relies on ALDH to quantify acetaldehyde, the enzyme also oxidises other aldehydes present in the sample, including propionaldehyde. This means that acetaldehyde is not distinguished from other aldehyde substrates of the recombinant ALDH. In many of the reported experiments that use this technique, ethanol is the major metabolic precursor administered and so it is reasonable to assume that the majority of aldehyde load detected is acetaldehyde. Additionally, enzymatic assays for the measurement of acetaldehyde are susceptible to inaccuracies due to the volatility of acetaldehyde as both a prepared standard for standard curve generation, and as a sample analyte in cell or plasma matrices. Enzymatic assays are performed at 25°C and so losses of acetaldehyde during sample collection and throughout the timecourse of the experiment is inevitable.

1.5.1.2 Chromatographic and Mass Spectrometric Assays for Aldehyde Quantification

1.5.1.3 Derivatisation of Aldehydes

The volatility and low response of aldehydes in liquid chromatography-mass spectrometry (LC-MS) presents analytical challenges. For analysis of highly polar aldehydes, derivatisation is a method that can be used to improve detection and quantitation in both gas chromatography-MS and LC-MS. Derivatisation involves the reaction of an analyte (aldehyde in this instance) with a reactive compound to yield a product that should be more amenable to analysis. Analyte derivatisation has many desirable effects on analyte characteristics, which improve the detectability and enhance chromatographic and fragmentation properties of analytes (Eggink et al., 2010):

- increase the stability of the analyte
- improve the separation from matrix components in sample pre-treatment and/or chromatography
- enhance the ionisation efficiency
- alter the fragmentation characteristics in MS

1.5.1.4 Agents for Carbonyl Derivatisation

Carbonyl groups of aldehydes can be readily derivatised using 2,4-dinitrophenylhydrazine (DNPH) (Figure 1.9). By derivatising aldehydes with DNPH to their corresponding aldehyde 2,4-dinitrophenylhydrazones, indirect detection of aldehydes is facilitated (Figure 1.10). The derivatisation reaction is relatively quick and simple and the resulting stable aldehyde 2,4-dinitrophenylhydrazone can be subjected to chromatographic and mass-spectromic analyses for sample detection and analysis. Derivatisation reagents contain a reactive functional group that selectively reacts with a complementary functional group in the analyte (Eggink et al., 2010). In this case, DNPH reacts with carbonyl groups of aldehydes. The advantage of this reactivity, afforded by the carbonyl functional group, is that it allows detection of multiple aldehydes in a complex mixture simultaneously. Despite possessing the same functional group, different aldehydes can be detected simultaneously because each aldehyde 2,4-dinitrophenylhydrazone exhibits a distinct molecular weight that will alter the retention time on the column material during HPLC separation and as DNPH has a molecular weight above the 50 Da detection limit of high-resolution accurate-mass mass spectrometers, all derivatised aldehydes should be detectable. Notably, in addition to raising the molecular weight of aldehydes, the reaction has the added benefit of reducing aldehyde volatility, preventing loss of aldehyde from the sample (Table 1.4).

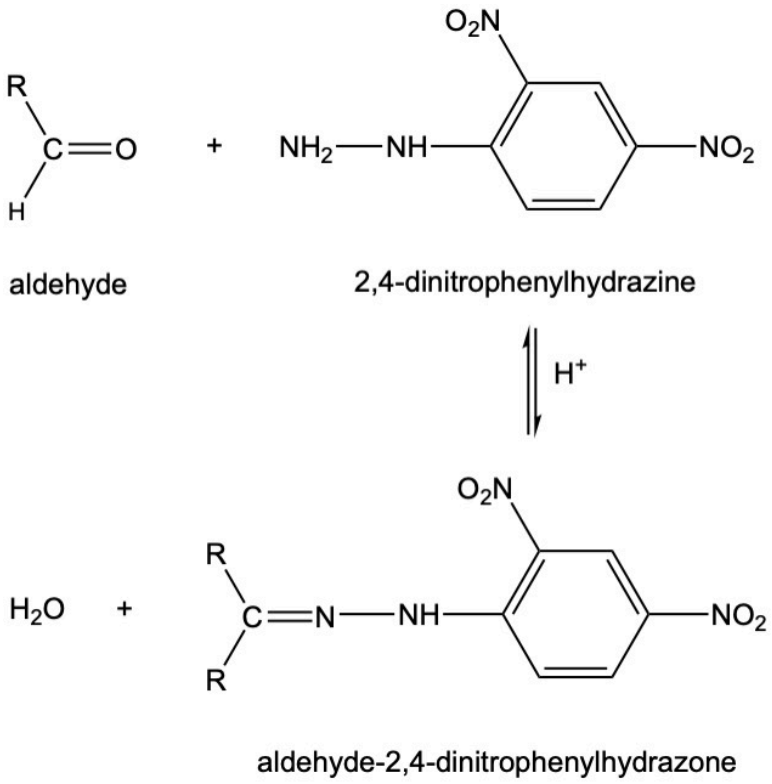

Figure 1.9: **Generic Derivatisation Reaction of DNPH with Aldehyde** DNPH reacts readily with carbonyl groups in aldehydes to generate hydrazone derivatives that have increased stability, are ionised more efficiently and have altered fragmentation characteristics making the compounds more amenable to analysis than non-derivatised aldehydes.

Figure 1.10: **Derivatisation of Aldehydes with DNPH**

Reaction of DNPH with aldehydes generates formaldehyde-, acetaldehyde- and propionaldehyde-specific hydrazone derivatives.

Table 1.4: Effect of Aldehyde Derivatisation on the Molecular Weight and Volatility of Aldehydes

	aldehyde	molecular mass	boiling point (°C)
	formaldehyde	30.03	-19
	acetaldehyde	44.05	20.2
	propionaldehyde	58.08	46
derivatised	formaldehyde-2,4-DNPH	210.2	357.8
derivatised	acetaldehyde-2,4-DNPH	224.2	382.5
derivatised	propionaldehyde-2,4-DNPH	238.2	391.7

1.6 Thesis Outline and Aims

There is ever-increasing evidence to show that ALDH enzymes are important in physiology and pathophysiology, especially as markers of cell populations. The importance and role of the major ALDH substrates and ALDH reaction products in relaying these biological effects is less understood. Understanding ALDH as a target of 5-nitrofuran prodrugs has relevance to current treatment strategies and the imminent application of nitrofurans as anticancer agents.

This thesis comprises three key research aims that span three chapters. Aims are as follows:

1. Understand whether the ALDH:5-NFN enzyme-drug interaction is relevant in mammalian systems and downstream effects of the interaction, focusing on the liver as the main site of nitrofuran metabolism and acetaldehyde detoxification.

2. Develop an aldehyde derivatisation approach suitable for LC-MS-detection to enable detection of multiple aldehydes in blood plasma.

3. Investigate transcriptional differences in $ALDH^{high}$, $ALDH^{low}$ and $ALDH^{null}$ populations in melanoma to determine whether ALDH1A3-expressing cells exhibit a differential gene expression that contributes to the tumour-resistant capacity of $ALDH^{high}$ populations.

Chapter 2

Materials and Methods

This chapter describes the general methods, reagents and instruments used to perform experiments performed in this thesis. Experimental methods relating to chromatographic and mass spectrometry analyses are detailed in Chapter 4.

2.1 Cell and Tissue Culture

2.1.1 Cell Line Maintenance and Culture Conditions

All cell culture work was performed in a laminar flow hood under aseptic conditions. Human hepatoma (HepG2) and human melanoma (A375) cell lines (Figure 2.1) were obtained from ECACC collections (ECACC 85011430, ECACC 88113005). All cell line experiments were performed on cells at passage 5 to 15. Cell lines were screened every three months for mycoplasma contamination. Cells were grown to confluence in growth medium; DMEM; L-Glutamine, 2 mM ; FBS, 10% (*v/v*). Cells were incubated at 37°C in a 5% CO_2 humidified atmosphere (Heraeus HERAcell 51013669 CO_2 incubator). Cell monolayers during growth phase or at 80% confluency were washed with phosphate buffered saline (PBS) and cells detached using 0.5% or 0.25% Trypsin-EDTA for A375 and HepG2 cells, respectively. Following detachment, trypsin was inactivated by addition of growth medium and cells were pelleted in 30 mL conical tubes by centrifugation at 1000 rpm for 5 min with a Eppendorf™ 5810 R centrifuge. Following pelleting, cells were gently resuspended in growth medium by pipetting. To minimise HepG2 cell clumping, cell suspension was passed through a 25 gauge needle attached to a 10 mL syringe. Cells were re-plated at split ratios appropriate to each cell line, 1:4 (HepG2) and 1:6 (A375) or were seeded into plate wells for experimental analysis.

For cryopreservation, cells in growth phase were trypsinised and pelleted as above and the resulting cell pellet cryopreserved in freezing medium; Ham's F-10 48% (*v/v*); tryptose phosphate broth (TPB), 40% (*v/v*); DMSO, 12% (*v/v*). Cryotubes were placed in Mr. Frosty™ freezing containers that were pre-equilibrated to -80°C before long-term cryostorage. For cell recovery, cryotube contents were rapidly thawed by immersion in a water bath at 37°C. Cells were resuspended in 10 mL pre-warmed growth medium and centrifuged at 1000 rpm before resuspension of the pellet and plating in fresh media. Cells were passaged at least three times after recovery before experimentation.

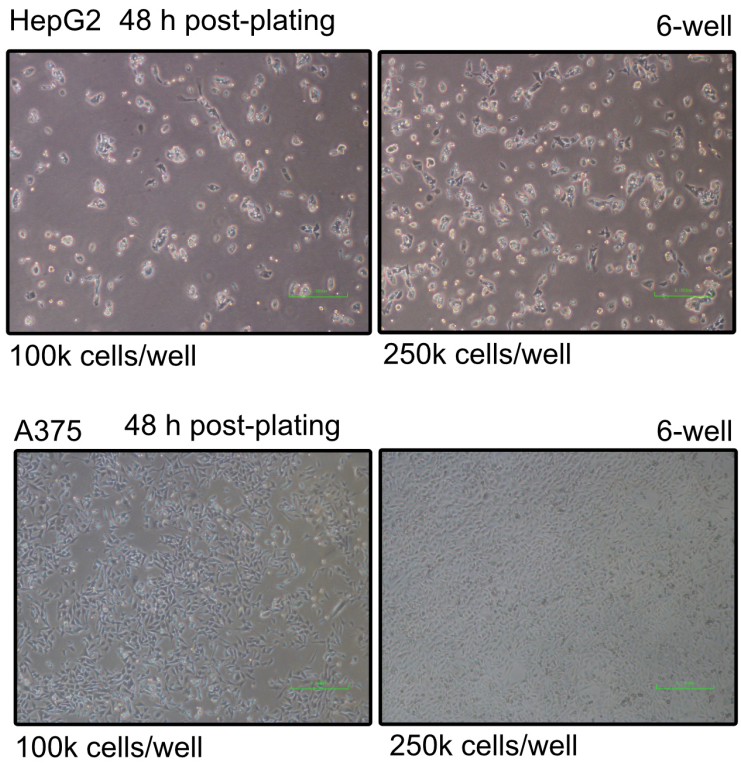

Figure 2.1: **Cell Line Morphology**

Human hepatoma (HepG2) and human melanoma (A375) cell lines obtained from ECACC collections (ECACC 85011430, ECACC 88113005).

Table 2.1: Cell Lines

Cell Line	*Source*	*Cat No*
HepG2, Human Hepatoma	ECACC	85011430
A375, Human Melanoma	ECACC	88113005
A375-Cas9	Sarvi et al. (2018)	-
A375-ALDH1A3^{C21}	Sarvi et al. (2018)	-

Table 2.2: Tissue Culture Media and Additives

Media and Additives	*Supplier*	*Cat No*
Dulbecco's Modified Eagle's Medium (DMEM)	Thermo Fisher Scientific	21969035
Gibco™ Heat-Inactivated Foetal Bovine Serum (FBS)	Thermo Fisher Scientific	11550356
Gibco™ GlutaMAX™Supplement (100X)	Thermo Fisher Scientific	35050-061
L-Glutamine (200 mM, 100X)	Thermo Fisher Scientific	25030081
Trypsin-EDTA (0.25%), phenol red	Thermo Fisher Scientific	25200056
Trypsin-EDTA (0.05%), phenol red	Thermo Fisher Scientific	25300054
Penicillin-Streptomycin (10,000 U/mL, 100X)	Thermo Fisher Scientific	15140122

Table 2.3: Cell and Tissue Culture Materials

Materials	*Supplier*	*Cat No*
Corning™ Costar™ 6-well plate, 96-well plate	Fisher Scientific	10578911, 10695951
Greiner CELLSTAR® 24-well plate	Sigma	M8562
Greiner CELLSTAR® T-25, T-75, T-175 flasks	Greiner Bio-One	690175, 658175, 660175
Single-edged blade	Fisher Scientific	1244-3170
Corning™ TC-Treated culture dish	Fisher Scientific	430167, 10075371
B. Braun Sterican 25 gauge needle	VWR	612-0153
Corning® cell strainer, 40 μm, 70 μm	Sigma	CLS431750, CLS431751
Falcon 50 mL Conical Centrifuge Tubes	Fisher Scientific	10788561
Greiner 30 mL Conical Tube	Greiner Bio-One	201150
Gibco™ Hank's Balanced Salt Solution (HBSS), 10X	Thermo Fisher Scientific	14065056
Lonza MycoAlert™ PLUS Mycoplasma Detection Kit	VWR	LT07-701
Corning® Costar® Stripette® serological pipette, 5 - 25 mL	Sigma-Aldrich	CLS4487-CLS4489

Table 2.4: Cryopreservation Materials

Materials	*Supplier*	*Cat No*
Gibco™ Ham's F-10 Nutrient Mix	Thermo Fisher Scientific	31550015
Dimethyl sulfoxide (DMSO) Hybri-Max™ ≥ 99.7%	Sigma-Aldrich	D2650
Tryptose Phosphate Broth solution (TPB)	Sigma-Aldrich	T8159
Thermo Scientific™ Nunc™ Cryogenic Tubes	Fisher Scientific	10577391
Mr. Frosty™ Freezing Container	Thermo Scientific	5100-0001

2.2 Cell Viability and Cytotoxicity

2.2.1 Growth Curves

To identify the optimal number of cells to plate for analysis of cell growth in the presence of small molecules and aldehydes, growth curve analysis was performed over seven days. Cells were resuspended in fresh growth medium and seeded in 96-well plates in a half-log dilution series ranging from 100,000 cells/well to 0 cells/well in 100 μL of media. Following incubation at 37°C and 5% CO_2 in a humidified atmosphere, cell growth was analysed every 24 h by PrestoBlue® assay.

2.2.2 Cell Viability and Cytotoxicity

Following trypsinisation, cells were resuspended in fresh growth medium and 1000 cells were plated/well of 96-well cell culture plates. Following overnight incubation, media was aspirated and 100 μL of fresh growth media containing half-log serial dilutions of desired compound (10 μM – 1 nM) or DMSO control (0.1%) was pipetted into each well via multichannel pipette. Cells were incubated at 37°C and 5% CO_2 in a humidified atmosphere for the treatment exposure period.

For acetaldehyde and NFN1 treatment of HepG2 cells, after overnight incubation of seeded cells, fresh growth media was supplemented with acetaldehyde at 10 mM, 5 mM, 2.5 mM and 0 mM concentrations and 95 μL/well supplemented growth media was added to the wells of each plate, with one plate per acetaldehyde condition. Five microliters of DMSO control or desired compound (NFN1) was added in half-log dilution series to the wells of each plate. Nitrofuran and acetaldehyde conditions were replenished daily by removal of media and addition of freshly-prepared NFN1, acetaldehyde

and DMSO control to cells. Cells were incubated at 37°C and 5% CO_2 in a humidified atmosphere for the treatment exposure period.

2.2.3 PrestoBlue® Assay

PrestoBlue® is a resazurin-based cell permeable redox indicator that is reduced in living cells to indicate viability. In living cells, PrestoBlue® is converted from its oxidised state (resazurin, blue) to its reduced form (resorufin, red). The reduced form absorbs at 570 nm and is highly fluorescent (λ_{ex} 535 nm, λ_{em} 612 nm). PrestoBlue® reagent, 10 μL was added to 100 μL of media in each well of the 96-well plate containing cells or blank wells. Cells were incubated with reagent for 30 min at 37°C and 5% CO_2 humidified atmosphere before measuring fluorescence (λ_{ex} 535 nm, λ_{em} 612 nm) using the automated 96-well plate reader Infinite® M200 PRO (Tecan, Switzerland) (Table 2.5).

Table 2.5: Fluorometer Settings for Analysis of the PrestoBlue Assay

Measurement Parameter	***Infinite® M200 Pro Settings***
Plates	Corning™ Costar™ 96 Flat Bottom
Shaking (prior to read)	Time: 20 s
	Amplitude: 1 mm
	Frequency: 432 rpm
	Mode: orbital
Mode	Top (T) / Bottom (B)
z-position (top fluorescence)	calculated from sample well
Excitation wavelength (λ_{ex})	560 nm
Emission wavelength (λ_{em})	600 nm
Gain	Optimal
Number of flashes	25
Settle time	0 ms
Lag time	0 μs
Integration time	20 μs
Reads per well	1

2.2.4 PrestoBlue® Quantification

All plate readings were performed using the Infinite® M200 PRO (Tecan, Switzerland). Data was exported with Magellan™ software (Tecan, Switzerland) and analysed in Prism 7 (GraphPad). The average value for each sample was calculated and corrected by subtracting the average blank. Fluorescence values (PrestoBlue®) were plotted against cell number to visualise cell growth curves. For cell viability curves, concentration of drug was plotted against fluorescence values and sigmoidal dose curves generated using Prism 7 (GraphPad). The average for each dilution was calculated (from six wells) and corrected by subtracting the average blank. This value was then related to the average of untreated control samples and the respective error bars were calculated. The mean half-maximal effective concentration (EC50) was used as an indicator of cytotoxicity to compare treatment conditions. Values represent the average mean of at least 3 experimental repeats and error bars represent the standard error of the mean (SEM).

2.2.5 Synergy vs Antagonism Modelling

To quantify synergistic or antagonistic effects of compound exposure, model-based quantification of drug combinations was performed with Combenefit (v2.02) (Di Veroli et al., 2016). Fluorescent intensity from PrestoBlue®-turnover was normalised to percentage cell viability, with DMSO control deemed to confer 100% cell viability. Dose-response (%) matrices for NFN1 and acetaldehyde single and combined exposure were generated and visualised with surface modelling. Synergy matrices were generated using the three most common models; highest single agent (HSA) model, Loewe additivity model and Bliss independence model. BLISS, HSA and LOEWE models were mapped to dose-response for graphical visualisation.

Table 2.6: Cell Viability and Cytotoxicity

Reagent	*Supplier*	*Cat No*
PrestoBlue™Cell Viability Reagent	Invitrogen	A13262
Invitrogen™Trypan blue stain (0.4%)	Fisher Scientific	10702404

Table 2.7: Reagents For Cell Treatments

Reagent	*Supplier*	*Cat No*
5-Nitrofurans		
Nifurtimox ≥98%	Sigma-Aldrich	N3415
Nifuroxazide ≥97%	EMD Millipore	481984
NFN1	Maybridge	BTB05727SC
Aldehyde		
Supelco™ Acetaldehyde ≥99.0%	Sigma-Aldrich	00071
Vehicle		
Dimethyl sulfoxide (DMSO) ≥ 99.7%	Sigma-Aldrich	D2650

2.3 Precision-Cut Liver Slices

2.3.1 PCLS Preparation

2.3.1.1 Liver Dissection

Six-to-eight week C57BL/6 mice were euthanised through CO_2 inhalation and livers were harvested rapidly to prevent ischaemic damage. Livers were perfused by administration of ice-cold PBS through the inferior vena cava and were dissected using scissors and forceps. Livers were stored on ice in HBSS before transfer to a cell culture dish containing ice-cold HBSS. Liver lobes were separated into lobular structures (Figure 2.2) using a single-edged blade and forceps.

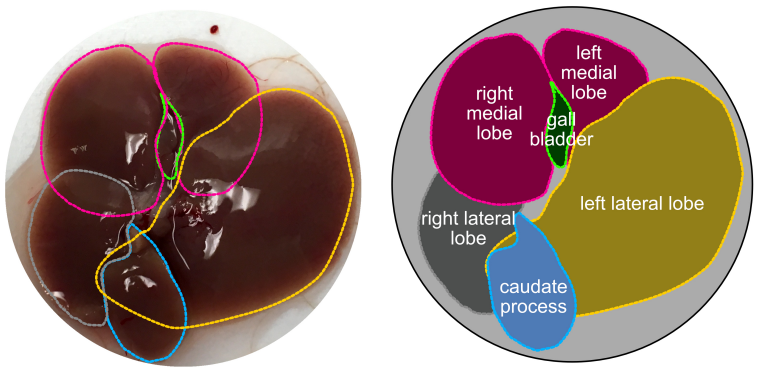

Figure 2.2: **Annotation of Liver Lobes Used for Preparation of PCLS** Liver tissue samples were prepared from the left lateral lobe (yellow dashed line) of 6-8 week C57BL/6 mice.

2.3.1.2 Liver Coring

A single liver lobe was transferred onto a dissection/coring board wetted with HBSS. The liver was cut into square fragments, maintaining the thicker, more central parts of the liver lobe that yield more intact, round liver slices. Fragmented liver tissue was placed under the tissue coring press (MD2000/2300, Alabama Research and Development) and as many cylindrical cores were obtained from large lobes as possible ($\approx$ 2 cores) and small lobes ($\approx$ 1 core). After each liver lobe was cored, cores were transferred using a stainless steel spatula to cell culture dishes containing ice-cold HBSS for a maximum of 20 min.

2.3.1.3 Liver Sectioning

The Krumdieck tissue slicer (TSE Systems) reservoir was filled with HBSS and the whole unit was pre-chilled in a cold room. Liver cores were individually transferred to the cylindrical core holder of the Krumdieck slicer and sectioned into PCLS of 200 μM thickness. Slices were transferred to a 2 L glass beaker by flushing through the system after the slicing of each individual core. After each core was sectioned and whilst the following core was being sectioned, liver slices were transferred with a stainless steel spatula to pre-warmed and oxygenated 24-well plates labelled with the type of lobe and sequential number of each section. Each well contained 1 mL supplemented DMEM; GlutaMAX™, 1X; FBS, 10% (*v/v*); penicillin-streptomycin 1% (*v/v*). Slices were pre-incubated for 3 h at 37°C, 5% CO_2 to increase viability of sections. Livers from 8-10 week mouse primary liver lobes generated enough material to prepare 20 slices. It has been previously reported that each liver slice remains viable for up to 96 h (de Graaf et al., 2010).

2.3.2 PCLS Drug Treatment

After pre-incubation, sections were transferred into 6 well plates containing 3 mL of supplemented DMEM; 1X GlutaMAX™; FBS 10%(*v/v*); penicillin-streptomycin 1% (*v/v*), containing the appropriate concentration of NFN1. Serial dilutions of NFN1 in media were prepared to give concentrations ranging from 0 μM - 10 μM (0.1% DMSO). Dilutions prepared in falcon tubes and then transferred to wells of 6-well plates. Liver sections were incubated for 20 h at 37°C in NFN1 or control vehicle (0.1% DMSO) before protein extraction and ALDH activity analysis.

2.4 Protein Extraction and Analysis

2.4.1 Protein Extraction and Quantification

2.4.1.1 Cell Lysate

To prepare cell lysates, growth media was removed from cells and cells were washed with ice-cold PBS. RIPA buffer, 50 - 500 μL containing protease and phosphatase inhibitors was added directly to the flask surface to lyse the cell monolayer. Plates or flasks were then incubated on ice for 30 min to promote cell lysis before scraping of lysate into pre-chilled 1.5 mL Eppendorf® tubes. Cell lysates were centrifuged at 13000 rpm for 2 min and the supernatant recovered into fresh 1.5 mL tubes. Cell lysates were either used immediately in downstream analyses or were snap-frozen using liquid nitrogen and stored at -80°C.

2.4.1.2 Tissue Lysate

For the preparation of PCLS lysates, growth media was removed from slices and slices were washed twice with ice-cold PBS. Each slice was transferred to a 2 mL microcentrifuge tube on ice and weighed before addition of 1 mL of ice-cold tissue homogenisation solution (100 mM Tris-HCl, 2 mM EDTA, pH 7.6) supplemented with protease and phosphatase inhibitor tablets. Tissues were homogenised using a single 3 mm Tungsten Carbide Bead per tube and a pre-cooled TissueLyser LT (Qiagen) for 6 min at a speed of 50 Hz (3000 oscillations/min). Tissue lysates were spun at 12000 rpm for 10 min before supernatant was removed and stored on ice ready for analysis. ALDH activity was measured immediately after harvesting of tissues, or supernatants were snap-frozen on liquid nitrogen and stored at -80°C before western blotting.

2.4.1.3 Protein Quantification

Protein concentration of cell and tissue lysate was determined using bicinchoninic acid (BCA) in 96-well plate format according to manufacturer protocol. Protein standards were generated by dilution of 2 mg/mL BSA in RIPA lysis buffer to yield 2000, 1500, 1000, 750, 500, 250, 125, 25, 0 μg/mL BSA standards. BCA working reagent was prepared in 50 mL conical tube with 50 mL of BCA reagent A added to 1 mL reagent B. If samples contained high protein concentrations, a small volume of sample was diluted in RIPA buffer prior to analysis. Twenty-five microliters of each standard or unknown sample was pipetted into the wells of a 96-well plate in triplicate. Two-hundred microlitres of working reagent was added to each well and the plate incubated at 37°C for 30 min. Optical density (OD) was measured using the automated 96-well plate reader Infinite® M200 PRO (Tecan, Switzerland) at a wavelength of 562 nm. OD values were converted to protein concentration through BSA standard curve interpolation using Prism 7 (GraphPad). If samples were pre-diluted, the protein concentrations were adjusted by the dilution factor.

Table 2.8: Protein Extraction and Quantification

Reagent	*Supplier*	*Cat No*
RIPA Buffer	SLS	Sigma-R0278
cOmplete™ ULTRA Protease Inhibitor	Roche	5892970001
PhosSTOP™	Roche	4906845001
Cell Scraper, 28 cm	Greiner Bio-One	541070
Gibco™ HEPES (1M)	Thermo Fisher	15630080
Tungsten Carbide Beads, 3 mm	QIAGEN	69997
Pierce™ BCA Protein Assay Kit	Thermo Scientific	23225
Corning™ Costar™ 96-well plate	Fisher Scientific	10695951
Pierce™ Bovine Serum Albumin	Thermo Scientific	23210
Microcentrifuge Tubes, 2 mL	Thermo Scientific	11838332

2.4.2 Protein Separation and Western Blotting

Twenty micrograms of protein per sample was added to sample buffer; sodium dodecyl sulfate-polyacrylamide gel electrophoresis (SDS-PAGE) sample loading buffer (6X) with 2-mercaptoethanol. Samples were totalled to a volume of 40 μL per well with radioimmunoprecipitation assay (RIPA) buffer. Samples were denatured by incubating at 95°C for 5 min. Samples were spun in a benchtop centrifuge to minimise loss of evaporated sample before loading alongside 5 μL of PageRuler™ prestained protein ladder onto Mini-PROTEAN TGX SDS-polyacrylamide precast gel. Proteins were separated by electrophoresis at 100 V in Tris-glycine running buffer; 25 mM Tris-Cl; 192 mM Glycine; 0.1% SDS, pH 8.3. Proteins were separated until the dye front reached the bottom of the gel. Mini-PROTEAN® tetra vertical electrophoresis cell (Bio-Rad) tank was used with an ice block to maintain temperature.

Separated proteins were transferred by western blotting to nitrocellulose membrane using the Trans-Blot Turbo Transfer System on TURBO mode (1704150, Bio-Rad). Transferred membranes were blocked in 5% (*w/v*) BSA in PBS-TWEEN®20, 0.1% (*v/v*) (PBS-T) for 1 h to minimise non-specific antibody binding. Blocked membranes were transferred to 50 mL tubes containing primary antibody diluted in 5% BSA in PBS-T (Table 2.10) and incubated overnight at 4°C. After incubation, membranes were washed with PBS-T, three times for 5 min each. Membranes were incubated in the appropriate fluorescent secondary antibody diluted in 5% BSA in PBS-T (Table 2.10) in conical tubes, protected from light, for 1 h, RT. Unbound secondary antibody was removed with three, 5 min washes in PBS-T. Specific bands were detected using the Odyssey® CLx Imaging System and Image Studio™ software.

Table 2.9: SDS-PAGE and Western Blotting

Reagent	*Supplier*	*Cat No*
Tris base	Fisher Scientific	AC167620010
Glycine	Sigma-Aldrich	G8898
SDS-PAGE Sample Loading Buffer (6X)	G-Biosciences	786-701
2-Mercaptoethanol	Sigma Aldrich	M6250
Mini-PROTEAN® TGX™ Gel, 4-15%	Bio-Rad	4561084
PageRuler™ Prestained Protein Ladder	Thermo Scientific	26616
Sodium Dodecyl Sulfate	Millipore	7910-OP
Trans-Blot® Turbo™ Midi Nitrocellulose	Bio-Rad	1704159
Bovine serum albumin (BSA)	Fisher	BP1605-100
TWEEN® 20	Sigma-Aldrich	P9416

All buffers were prepared at room temperature on a magnetic stirrer.

Table 2.10: Antibodies for Western Blotting

antibody (species)	*band (kDa)*	*concentration*	*supplier*	*cat. no*
Primary				
ALDH1B1 (rabbit)	55	1:1000	Proteintech	15560-1-AP
ALDH2 (rabbit)	56	1:1000	Boster	PB9472
ALDH2 (rabbit)	56	1:1000	abcam	EPR4493
GAPDH (D4C6R) (mouse)	37	1:10000	cell signalling tech	97166
Secondary				
IRDye®800CW anti-Rabbit IgG H&L (donkey)	-	1:10000	LI-COR®	926-32212
IRDye®680RD anti-Mouse IgG H&L (donkey)	-	1:10000	LI-COR®	926-68072

2.5 *In vitro* ALDH Activity Analysis

2.5.1 Recombinant ALDH1B1 Expression and Purification

His-tagged ALDH1B1 recombinant enzyme was expressed and purified by Dr Zhiping Feng, James Chen laboratory, Stanford University.

Expression

Plasmid containing the DNA sequence encoding ALDH1B1 (pET15b-ALDH1B1) was transformed into TunerDE3 chemically competent cells according to the manufacturer protocol. Single colonies were used to inoculate 5 mL lysogeny broth (LB) supplemented with Ampicillin (100 μg/mL) and Spectinomycin (50 μg/mL). Cells were grown at 37°C, overnight. Cultures were transferred to 1 L of LB and once culture OD_{600} = 0.6, cultures were induced with Isopropyl-β-D-thiogalactoside (IPTG) (0.5 mM final concentration) and grown at 16°C overnight. Cultures, 250 mL/tube were pelleted by centrifugation at 5000 rpm, 25 min, 4°C. Cultures were stored at -20°C for $\approx$ 1 h.

Purification

Cells were lysed with BugBuster Master Mix, 10 mL containing cOmplete™ ULTRA Protease Inhibitor. Cultures were rocked at RT for ≈ 20 min. Lysed samples were spun down at 16000 x *g* at 4°C for 25 min. The soluble fraction was retained and 2 mL of nickel-nitrilotriacetic acid (Ni-NTA) superflow agarose resin was added. The resin and soluble fraction were incubated in 50 mL conical tube at 4°C for ≈ 1 h. The mixture was flowed through the column for the resin to settle. Beads were washed with 40 mL buffer B1, followed by buffer W1. Bound protein was eluted with 500 μL of buffer E1. Glycerol, 500 μL was added to each 500 μL fraction. Purified recombinant protein was stored at -80°C in 1:1 (*v/v*) glycerol and E1.

Binding buffer (B1): 500 mM sodium chloride, 20 mM sodium phosphate, 1 mM dithiothreitol, 20 mM imidazole, 5% glycerol, pH 7.4.

Wash buffer (W1): 500 mM sodium chloride, 20 mM sodium phosphate, 1 mM dithiothreitol, 40 mM imidazole, 5% glycerol, pH 7.4.

Elution buffer (E1): 500 mM sodium chloride, 20 mM sodium phosphate, 1 mM dithiothreitol, 400 mM imidazole, 5% glycerol, pH 7.4.

2.5.2 Recombinant ALDH2 Expression and Purification

His-tagged ALDH2 recombinant enzyme was expressed and purified by Dr Matt Nowicki, Edinburgh Protein Production Facility, Edinburgh University.

Expression Plasmid containing the DNA sequence encoding ALDH2 (pET3a) was transformed into C41 chemically competent cells according to the manufacturer protocol. Single colonies were used to inoculate 2 mL LB supplemented with Carbenicillin (100 μg/mL). Cultures were incubated at 37°C, 250 rpm for 7 h. Starter culture, 0.5 mL was incubated in pre-warmed EnPresso® B media (2 media tablets, 25 μL Reagent A, 100 μg/mL carbenicillin). Cultures were incubated overnight at 30°C, 250 rpm. Following incubation, expression was induced by adding 1 mM IPTG and the media was supplemented with 1 booster tablet and 25 μL Reagent A. Cultures remained incubating at 30°C, 250 rpm for 24 h. Cells were harvested by centrifugation at 4000 x *g* and the resultant pellets were flash frozen in liquid nitrogen and stored at -80°C.

Purification Cells were resuspended in lysis buffer (W2), 30 mL containing cOmplete™ ULTRA Protease Inhibitor and 10 mg/mL DNase 1 (15 μL). Cells were lysed by mechanical lysis (25 kPsi, Constant Systems cell disruptor). Lysed samples were spun down at 25000 x *g* at 4°C for 45 min. The soluble fraction was filtered (0.2 μm) and loaded onto a HiTrap SP FF (1 mL, pre-equilibrated in W1 buffer) at a flow rate of 1 mL/min. The column was washed with 20 column volumes (CV) of W2 buffer. Bound protein was eluted through an E2 gradient; 6% E2, for 5 CV; 9% E2 for 10 CV; 9–26% for 10 CV; 26% E2 for 5 CV; 26–100% for 10 CV. Fractions associated with the ALDH2 were pooled and concentrated to 150 μL using a spin concentrator (30 kDa cut-off). ALDH2 was further purified by gel filtration using a superdex200 10/300 column and buffer E2. ALDH2 eluted as a single peak with a retention volume of 12.1 mL. The fractions containing ALDH2 (as analysed by SDS-PAGE) were pooled to give a final concentration of 0.37 mg/mL (3 mL). Purity was calculated to be >95% by analytical gel filtration and SDS-PAGE density analysis.

Lysis and Wash buffer (W2): 100 mM sodium acetate, pH 5.0; 50 mM sodium chloride.

Elution buffer (E2): 100 mM sodium acetate, pH 5.0; 1 M sodium chloride.

Gel filtration/enzyme buffer (F1): 20 mM HEPES, pH 7.5; 100 mM sodium chloride; 1 mM dithiothreitol.

2.5.3 ALDH Activity

2.5.3.1 Dehydrogenase

Purified His-tagged ALDH1B1 was diluted from glycerol stock to 25 μg/mL in 100 mM sodium phosphate buffer. 0.5 μg of ALDH1B1 (20 μL volume) was added per well followed by pre-incubation with 20 μL 2-mercaptoethanol (5 mM) for 2 min. 5 mM NAD^+, 1 mM $MgCl_2$ in 100 mM sodium phosphate buffer (20 μL) was added to the enzyme reaction and pre-incubated for 20 min. 5-nitrofurans or control compounds (daidzin, disulfiram) were diluted in DMSO and 20 μL added to the enzyme reaction. Drugs were preincubated for 10 min. NADH standard curve was generated and background absorbance was recorded at Ex/Em 340/460 nm. Acetaldehyde (5 mM, 20 μL) was used to initiate the dehydrogenase reaction and NADH generated was recorded by fluorescence emitted at Ex/Em 340/460 nm in kinetic mode for 30 min. Daidzin and disulfiram (10 μM) were used as positive controls for ALDH inhibition.

Table 2.11: UV-Vis Settings for Analysis of Dehydrogenase Assay

Measurement Parameter	***Infinite® M200 Pro Settings***
Plates	Corning™ Costar™ 96 Flat Bottom
Shaking (prior to read)	Time: 20 s
	Amplitude: 1 mm
	Frequency: 432 rpm
	Mode: orbital
Mode	Top (T) / Bottom (B)
z-position (top fluorescence)	calculated from sample well
Excitation wavelength (λ_{ex})	340 nm
Emission wavelength (λ_{em})	460 nm
Gain	Determined by well containing 1 nmol NADH
Number of flashes	1
Settle time	0 ms
Lag time	0 μs
Integration time	20 μs
Reads per well	1

Table 2.12: ALDH Dehydrogenase Activity Analysis

Reagent	*Supplier*	*Cat No*
Corning® white 96 well plate	Sigma-Aldrich	CLS3922
Acetaldehyde ACS reagent, ≥99.5%	Sigma-Aldrich	402788
β-Nicotinamide adenine dinucleotide sodium salt, NAD^+≥95%	Sigma-Aldrich	N0632
NADH disodium salt trihydrate, ≥95%	abcam	ab146315
Sodium phosphate monobasic, ≥99.9%	Sigma-Aldrich	S0751
Sodium phosphate dibasic, ≥99.0%	Sigma-Aldrich	71640
Magnesium chloride hexahydrate, ≥99.0%	Sigma-Aldrich	M2670
Daidzin ≥98%	Cambridge Bioscience	CAY13202
Supelco™ Disulfiram	Sigma-Aldrich	PHR1690
Dimethyl sulfoxide (DMSO) Hybri-Max™ ≥ 99.7%	Sigma-Aldrich	D2650
Nifurtimox ≥98%	Sigma-Aldrich	N3415
Nifuroxazide ≥97%	EMD Millipore	481984
NFN1	Maybridge	BTB05727SC

2.5.3.2 Esterase

Purified recombinant ALDH2 was diluted in HEPES buffer (60 nM/well) and preincubated with 0.5 mM or 0.05 mM NAD^+ in HEPES. 5-NFNs were incubated with the enzyme for 20 min with shaking prior to reaction initiation. 4-Nitrophenol (4-NP) was serially diluted into wells of the reaction plate to generate a 4-NP standard curve. 4-Nitrophenylacetate (4-NPA) was prepared (4 mM in 6% (*v/v*) DMSO) and was added to substrate wells at a final concentration of $\approx$ 1 mM. Formation of 4-NP was monitored by measuring absorbance at 405 nm. All experiments were performed in triplicate with 60 nM recombinant human ALDH2. All reactions were performed in a white 96-well plate with 50 μL final reaction volume. Absorbance was measured at λ = 405 nm using the automated 96-well plate reader Infinite® M200 PRO (Tecan, Switzerland) (Table 2.13). Enzymatic rates were determined using the initial linear change of absorbance and all data analysed using Prism 7 (GraphPad).

Table 2.13: Fluorometer Settings for Analysis of Esterase Activity

Measurement Parameter	***Infinite® M200 Pro Settings***
Plates	Corning™ Costar™ 96 White Flat Bottom
Shaking (prior to read)	Time: 10 s
	Amplitude: 1 mm
	Frequency: 432 rpm
	Mode: orbital
Absorbance	405 nm
Number of reads	25 ms
Settle time	0 ms

Table 2.14: ALDH Esterase Activity Analysis

Reagent	*Supplier*	*Cat No*
4-Nitrophenol, ≥99%	Fisher Scientific	AC157051000
4-Nitrophenyl acetate, ≥98%	Alfa Aesar	L00314
Corning® white 96 well plate	Sigma-Aldrich	CLS3922
Recombinant human ALDH2 protein (active)	abcam	ab87415
β-Nicotinamide adenine dinucleotide, NAD^+≥95%	Sigma-Aldrich	N0632

2.6 ALDH Assays on Liver Tissue

2.6.1 Dehydrogenase

PicoProbe™ analysis of ALDH activity was performed on freshly extracted protein from liver or PCLS in Tris-Cl buffer. The assay was performed according to manufacturer protocol, with the exception that Tris-Cl buffer was used instead of the kit assay buffer. Briefly, NADH standard curve was prepared. Protein extracts from fresh liver were pre-incubated in wells alongside substrate mix and small molecules (NFN1, NAZ, NFX) diluted in DMSO. PCLS protein extracts were aliquotted into corresponding wells before addition of PicoProbe™ in Tris-Cl buffer. Background control readings, containing no addition of acetaldehyde were prepared. The dehydrogenase reaction was initiated with acetaldehyde. For quantitation of ALDH activity, fluorescence was recorded at Ex/Em 535/587 nm for 0 - 60 min. For analysis, background readings were subtracted from sample readings and NADH generated during the reaction time was interpolated from the NADH standard curve.

Table 2.15: PicoProbe™ ALDH Activity Analysis

Reagent	*Supplier*	*Cat No*
PicoProbe™	BioVision	K741-100
Corning™ 96-Well Black Polystyrene Microplate	Sigma-Aldrich	CLS3603

2.7 ALDEFLUOR™ Staining and Flow Cytometry

A375 cells were seeded at a density of 250,000 cells per T175 flask. Cells were harvested during growth phase. ALDEFLUOR™ assay was performed according to the manufacturer protocol. Cells were harvested by trypsinisation as described above. Cell number was determined using a haemocytometer and staining non-viable cells with trypan blue; 10 μL of cell suspension was added to 10 μL Trypan blue stain and 10 μL was loaded into each chamber of the haemocytometer. Thirty million A375-Cas9 cells were incubated with fluorescent Bodipy™-aminoacetaldehyde diethyl acetal (BAAA-DA) reagent for 30 min at 37°C. To negatively control for FACS-analysis, cellular ALDH activity was blocked with diethylamino-benzaldehyde (DEAB) and an unstained sample of trypsinised cells was treated in parallel to the ALDEFLUOR™ and DEAB-treated samples. ALDEFLUOR™-stained cells were sorted using the BD FACSAria™ II (BD Biosciences). The top 5% and bottom 5% of ALDEFLUOR™-stained cells were sorted by fluorescence-activated cell sorting (FACS) into two populations and cells were collected into DMEM containing 2% (*v/v*) FBS in conical tubes on ice. ALDEFLUOR™ was detected on 488 nm excitation and 525/50 nm BP filter for detection. Dead cells were excluded using 12 μM propidium iodide solution or 3 μM 4′,6-Diamidine-2′-phenylindole dihydrochloride (DAPI). Data were analyzed using FlowJo software. For measurement of ALDEFLUOR™ staining of A375-ALDH1A3^{C21} cells, A375-ALDH1A3^{C21} and A375-Cas9 cells were treated with ALDEFLUOR™ (and DEAB inhibitor/unstained control) as above and quantitated using the BD LSRFortessa™ (BD Biosciences).

Table 2.16: FACS ALDEFLUOR™ Analysis

Reagent	*Supplier*	*Cat No*
ALDEFLUOR™ kit	STEMCELL™ Technologies	01700
DAPI, 1 mg/mL	MBD0015	Sigma-Aldrich
Propidium iodide solution	Sigma-Aldrich	P4864

2.8 RNA Extraction

Ribonucleic acids were purified from cell lines through phenol-chloroform extraction according to the TRIzol™ manufacturer protocol. Briefly, FACS-sorted cells were pelleted by centrifugation at 1000 rpm and the cell pellet was resuspended in 0.75 mL of TRIzol™ per 5 million cells. Alternatively, adherent monolayers of cells were directly lysed, after removal of media, by addition of TRIzol™ to the culture flask. Cells were incubated with TRIzol™ for 5 min to dissociate and solubilise nucleoproteins. Lysate was transfered to LoBind tubes and homogenised by pipetting. Chloroform, 200 μL per 1 mL TRIzol™ was added to lysates to promote phase separation. Samples were then bench vortexed, incubated for 5 min and centrifuged for 15 min at 12,000 x *g*, 4°C. The resulting aqueous phase was collected and RNA precipitated from the aqueous phase with addition of isopropanol and incubation for 10 min. Precipitated RNA was collected by centrifugation for 10 min at 13,000 x *g*, 4°C. The resulting RNA pellet was washed by re-suspension in 75%ethanol, homogenised by bench vortex and centrifuged at 13,000 x *g*, 4°C. The RNA pellet was air-dried and was resuspended in 50 μL RNase-Free water.

Table 2.17: RNA Extraction

Reagent	*Supplier*	*Cat No*
TRIzol™	Invitrogen™	15596018
Chloroform	Fisher Scientific	10071970
Isopropanol	Fisher Scientific	10215390
RNeasy MinElute Cleanup Kit	Qiagen	74204
DNA LowBind Micro tube, 2 mL	SARSTEDT	72.695.700
RNasin® Ribonuclease Inhibitor	Promega	N251B
LightCycler® 480 SYBR Green I Master	Roche	23724620
SuperScript™ III Reverse Transcriptase	Invitrogen™	18080093
Invitrogen™ UltraPure™Water	Fisher Scientific	11538646
Invitrogen™RNA*later*™	Thermo Fisher Scientific	AM7020
Ethanol absolute, ≥99.8%	VWR Chemicals	437433T

2.9 Transcriptome Analysis

2.9.1 RNA Sequencing

2.9.1.1 Quality Control

After preparation of total RNA from samples as described above, RNA samples (2 μL, heated to 70°C for 2 min) were quality controlled with the Agilent 2100 Bioanalyser System (Agilent Technologies, GS2938B) and Agilent RNA 6000 Nano assay kit. Quality-controlled RNA samples were submitted for library preparation and next generation RNA sequencing to the Wellcome Trust Edinburgh Clinical Research Facility Genetics Department.

2.9.1.2 Library Preparation

Libraries were prepared from 500 ng of each total-RNA sample using the TruSeq Stranded mRNA Library Kit according to manufacturer protocol. Poly-A containing mRNA molecules were purified using poly-T oligo attached magnetic beads. Following purification, mRNA was fragmented using divalent cations under elevated temperature and primed with random hexamers. Primed RNA fragments were reverse transcribed into first strand cDNA using reverse transcriptase and random primers. RNA templates were removed and a replacement strand synthesised incorporating dUTP in place of dTTP to generate double stranded cDNA. The incorporation of dUTP in second strand synthesis quenches the second strand during amplification as the polymerase used in the assay is not incorporated past this nucleotide. AMPure XP beads were then used to separate the ds cDNA from the second strand reaction mix, providing blunt-ended cDNA. A single 'A' nucleotide was added to the 3' ends of the blunt fragments to prevent them from ligating to another during the subsequent adapter ligation reaction, and a corresponding single 'T'

nucleotide on the 3' end of the adapter provided a complementary overhang for ligating the adapter to the fragment. Multiple indexing adapters were then ligated to the ends of the ds cDNA to prepare them for hybridisation onto a flow cell, before 12 cycles of PCR were used to selectively enrich those DNA fragments that had adapter molecules on both ends and amplify the amount of DNA in the library suitable for sequencing. After amplification libraries were purified using AMPure XP beads.

2.9.1.3 Library Quality Control

Libraries were quantified by fluorometry using the Qubit dsDNA HS assay and assessed for quality and fragment size using the Agilent Bioanalyser and High Sensitivity DNA Analysis kit.

2.9.1.4 Sequencing

Sequencing was performed using the NextSeq 500/550 High-Output v2 kit on the NextSeq 550 platform (Illumina Inc, SY-415-1002). Libraries were combined in an equimolar pool based on the library quantification results and run across a single High-Output Flow Cell.

Table 2.18: RNA-Sequencing

Reagent	*Supplier*	*Cat No*
Agilent RNA 6000 Nano assay kit	Aligent	5067-1511
TruSeq® Stranded mRNA Library Prep Kit	Illumina	20020594
Agencourt AMPure XP	Beckman Coulter	A63881
Bioanalyzer High Sensitivity DNA Analysis	Aligent	5067-4626
NextSeq 500/550 High-Output v2 Kit	Illumina	FC-404-2002

2.9.2 RNA-Seq Analysis Pipeline

2.9.2.1 FASTQ Generation

Basecall data produced by the NextSeq 550 was uploaded to BaseSpace (Illumina). Basecall data is converted into FASTQ files to allow analysis using a number of apps accessible directly through BaseSpace, or to download so that alternative analysis pipelines can be used.

2.9.2.2 Read Quality Control

A 2 x 75 bp sequencing run on the Nextseq 550 using a high output flow cell is expected to generate up to 400 M reads with a data quality of > 80% higher than Q30, based on a cluster density of 170-230 K/mm^2. When multiplexing 12 samples per flow cell we would therefore expect to see up to 33 M paired end (PE) reads per sample.

The flow cell achieved a cluster density of 189 K/mm^2 with 91.1% of clusters passing quality filters (PF). The generated data had 93.2% >Q30. Coverage of each sample was a little uneven, though all libraries sequenced generated > 28 M PE reads (Min: 28.9 M, Max: 49.9 M, Mean: 36.3 M). Table 2.19 provides the number of clusters PF for each library, corresponding to the number of PE reads.

2.9.2.3 Mapping Reads and Analysis

The matrix of RNA-seq unnormalised counts was mapped and DEG analysis performed with the DESeq2 bioconductor package (Love et al., 2014) by Graeme Grimes, MRC Human Genetics Unit, Edinburgh. I performed all downstream analyses using RStudio (v 1.1.463).

Table 2.19: Number of Clusters Passing Quality Filters per Sample

Sample ID	*Clusters Passing Quality Filters*
CAS9 1	49,922,016
HIGH 1	29,072,686
LOW 1	41,657,120
CAS9 2	39,526,394
HIGH 2	27,664,649
LOW 2	3,323,659
CAS9 3	28,977,277
HIGH 3	36,954,983
LOW 3	30,580,977
1A3 1	33,690,175
1A3 2	36,722,591
1A3 3	37,621,698

2.10 Aldehyde Derivatisation and Quantification

2.10.1 Aldehyde Derivativatisation

Extended methods specific to each analytical step are described in Chapter 4.

2.10.1.1 Derivatisation

Mouse plasma and MS-grade water were used as matrices to test the derivatisation of aldehydes with DNPH. Matrices were fortified with acetaldehyde and/or the internal standard (d_4-acetaldehyde). Fortified samples (100 μL) were deproteinated by addition of 1 volume acetonitrile and 2.5 volumes methanol. Samples were centrifuged at 15000 x *g*, 15 min, 4°C and the supernatant removed to glass vial. Acetaldehyde and (d_4-acetaldehyde) in the samples was derivatised by addition of a molar-excess of DNPH in 6N (other solvents were tested as described in chapter 4). The pH of each reaction mixture checked using pH indicator paper. The pH of each reaction was increased to pH 4 using sodium acetate solution. Derivatisation reactions proceeded for 1 h at RT on a desktop plate shaker. The derivatisation reaction was stopped by altering the pH with addition of 3 volumes sodium acetate. Samples were vacuum concentrated using an Eppendorf™ Concentrator Plus (Fisher Scientific, 12884952) and resulting samples were resuspended to their initial volume before chromatographic analysis.

Table 2.20: Aldehydes and Aldehyde-2,4-DNPH Reference Standards

Reagent	*Supplier*	*Catalogue Number*
acetaldehyde-2,4-DNPH	Sigma	442434
formaldehyde-2,4-DNPH	Sigma	442597
propionaldehyde-2,4-DNPH	Sigma	442768
d_4-acetaldehyde	Sigma-Aldrich	176567

Table 2.21: Aldehyde Derivatisation Reaction

Reagent	*Supplier*	*Catalogue Number*
Clear Glass Threaded Vials, 2 mL	Fisher Scientific	11503532
Screw Vial, 9 mm, 350 μL	Thermo Scientific	MSCERT5000-37LVW
Nunc™96-Well Cap Mats	Thermo Scientific	276011
EasyLoad clear, 1000 μL, 200μL	Greiner Bio-One	741035, 741000
2,4-dinitrophenylhydrazine	VWR	DI149-100GM
BD Plastipak™ Syringe	Fisher Scientific	10080264
Millex™ PES Filter, 0.22 μm	Merck	SLGP033RS
methanol	Fisher Chemical	10675112/10499560
acetonitrile	Fisher Chemical	10407440
water	Fisher Chemical	10449380
Sodium acetate, ≥99.0%	Sigma-Aldrich	S8750
Normal Mouse Serum	Invitrogen	10410
Fisherbrand™ pH Indicator Paper	Fisher Scientific	11316454

2.10.2 LC-MS Analysis of Derivatised Aldehydes

Extended methods are reported in Chapter 4. All reagents used were of HPLC grade.

2.10.2.1 Analysis of Commercial Standards

Freshly harvested mouse plasma and MS-grade water was spiked with the aldehyde-DNPH standards acetaldehyde-2,4-DNPH, formaldehyde-2,4-DNPH and propionaldehyde-2,4-DNPH. Samples were spiked with aldehyde-DNPH standards to a final concentration of 10 μM (1:9 (*v/v*) acetonitrile:water). Samples were deproteinated using 1 volume acetonitrile and 2.5 volumes methanol followed by centrifugation at 15000 x *g*, 15 min, 4°C. Supernatant was vacuum concentrated using an Eppendorf™ Concentrator Plus (Fisher Scientific, 12884952) and resulting pellets were resuspended to their initial volume in 2% (*v/v*) acetonitrile before chromatographic analysis.

2.10.2.2 LC-MS Instrumentation

Samples were analysed with the following instrumentation:

Table 2.22: LC-MS Instrumentation

Column	*LC-MS*
Accucore™ C18 column 80Å, 2.6 μm, 2.1 mm x 100 mm	UltiMate™3000 HPLC (Thermo) Q Exactive™Orbitrap system (Thermo)
ACQUITY UPLC HSS T3 Column 100 Å, 1.8 μm, 2.1 mm x 150 mm	Acquity™Ultra Performance LC (Waters) QTrap 5500 (AB Sciex)

2.10.2.3 LC Conditions

Table 2.23: Chromatographic Gradient on Accucore™ C18 column with UltiMate™3000 HPLC

Retention (min)	Flow (mL/min)	% A	% B	Curve
0	0.05	98	2	5
0	0.3	80	20	5
0.3	0.3	80	20	5
0.5	0.3	80	20	5
4	0.3	70	30	5
7	0.3	10	90	5
9.5	0.3	10	90	5
10	0.3	80	20	5
12	0.3	80	20	5
12.1	0.02	80	20	5

Mobile Phase A, MS-grade water; Mobile Phase B, acetonitrile.

Gradient flow rate, 0.3 mL/min.

Column temp, 45°C.

Column Type, Accucore™ C18 LC Column 80Å, 2.6 μm, 2.1 mm X 30 mm. Column Type, Accucore™ C18 LC Column 80Å, 2.6 μm, 2.1 mm X 30 mm.

Table 2.24: Chromatographic Gradient on ACQUITY T3 column with Acquity™Ultra Performance LC

Retention (min)	Flow (mL/min)	%A	%B	Curve
1.5	0.4	75	15	5
2.00	0.4	15	85	5
5.00	0.4	15	85	5
5.50	0.4	85	15	5
7.50	0.4	85	15	5

Buffer A, MS-grade water; Buffer B, acetonitrile.

Gradient flow rate = 0.4 mL/min

Column temp = 45°C

Column Type = Waters ACQUITY UPLC HSS T3 Column, 100Å, 1.8 μm, 2.1 mm X 150 mm.

2.10.2.4 MS Conditions

Table 2.25: MS Conditions for Analysis of Aldehyde-DNPHs on Orbitrap MS

Parameter	
Method	Full MS Single Ion Monitoring
Runtime	12 min
Polarity	negative
Resolution	70,000
AGC target	$1E_6$
Maximum Injection Time	200 ms
Scan Range	206-212 *m/z*, 220-226 *m/z*, 234-240 *m/z*
Spectrum Data Type	Profile

Table 2.26: Tuning Conditions for Analysis of Hydrazone Derivatives of Acetaldehyde and d_4-Acetaldehyde

Analyte	Ion Transition (*m/z*)	Time (ms)	CE (*V*)	CXP (*V*)	DP (*V*)
AA-2,4-DNPH	223.000>223.000	50.0	-5.000	-6.000	-60.000
	223.000>151.000	50.0	-14.000	-13.000	-60.000
	223.000>122.000	50.00	-28.000	-11.000	-60.000
	223.000>59.100	50.0	-26.000	-7.000	-60.000
	223.000>76.000	50.0	-18.000	-7.000	-60.000
d_4-AA-2,4-DNPH	227.000>227.000	50.0	-5.000	-15.000	-90.000
	227.000>167.000	50.0	-16.000	-17.000	-90.000
	227.000>137.000	50.0	-26.000	-15.000	-90.000
	227.000>76.000	50.0	-20.000	-7.000	-90.000
	227.000>123.000	50.0	-28.000	-9.000	-90.000

Gradient flow rate = 0.4 mL/min, Column temp = 45°C, Column Type = Waters ACQUITY UPLC HSS T3 Column, 100Å, 1.8 μm, 2.1 mm X 150 mm. Ionisation Parameters; Turbo Spray. Curtain Gas, 40.00; Collision Gas, Medium; IonSpray Voltage (IS), -4500; Temperature, 500.0; Ion Source Gas 1, 40.00; Ion Source Gas 2, 60.00. Collision energy (CE); Voltage (V); A1 (acetaldehyde-2,4-DNPH); d_4-A1 (d_4-acetaldehyde-2,4-DNPH); Collision cell exit potential (CXP); De-clustering potential (DP).

2.10.2.5 Data Analysis

HPLC-MS data from the Q-Exactive Mass Spectrometer was acquired with CHROMELEON™ and XCalibur 4.0 (Thermo). AssayR was used for generation of histograms to represent absolute peak area for analysis of QE-generated HPLC-MS data (Wills et al., 2017). UPLC-MS Data from the QTrap 5500 was acquired and processed using Analyst 3.0 software (AB Sciex).

2.11 Laboratory Animal Work

2.11.1 Facilities and Project License

All animal work was conducted in accordance to the UK Home Office Animals (Scientific Procedures) Act (1986), under Home Office project licence (70/7950 and PD702DCD2) and personal licences (IBC155803) with approval from Veterinary services at the Human Genetics Unit Biomedical Research Facility.

2.11.2 Mouse Strain Origins and Husbandry

The *ALDH1b1* mouse line was provided by Prof. M.J. Arends (CRUK, Edinburgh). *Aldh1b1*$^{-/-}$ mice possess a complete knockout of exon 2 of the murine *Aldh1b1* gene. The *Aldh1b1*$^{-/-}$ mouse line was generated with a gene-trap approach that uses the knockout-first strategy (Skarnes et al., 2011). The knockout-first allele contains a gene trap cassette and neomycin cassette driven by a floxed promoter that was inserted into the second intron of the *Aldh1b1* gene. The knockout-first allele was converted to a conditional allele by Flp recombinase and the tm1d (complete knockout) mouse line was generated after crossing Flp+ mice with Cre transgenic mice to delete the floxed exon. The *Aldh1b1* mouse line was maintained on the C57BL/6 line for five generations. Mice were fed a standard chow diet and water *ad libitum* and housed in conventional barrier cages with enrichment. Mice were kept on a 12 hour light-dark cycle: During the dark cycle, lights were not used and researchers and technicians did not enter the mouse room.

2.11.3 Mouse Genotyping

2.11.3.1 DNA extraction, Amplification and Analysis

Table 2.27: DNA Extraction and Analysis

Reagent	*Supplier*	*Cat No*
QIAprep spin miniprep kit	Qiagen	27106
DirectPCR Lysis Reagent (Ear)	Viagen Biotech	402-E
PCR 8 Tube Strips, 0.2 mL	Alpha Laboratories	LW2570
DreamTaq Green PCR Master Mix (2X)	Thermo Scientific™	K1081
UltraPure™ Agarose	Invitrogen™	15510027
Quick-Load® 1 kb DNA Ladder	New England BioLabs	N0468S
Quick-Load® Purple 100 bp DNA Ladder	NEB®	N0551S
SYBR Safe DNA gel stain	Invitrogen™	S33102

PCR genotyping was performed on ear biopsies of *Aldh1b1* mice. Ear biopsies, 0.2 cm were digested in 100 μL of DirectPCR ear lysis reagent containing 0.4 mg/mL Proteinase K in autoclaved 1.5 mL Eppendorf® tubes. Ears were lysed overnight in a water bath at 55°C followed by Proteinase K inactivation for 1 h at 85°C. Crude lysates were stored at -20°C. PCR reactions were set up according to Table 2.29 and DNA amplified through PCR with cycles detailed in Table 2.30. Amplified PCR product was separated on agarose gel. Agarose gels were prepared with agarose in 1X Tris/Borate/EDTA (TBE) buffer. The PCR product of *Aldh1b1 reaction 1* was separated on 2% (*w/v*) agarose gel and the PCR product of *Aldh1b1 reaction 2* was separated on 3% (*w/v*) agarose gel. SYBR Safe DNA stain was added to molten agarose (1:10000) before casting the gel to enable DNA visualisation under Ultraviolet (UV) light. Five microlitres of DNA ladder (100 bp / 1 kb) was loaded onto each well to enable sizing of PCR products.

Mini-Sub® GT Cell (Bio-Rad, 1704406) reservoir was filled with 1X TBE and the solidified agarose gel. PCR reactions at end point were loaded directly into wells before electrophoretic separation at 100 V in 1X TBE buffer until adequate separation was achieved. Resolved DNA was photographed under UV light using the CHEMI Genius2 BioImaging System (Syngene) and GeneSnap™ analysis tool. A representative image of the presence of targeted homozygous knockout, heterozygous knockout or wildtype *Aldh1b1* alleles is in Figure 2.3.

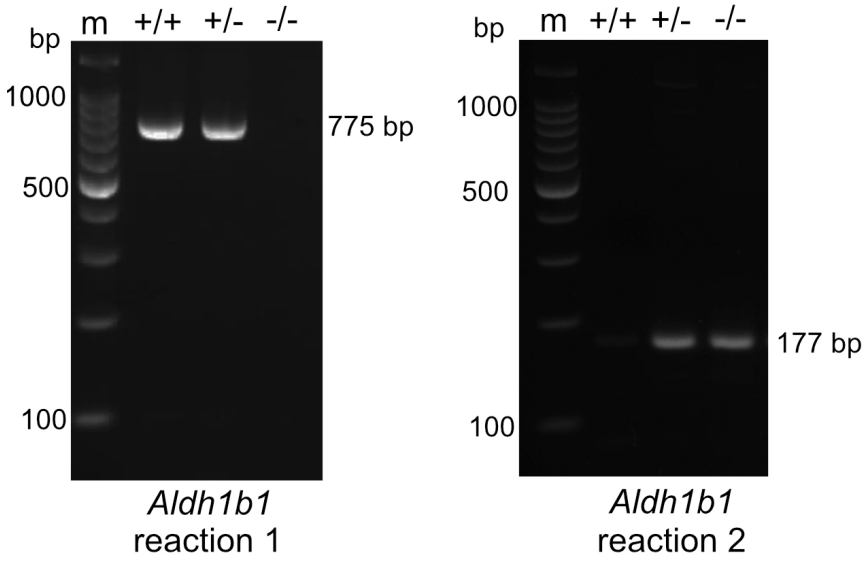

Figure 2.3: **Genotyping for *ALDH1B1* allele status**

Gel 1: PCR reactions of earclip DNA for the floxed allele. Lane 1, DNA Ladder; Lane 2, wild-type, heterozygous; Lane 3, homozygous. Gel 2: PCR Reaction of earclip DNA for the floxed allele.

Table 2.28: Genotyping Primers

Primer Name		*Sequence 5'-3'*
Aldh1b1(FL065)	forward	TTTCACGGTGTGGGCTTTTCCTCAAAT
Aldh1b1(FL066)	reverse	TGACTTCATCCAGATCCAAGACAT
Aldh1b1(Tm1c)	forward	AAGGCGCATAACGATACCAC
Aldh1b1(FL_LR)	reverse	ACTGATGGCGAGCTCAGACC

Table 2.29: Genotyping PCR Reactions

Reagent	*Volume* (μL)
***Aldh1b1* Reaction 1**	20
FL065 forward primer	0.5
FL066 reverse primer	5
2X Taq Polymerase	10
Water	3.5
DNA template	1
***Aldh1b1* Reaction 2**	20
Tm1c forward primer	0.2
FL_LR reverse primer	0.2
2X Taq Polymerase	10
Water	8.6
DNA template	1

Table 2.30: Genotyping PCR Cycles

PCR Step	*Temperature* (°C)	*Time* (s)	*number of cycles*
***Aldh1b1* Reaction 1**			
Preheat	95	120	1
Denaturation	95	30	32
Annealing	58	30	
Extension	72	90	
Termination	72	300	1
	4	∞	1
***Aldh1b1* Reaction 2**			
Preheat	95	120	1
Denaturation	95	30	35
Annealing	58	30	
Extension	72	180	
Termination	72	300	1
	4	∞	1

2.12 Mouse *In Vivo* Studies

2.12.1 Nifuroxazide and Ethanol Cotreatment

ALDH1b1 heterozygous and homozygous mutant mice on C57BL/6 background at 6-8 weeks were administered over seven days with 20% ethanol in drinking water, which is well tolerated in mice. On the eighth day, ethanol treatment was continued and nifuroxazide was administered at a dose of 150 mg/kg in sunflower oil for four days. Mice were weighed and general health was monitored daily. At the experimental end-point, mice were culled through schedule 1 exposure to carbon dioxide at rising concentration. Terminal blood collection was performed by puncture of the inferior vena cava, to allow collection of larger blood volumes than cardiac puncture. Blood was stored in pre-cooled heparin-coated tubes on ice but was processed under cold conditions and as rapidly as possible to minimise aldehyde loss from samples.

2.13 Acetaldehyde Plasma Detection

Freshly-harvested plasma was prepared from heparinized blood with centrifugation at 3000 × *g* for 15 min, 4°C immediately after withdrawal. Acetaldehyde levels in the plasma were analysed immediately to ensure maximal recovery of acetaldehyde in samples. Plasma acetaldehyde concentrations were determined using an enzymatic acetaldehyde assay. Samples were assayed according to the manufacturer instructions, and 50 μL of plasma used for one reaction per well.

Table 2.31: Mouse *In Vivo* studies and Blood Collection

Reagent	*Supplier*	*Catalogue Number*
Ethanol absolute ≥99.8%	VWR Chemicals	437433T
B. Braun Sterican 25 gauge needle	VWR	465785, 612-0153
BD PlastiPak™ Syringe	Fisher Scientific	15544835
Lithium Heparin Blood Collection Tube	Greiner Bio-One	459084
Nifuroxazide	Millipore	481984
Supelco™ sunflower seed oil	Sigma-Aldrich	47123
Acetaldehyde Assay Kit	MegaZyme	K-ACHYD

Chapter 3

Aldehyde Dehydrogenase: 5-Nitrofuran Protein-Drug Interactions

3.1 Introduction

3.1.1 Overview

The 5-nitrofurans (5-NFNs) are a class of prodrugs with antibiotic and antiparasitic activities. Interactions between ALDH and 5-nitrofurans are critical mediators of 5-nitrofuran-induced melanocyte cell death in zebrafish, where is has been shown that the zebrafish Aldh2b (Aldh2) enzyme bio-activate 5-nitrofuran (nifurtimox, NFN1) prodrugs (Zhou et al., 2012). Furthermore, 5-nitrofurans (nifurtimox, NFN1) have been indicated as competitive substrates for human ALDH2 *in vitro* (Zhou et al., 2012). While the Patton laboratory Zhou et al. (2012) has investigated ALDH2-mediated bio-activation of 5-nitrofuran prodrugs in zebrafish, the relevance of this interaction in mammals, its involvement in mechanisms underpinning 5-nitrofuran side effects and how genetic mutations alter the ALDH:5-NFN interaction remains unknown.

3.1.2 Aims

The Patton laboratory has previously demonstrated bio-activation of 5-nitrofurans by zebrafish Aldh2b. I hypothesised that 5-nitrofurans inhibit the activity of ALDH enzymes expressed in mammalian liver and as a consequence, alter the metabolism of endogenous ALDH substrates. This first results chapter encompasses this aim to explore the potential for ALDH:5-NFN interactions in mammalian systems. To this end, the experiments in this chapter were performed under three objectives:

1. Identify protein-drug interactions between ALDH and 5-nitrofuran *in vivo* and *ex vivo*.

   To achieve this objective, studies to establish the effect of 5-nitrofurans on enzyme activity were performed on human recombinant ALDH proteins.

2. Investigate whether ALDH:5-NFN protein-drug interactions are physiologically relevant and occur with ALDH enzymes expressed in the liver.

   To fulfil this objective, precision cut liver slices were developed and characterised as mammalian *ex vivo* tools to study ALDH:gene-drug interactions. ALDH isoform transcript and protein expression in liver slices was analysed and methods of detecting ALDH activity in liver extracts and slices were applied to explore to the effects of the 5-nitrofurans *ex vivo*.

3. Determine the impact of 5-NFN and ethanol exposure on ALDH-mediated pathways *in vivo* and the involvement of the ALDH isoform *Aldh1b1* on the ALDH:5-NFN interaction. Studies on *Aldh1b1*

knockout mice were used to elucidate the *in vivo* impact of 5-NFN exposure on ALDH enzymes and to address the importance of the ALDH1B1 isoform on the ALDH:5-NFN interaction *in vivo*. To fulfil this objective, ELISA-based aldehyde analysis was used to determine the response to ethanol and nifuroxazide-exposure *in vivo* through monitoring the relative abundance of circulating plasma acetaldehyde.

3.2 Results

3.2.1 Nitrofurans are Competitive Substrates for ALDH Enzymes *In Vitro*

Given that 5-nitrofurans are bioactivated by Aldh2b in zebrafish melanocytes (Zhou et al., 2012), and ALDH enzymes are expressed across species in liver, I hypothesised that 5-nitrofurans bind to ALDH enzymes present in mammalian liver. ALDH2 and ALDH1B1 were chosen as candidate targets of 5-nitrofurans in mammals. These candidates were chosen because:

- Zebrafish ALDH2b is homologous to mouse/human ALDH2.
- ALDH1B1 and ALDH2 isoforms share a high degree of sequence similarity and substrate specificity: ALDH2 and ALDH1B1 are two main enzymes involved in acetaldehyde metabolism.
- Patients treated with the 5-NFN, nifurtimox are intolerant to ethanol, which when metabolised, gives rise to acetaldehyde, the main substrate of ALDH2 and ALDH1B1 enzymes.

3.2.1.1 ALDH Dehydrogenase Activity

To determine whether 5-nitrofurans interact with ALDH1B1, recombinant ALDH1B1 protein was tested in an *in vitro* dehydrogenase activity assay. The assay entails incubation of recombinant ALDH1B1 or ALDH2 enzyme with 5-nitrofurans, followed by addition of the endogenous ALDH1B1/2 substrate, acetaldehyde. Metabolism of acetaldehyde by ALDH enzymes is NAD^+ (nicotinamide adenine dinucleotide) dependent; during conversion of acetaldehyde to acetic acid, NAD^+ is reduced to NADH. NADH production can be quantified by monitoring sample absorbance at 360 nm using ultraviolet-visible spectroscopy (UV-Vis). Alternatively, NADH can be coupled to PicoProbe™, a fluorescent NADH-binding probe which can be quantified with fluorescence detection (Ex/Em = 535/587 nm). Together, these methods of quantifying NADH generation provide a useful tool to analyse ALDH activity (Figure 3.1). Incubation of ALDH1B1 protein with 5-nitrofurans resulted in concentration-dependent and drug-specific inhibition of the dehydrogenase activity of ALDH1B1 (Figure 3.2). NFN1 and NFX induced inhibition of ALDH1B1 activity, whereas NAZ did not induce significant inhibitory effects. The pan-ALDH inhibitor disulfiram significantly inhibited ALDH1B1 activity and the selective ALDH2 inhibitor daidzin also inhibited ALDH1B1 activity, albeit not the the same extent as disulfiram.

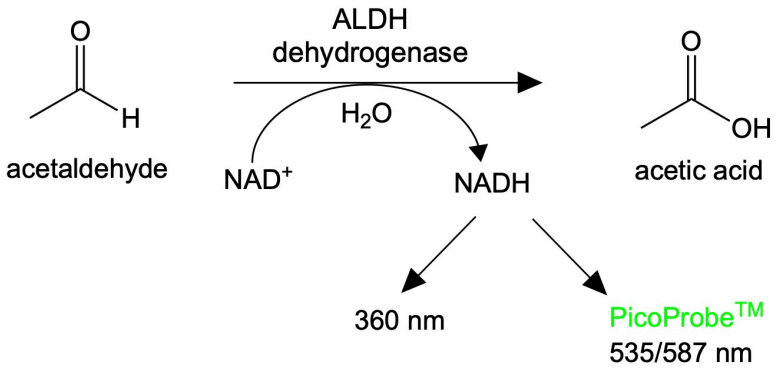

Figure 3.1: **Quantification of ALDH Dehydrogenase Activity**
ALDH enzymes (isoforms 1A1, 1B1, 2) catalyse metabolism of acetaldehyde to acetic acid. This reaction is NAD^+-dependent. During oxidation of acetaldehyde substrate, NAD^+ is reduced to NADH. NADH is used as a readout of ALDH activity. NADH can be quantified by UV-Vis at 360 nm or with PicoProbe™-induced fluorescence at excitation/emission 535/587 nm.

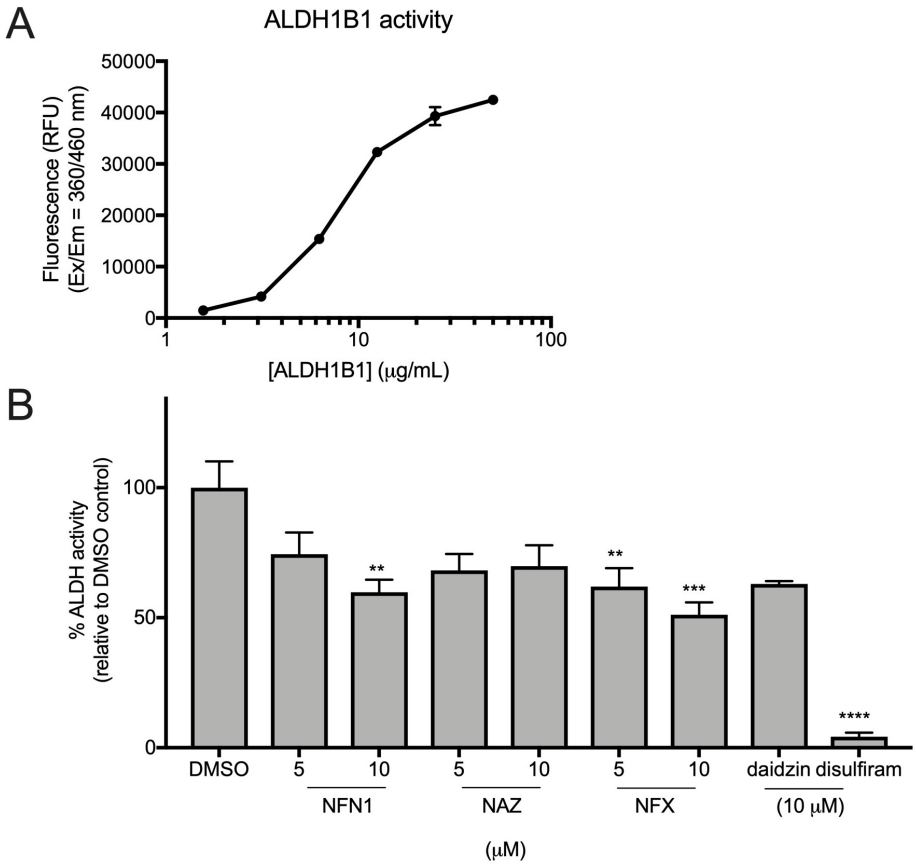

Figure 3.2: **5-Nitrofurans Inhibit the Dehydrogenase Activity of ALDH1B1** The effect of 5-nitrofurans on ALDH1B1 activity was tested through incubation of 0.5 μg ALDH1B1 with Mg^{2+} and NAD^{+} with the 5-NFNs; NFN1, nifuroxazide (NAZ), nifurtimox (NFX) (5 μM, 10 μM). The dehydrogenase reaction was initiated with the addition of 1 mM acetaldehyde and reduction of NAD^{+} to NADH was quantified with the excitation/emission pair 340/460 nm. All reactions were performed in triplicate wells per condition and ANOVA used to test statistical significance. Error bars represent standard deviation.

3.2.2 ALDH Esterase Activity

Although designated the aldehyde dehydrogenase family, the enzymatic activity of ALDHs is not limited to dehydrogenase action on aldehyde substrates. The ALDH enzymes have multiple additional enzymatic activities including esterase functions. I hypothesised that other ALDH enzymatic activities, other than dehydrogenase activity would also be disrupted upon exposure to 5-nitrofurans. To determine whether 5-nitrofurans inhibit the esterase activity of ALDH2, recombinant ALDH2 was subjected to an *in vitro* esterase activity assay: Recombinant ALDH2 enzyme was incubated with 5-nitrofurans, followed by reaction initiation with ALDH esterase substrate. Currently, there are no identified endogenous ester substrates of ALDH enzymes, so the ester, 4-nitrophenylacetate (4-NPA) was used as a substrate. For analysis of esterase activity, the substrate 4-NPA is converted to 4-NP, which absorbs at 405 nm, so affords quantification by UV-Vis (Figure 3.3).

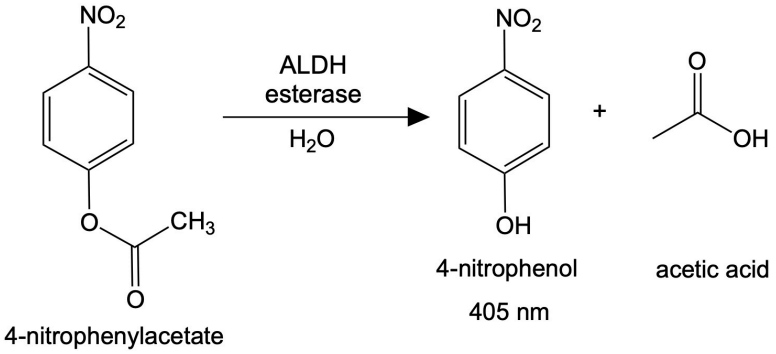

Figure 3.3: **Quantification of ALDH Esterase Activity**
ALDH enzymes catalyse conversion of 4-nitrophenylacetate (4-NPA) to 4-nitrophenol (4-NP). Generation of 4-NP by active ALDH enzyme can be measured by UV-Vis absorbance at 405 nm and used to quantify ALDH esterase activity.

3.2.2.1 ALDH Esterase Dynamics

Determining ALDH enzyme kinetics

To accurately determine the effects of tested compounds on esterase activity, ALDH enzyme velocity was studied. For this, it was important to establish reaction conditions where the ALDH2 enzyme exhibited linear kinetics. ALDH2 substrate saturation dynamics were measured by incubating recombinant ALDH2 protein with differing concentrations of the esterase substrate, 4-NPA. Increased absorbance at 405 nm, representing 4-NP production by ALDH2 was tracked over a 40 min timescale (Figure 3.5).

The resulting enzyme reaction curves demonstrated increases in absorbance at 405 nm over the time course. Furthermore, higher concentrations of 4-NPA yielded corresponding increases in absorbance at 405 nm, reflecting accumulation of the 4-NP product. Reassuringly, under these reaction conditions, turnover of substrate by ALDH enzyme was concentration-dependent. Given that the highest change in absorbance was observed with 700 μM 4-NPA and that at this substrate concentration, linear enzyme activity was retained for the reaction time, 700 μM 4-NPA was used for subsequent esterase activity experiments. Notably, comparatively low absorbance values were detected for the initial 500 s of the reaction.

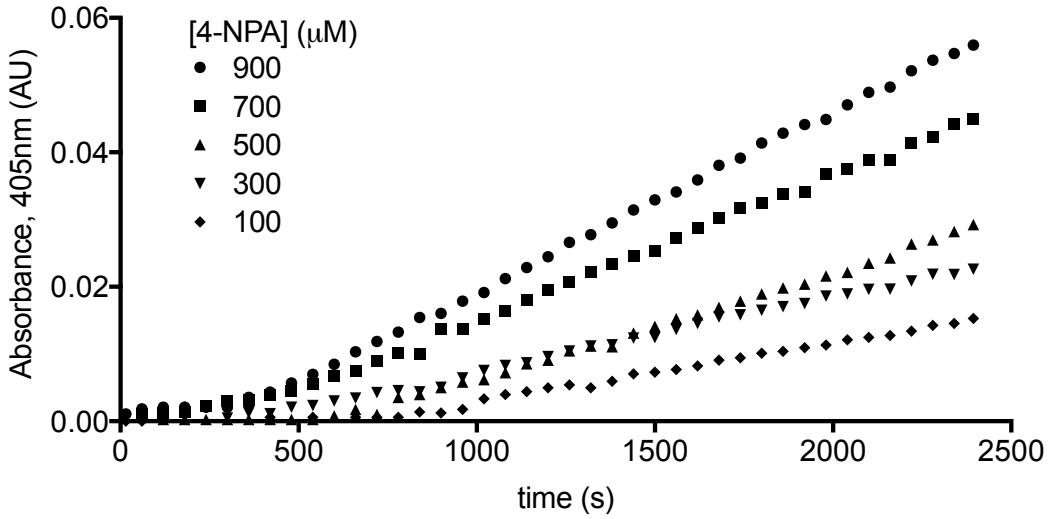

Figure 3.4: **ALDH2 Ester Substrate Dynamics**

Production of 4-NP by recombinant ALDH2 with increasing 4-NPA substrate concentrations. Generation of 4-NP was determined by measuring absorbance at 405 nm with 30 s intervals. Data points are mean of 3 technical replicates.*This experiment was performed with honours student, Marija Zarocsinceva under my direct supervision.

Determining molar extinction coefficients

For all experiments, a standard curve of known 4-NP concentration alongside corresponding absorbance was generated. This enabled interpolation of the amount of 4-NP generated by ALDH2 during the experimental procedure (3.5). To determine the molar extinction coefficient, ε of 4-NP, Beer-Lambert law ($A = \varepsilon cl$) was applied to the absorbance values (ε = 3400 M^{-1} cm^{-1}) and path length, (l) of 0.2.

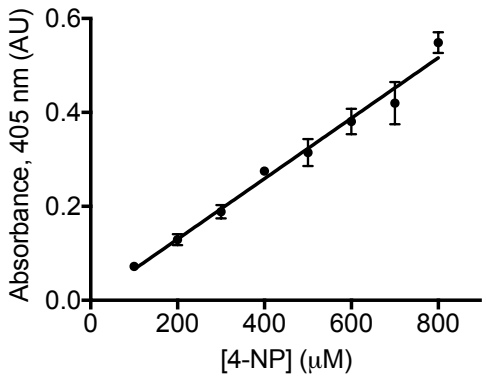

Figure 3.5: **4-Nitrophenol Standard Curve (405 nm)**

Absorbance at 405 nm plotted against known 4-NP concentrations (100 - 800 μM). Data points are the mean of 3 technical replicates, error bars represent standard deviation. *This experiment was performed with honours student, Marija Zarocsinceva under my direct supervision.

Absorbance Spectra of Compounds

To confirm that compounds to be tested for esterase inhibition did not have intrinsic absorbance that would interfere with UV-Vis detection of 4-NP, the absorbance of several nitrofurans and the esterase inhibitor, Aldi-2 was evaluated. Absorbance of the compounds was quantified between 230 nm and 700 nm at 5 nm intervals (Figure 3.6). None of the tested compounds absorbed at the 405 nm wavelength used for monitoring 4-NP (reporter of esterase activity) and so the effect of compounds on ALDH esterase activity could be investigated.

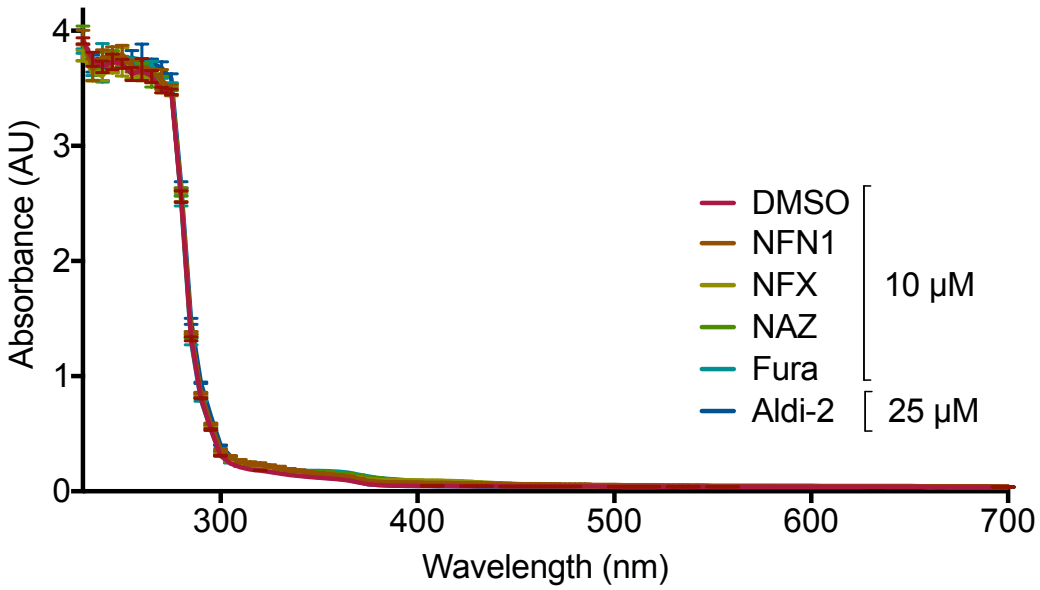

Figure 3.6: **Absorbance Spectra of Compounds Tested for Inhibitory Action on ALDH Esterase Activity**

The 5-nitrofurans; nifurtimox (NFX), nifuroxazide (NAZ), tool 5-NFN compound (NFN1), vehicle (DMSO) and esterase inhibitor (Aldi-2) did not absorb at wavelengths used for the esterase assay (405 nm) and so the effects of these compounds on esterase inhibition could be measured using 4-NPA metabolism as a readout. Spectra measured λ= 700 – 230 nm. Data points are the mean of 3 technical replicates, error bars represent standard deviation. *This experiment was performed by honours student, Marija Zarocsinceva under my direct supervision.

3.2.3 ALDH Esterase Activity is Enhanced by Oxidised Nicotinamide Adenine Dinucleotide

The dehydrogenase activity of ALDH2 is NAD^+-dependent. To decipher whether the esterase activity of ALDH2 also required the NAD^+ co-factor, the rate of 4-NP production by ALDH2 under varying concentrations of NAD^+ was determined (Figure 3.7). In the absence of NAD^+, ALDH2 generated 4-NP from 4-NPA. Addition of NAD^+ at 0.05 mM and 0.5 mM enhanced the esterase activity of ALDH2: Under these NAD^+ concentrations, the rate of 4-NP production increased by 26% ($P = 0.0023$) and 66% ($P = 0.0010$), respectively when compared to NAD^+-deficient conditions.

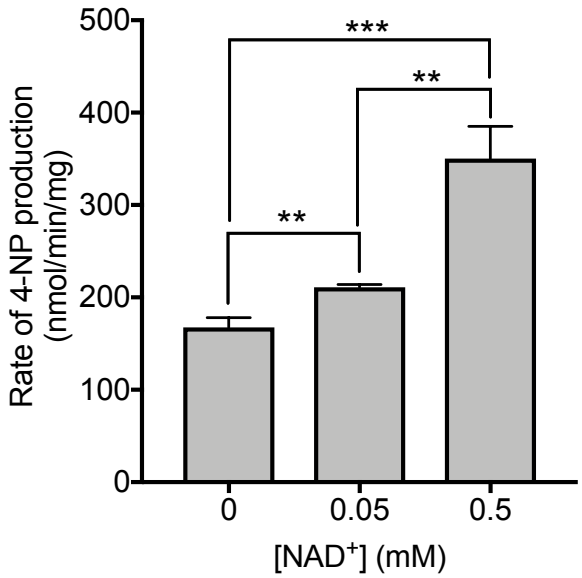

Figure 3.7: **The Esterase Activity of ALDH2 is Enhanced By NAD^+**
Recombinant ALDH2 was incubated with 4-NPA as substrate. Generation of 4-NP was monitored over 40 min. The possibility of background interfering absorbance was corrected for by subtracting absorbance in samples not containing substrate (4-NPA) from substrate-containing samples. Rate of 4-NP generation and ALDH esterase activity was determined by change in absorbance / (time x mg protein). The presence of NAD^+ at concentrations of 0.05 mM and 0.5 mM led to increased 4-NP production by 26% (P = 0.0023) and 66% (P = 0.0010), respectively. Data points are the mean of 3 technical replicates, error bars represent standard deviation. Statistical significance tested by unpaired t-test. *This experiment was performed by honours student, Marija Zarocsinceva under my direct supervision.

3.2.4 Nitrofurans Inhibit the Esterase Activity of Recombinant ALDH2

To determine whether 5-nitrofurans inhibit ALDH2 and disrupt the enzymatic capacity of ALDH to metabolise ester substrates, recombinant ALDH2 was subjected to an in vitro esterase activity assay in the presence of 5-nitrofurans or control compounds using the esterase substrate, 4-NPA (Figure 3.8). Reassuringly, the ALDH2 esterase inhibitor, Aldi-2 significantly ablated generation of 4-NP compared to DMSO control ($P < 0.0001$). The tool nitrofuran compound, NFN1 exhibited significant concentration-dependent inhibition of ALDH2 esterase activity at 3 μM ($P = 0.0001$) and 100-fold lower, 30 nM concentration ($P = 0.0012$).

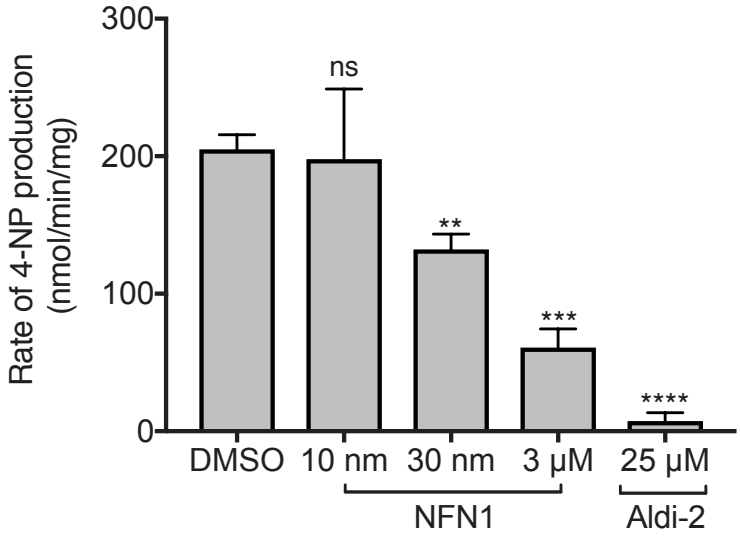

Figure 3.8: **NFN1 inhibits ALDH2 esterase activity**

Recombinant ALDH2 was incubated with 4-NPA as substrate with NFN1 (10 nm – 3 μM) or vehicle (DMSO 1.2%). Generation of 4-NP was monitored over 40 min. The possibility of background interfering absorbance was corrected for by subtracting absorbance in samples not containing substrate (4-NPA) from substrate-containing samples. Data points are the mean of 3 technical replicates, error bars represent standard deviation. Statistical significance tested by unpaired t-test. *This experiment was performed by honours student, Marija Zarocsinceva under my direct supervision.

3.2.5 ALDH Transcript Expression in Mammalian Liver

To address which ALDH isoforms are expressed in mammalian liver and to confirm that ALDH1B1 and ALDH2 proteins are expressed in liver and therefore could potentially be targets of 5-nitrofurans, transcript expression of the 19 and 21 ALDH genes was probed in human HepG2 and mouse liver respectively. Murine ALDH transcripts were probed similarly using the BioGPS data set available at code GeneAtlas MOE430, gcrma. The ALDH transcript most abundantly expressed in mouse liver from this stage is *ALDH1A1* (*RALDH1*) with ALDH1B1 and ALDH2 also expressed.

By analysing the transcript levels of a liver cancer cell line, HepG2, the same ALDH isoforms were seen enriched in this tissue (Figure 3.9). Of all 19 ALDH enzymes expressed in the HepG2 cell line, *ALDH1A1* (*RALDH1*) had the highest expression level, similar to in mouse. The previously-characterised acetaldehyde-metabolising ALDH enzymes, *ALDH1A1*, *ALDH1B1* and *ALDH2* were all expressed in the HepG2 cell line.

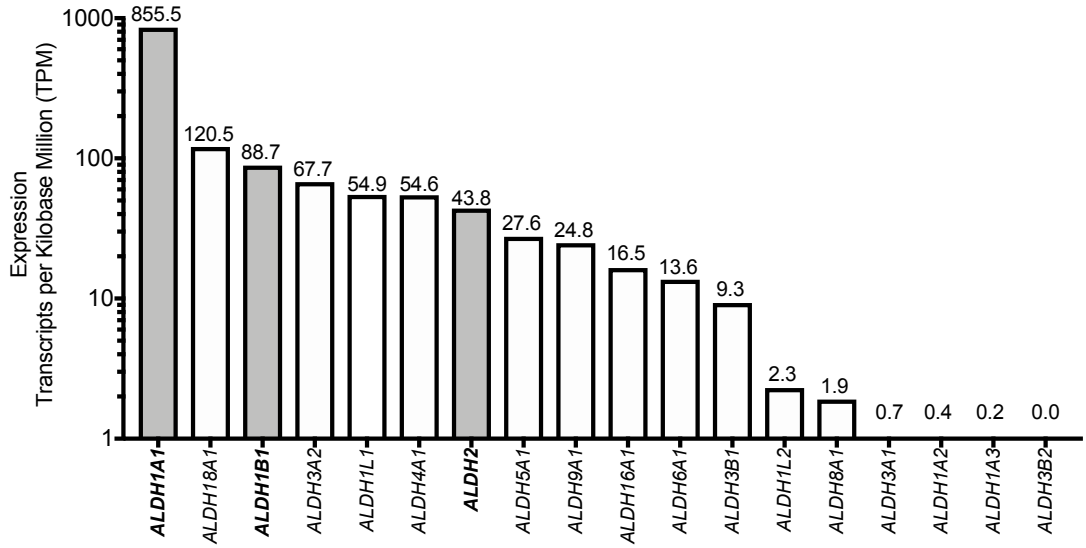

Figure 3.9: **Expression of ALDH Isoforms in the HepG2 Cell Line**
Transcriptional levels of ALDH isoforms in the HepG2 in vitro cultured cell line according to the Human Protein Atlas database. ALDH1B1 and ALDH2 genes are both expressed in HepG2 cells.Data curated from the Human Protein Atlas (Uhlén et al., 2015). Isoforms plotted by expression level. If the TPM value exceeds 1, it is generally accepted that this level of transcript results in functional expression of protein.

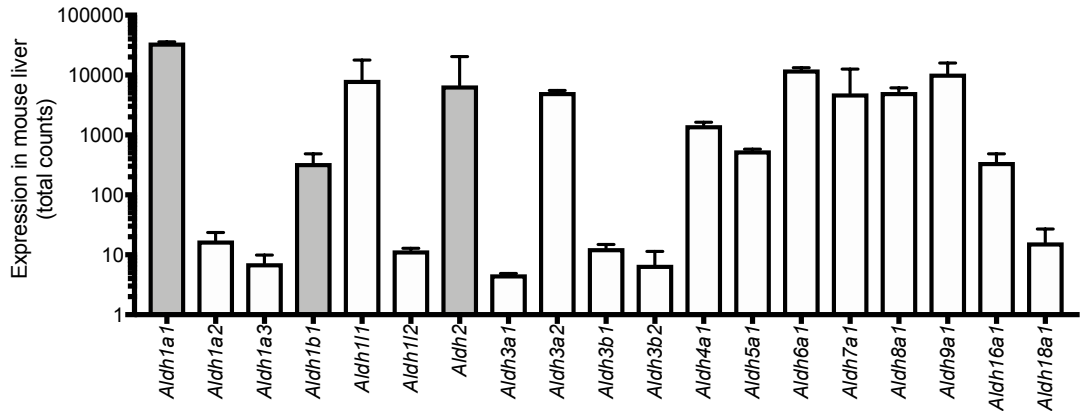

Figure 3.10: **Expression of ALDH Isoforms in Mouse Liver**
Transcript levels of ALDH genes in 6-8 week C57BL/6 mouse liver. ALDH1B1 and ALDH2 genes are both expressed in the liver of C57BL/6 mice. Data curated from BioGPS-deposited data. Error bars represent standard deviation.

3.2.6 ALDH Protein Expression and Activity in Mammalian Liver, *Ex Vivo*

To validate these computational data sets and to ensure that precision cut liver slices derived from C57BL/6 mice were viable tools to explore *ex vivo* gene-drug interactions involving ALDH, ALDH expression and activity in precision cut liver slices was analysed using ALDH enzymatic activity assays and was complemented with western blot methods.

Precision cut liver slices were analysed for their expression of ALDH1B1 and ALDH2 protein following 24 h culture (Figure 3.11). These isoforms yielded intense-staining bands at the respective positions for ALDH1B1 and ALDH2, 57 kDa and 56 kDa and so I explored ALDH:5-NFN interactions using this experimental model.

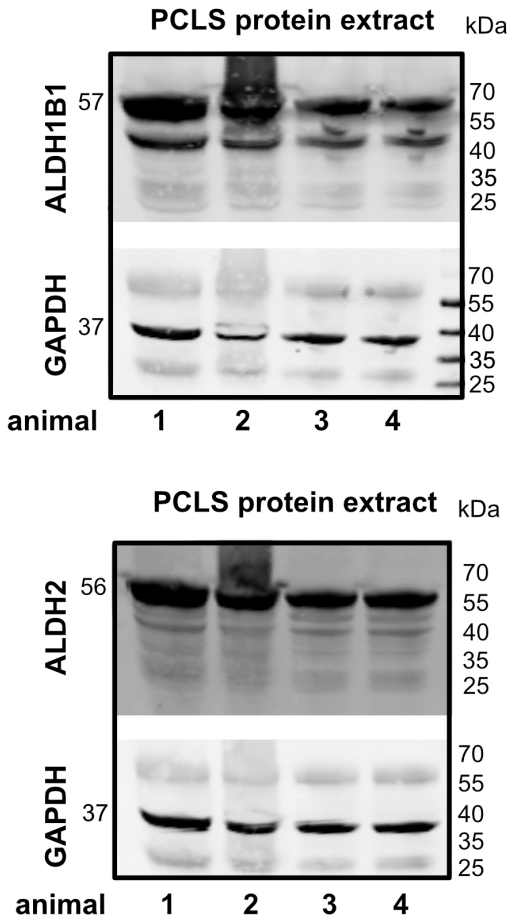

Figure 3.11: **Expression of ALDH Isoforms in Mouse Precision Cut Liver Slices**

Protein levels of ALDH1B1 (57 kDa) and ALDH2 (56 kDa) isoforms in precision cut liver slices from 6-8 week C57BL/6 mice. GAPDH loading control (37 kDa).

3.2.7 Nitrofurans are Competitive Substrates of ALDH in Mammalian Liver

Given that ALDH enzymes are expressed in human and mouse liver and the main organ responsible for nitrofuran metabolism and elimination is the liver, the possibility of an interaction between 5-nitrofurans and ALDHs, and consequence on ALDH enzymatic activity in live liver tissues was examined.

3.2.7.1 Nitrofurans are Competitive Substrates of ALDH in Mammalian Liver, *In Vitro*

First, whole liver extracts were prepared from the liver of C57BL/6 mice. For liver preparation, protein samples were prepared from the left lateral lobe (Figure 2.2). Left and right lateral lobes have similar ALDH activity when tested with PicoProbe™assay (Figure 3.12). For testing 5-NFN compounds and for consistency, the left lateral lobe was chosen to prepare protein extracts as this is the larger of both lobes. Extracts from the left lateral liver lobe were incubated with different nitrofuran compounds, nifurtimox (NFX), nifuroxazide (NAZ) and NFN1. Following incubation, the ALDH activity of liver extracts was tested by PicoProbe™ assay (Figure 3.13). Exposure of liver extracts to 5-NFNs resulted in dose dependent inhibition of ALDH activity. NFN1 demonstrated the most potent inhibition of acetaldehyde-metabolising ALDH enzymes, followed by NFX and NAZ.

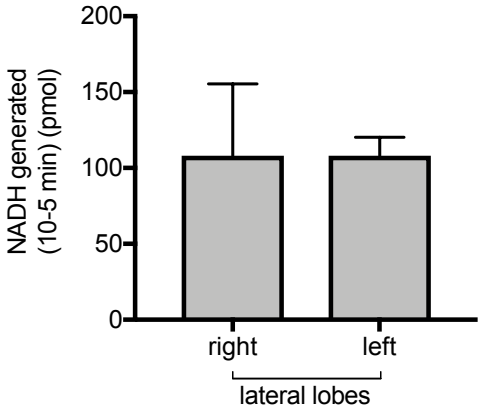

Figure 3.12: **ALDH activity in Mouse Lateral Liver Lobes**
Liver tissue samples from the left and right lateral lobes of 6-8 week C57BL/6 mice were prepared and endogenous ALDH activity monitored by PicoProbe™assay.

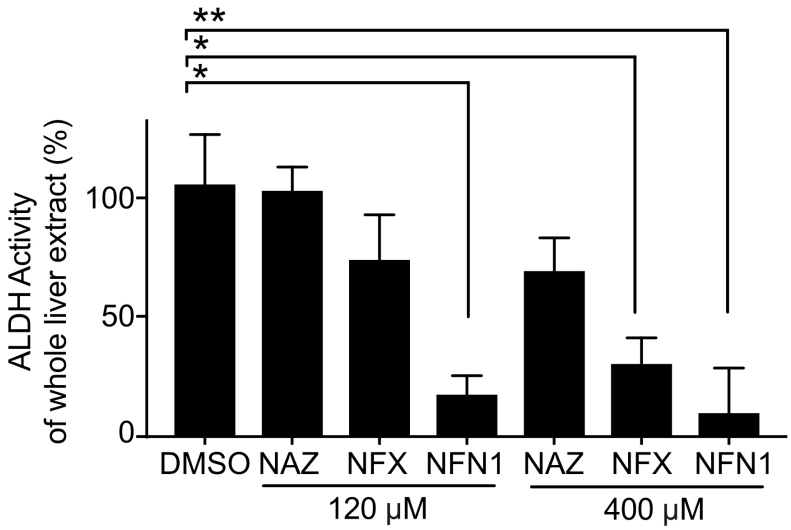

Figure 3.13: **5-NFNs Inhibit ALDH activity in Liver Extracts *In Vitro***
Liver tissue protein extracts prepared from the left lateral lobe of 6-8 week C57BL/6 mice were incubated with NFN compounds before analysis of ALDH activity via PicoProbe™assay. Extracts exhibited concentration-dependent reduction in ALDH activity when incubated with the 5-NFNs, NFN1 and NFX. Data points are the mean of 3 technical replicates. Statistical significance was tested by ANOVA. Error bars represent the standard error of the mean.

3.2.7.2 Nitrofurans are Competitive Substrates of ALDH in Mammalian Liver, *Ex Vivo*

To test whether 5-NFNs maintained inhibitory activity against ALDH enzymes in live tissue, precision cut liver slices were used as an *ex vivo* tool. Precision cut liver slices (PCLS) were prepared from the left lateral liver lobe of 6-8 week C57BL/6 mice (Figure 3.14) and incubated for 24 h with NFN1 (Figure 3.15). NFN1 exhibited concentration-dependent reduction in ALDH activity of live, *ex vivo* tissue slices.

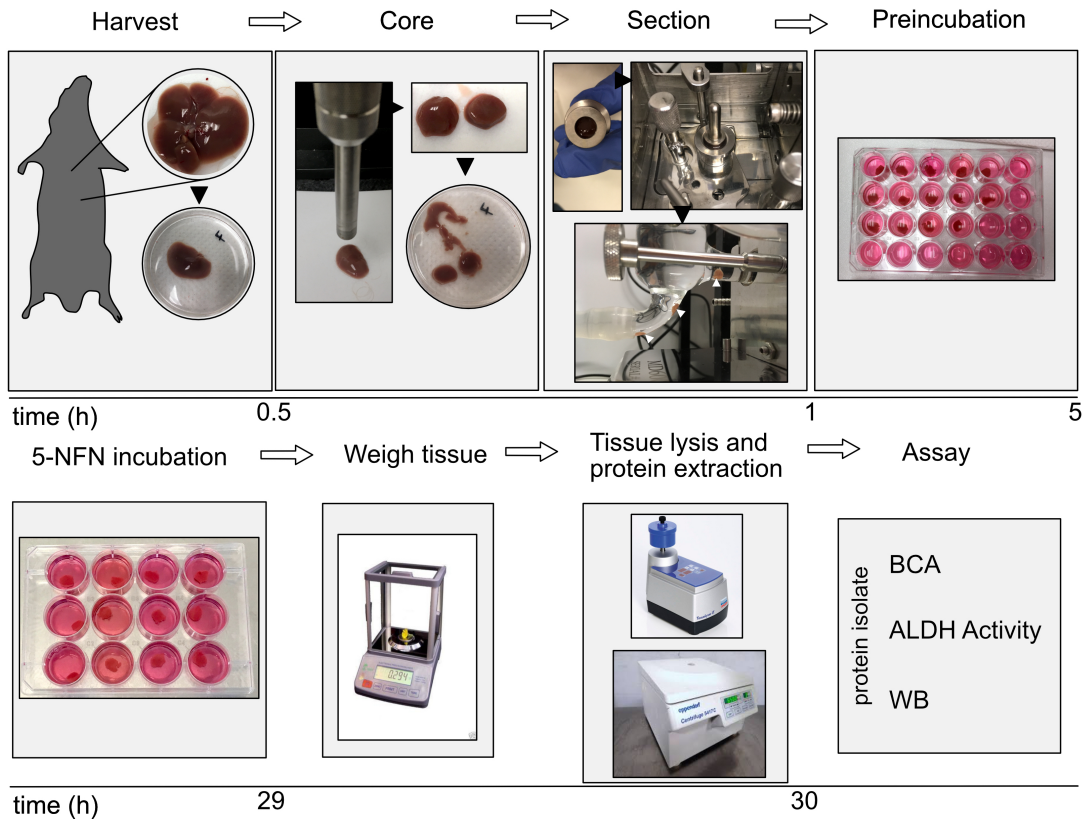

Figure 3.14: **Preparation of Precision Cut Liver Slices**
PCLS were prepared from the left lateral lobe of 6-8 week C57BL/6 mice and incubated with 5-NFN compounds before analysis of ALDH activity via PicoProbe™ ALDH assay.

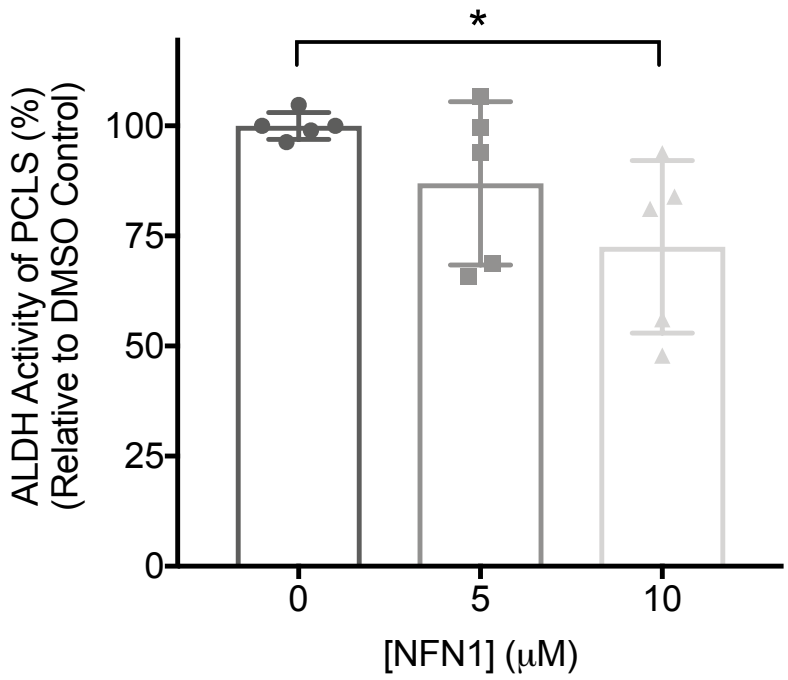

Figure 3.15: **NFN1 Decreases ALDH Activity in PCLS**

PCLS were prepared from the left lateral lobe of 6-8 week C57BL/6 mice and incubated with NFN compounds at 5 μM and 10 μM concentration for 24 h before analysis of ALDH activity via PicoProbe™ ALDH assay. Data points are the mean of 3 PCLS replicates, performed with three picoprobe technical replicates. Error bars represent standard deviation. Statistical significance was tested by ANOVA.

3.2.7.3 ALDH Substrates Increase the Cytotoxic Effects of 5-NFNs on Liver Cells

Given that incubation of liver tissue with 5-NFNs resulted in concentration-dependent reduction of ALDH activity, the potential of ALDH substrates in increasing the cytotoxic effects of 5-NFNs was addressed. HepG2 cells have active ALDH metabolism when measured through ALDEFLUOR™ (Figure 3.16A) and expression of the ALDH2 isoform was confirmed through western blotting (Figure 3.16B). Three day incubation of 5-NFNs in presence or absence of 2.5 mM acetaldehyde, in combination with different concentrations of NFN1 led to a four-fold reduction of the EC50 for NFN1 from 1.04 x 10^{-6} M to 2.26 x 10^{-7} M, indicating that acetaldehyde invokes sensitisation of HepG2 cells to the cytotoxic effects of NFN1 (Figure 3.17).

To establish whether this sensitisation effect was the result of synergistic or additive effects of acetaldehyde and NFN1 on the cell line, model-based quantification of drug combinations was performed. BLISS, HSA and LOEWE dose-response models were used to quantify whether synergistic or antagonistic interactions underlied the cytotoxicity of acetaldehyde and NFN1 in HepG2 cells. Dose response matrices and surface models generated from all mathematical models tested indicate enhanced cytotoxicity at the highest concentration of acetaldehyde and NFN1. The interaction between acetaldehyde and NFN1 is synergistic (synergy value > 10) at 10 μM NFN1 and this synergy is most prevalent when coupled with higher concentrations of acetaldehyde. At lower concentrations of 5-NFN and acetaldehyde, the interaction tends towards additivity (-10 < synergy value < 10) or antagonism (synergy value < -10).

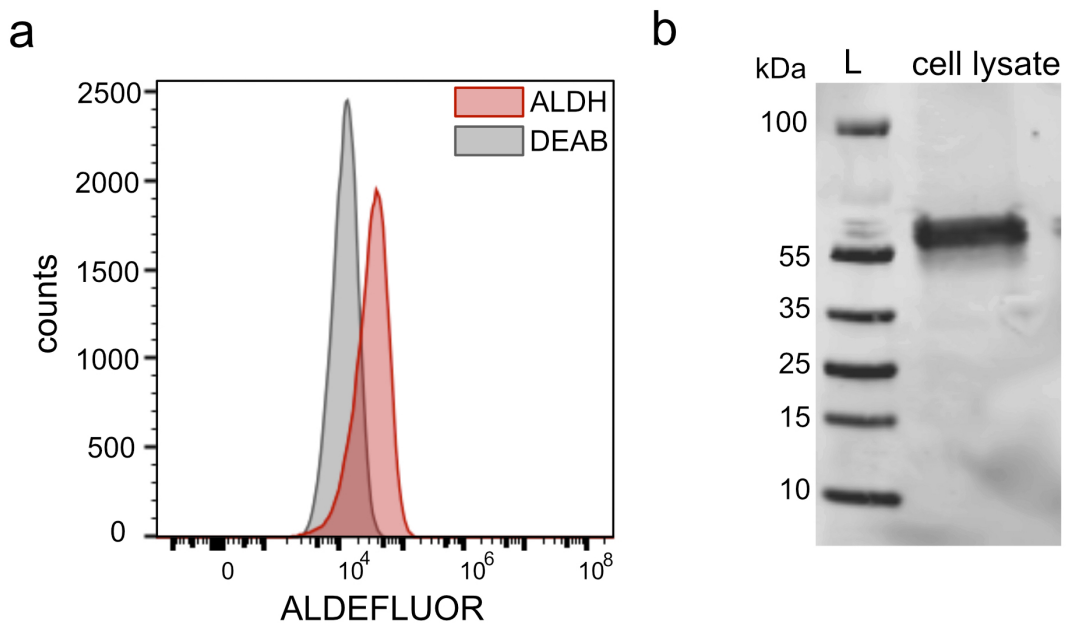

Figure 3.16: **HepG2 Cells Express ALDH2 and Exhibit Proficient ALDH Activity**

A. HepG2 cells metabolise the BAAA substrate of the ALDEFLUOR™ assay, a reporter of ALDH activity.

B Western blotting of cell lysate reveals expression of ALDH2 protein.

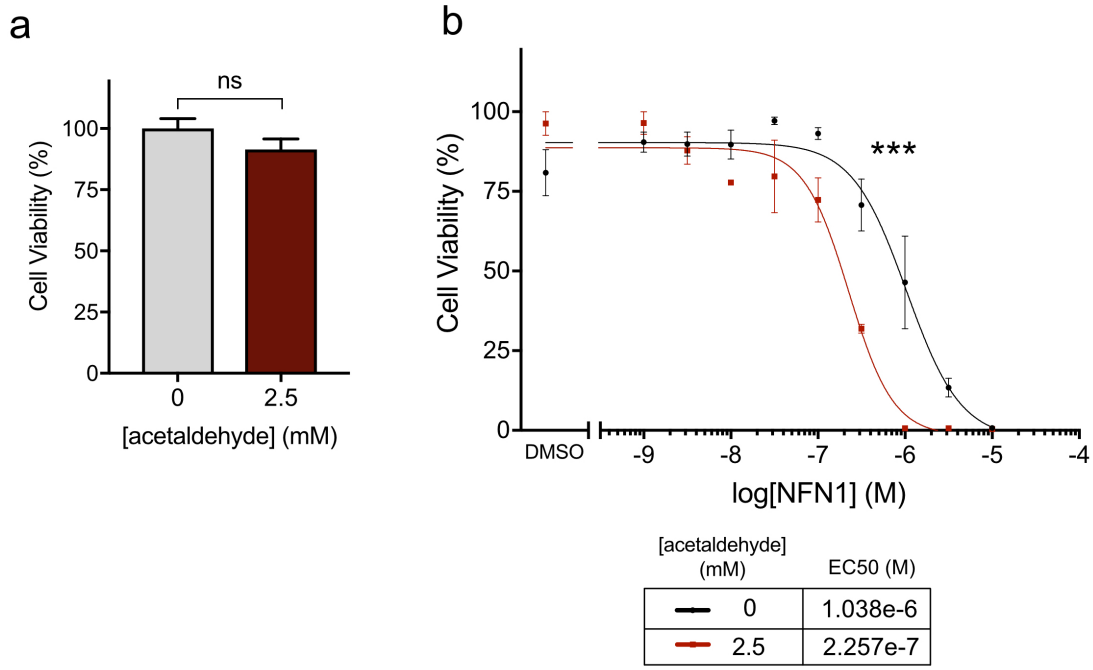

Figure 3.17: **Acetaldehyde Increases the Cytotoxic Effects of 5-NFNs on ALDH-Expressing Liver Cells**

A. Exposure of HepG2 cells to 2.5 mM acetaldehyde does not significantly impact upon cell viability. Statistical significance was tested by unpaired t-test (N=6). Error bars represent standard error of the mean.

B. Exposure of HepG2 cells to acetaldehyde (2.5 mM) sensitises cells to the cytotoxic effects of NFN1. Statistical significance was tested by Ordinary Two-way ANOVA (N=6). Error bars represent standard error of the mean.

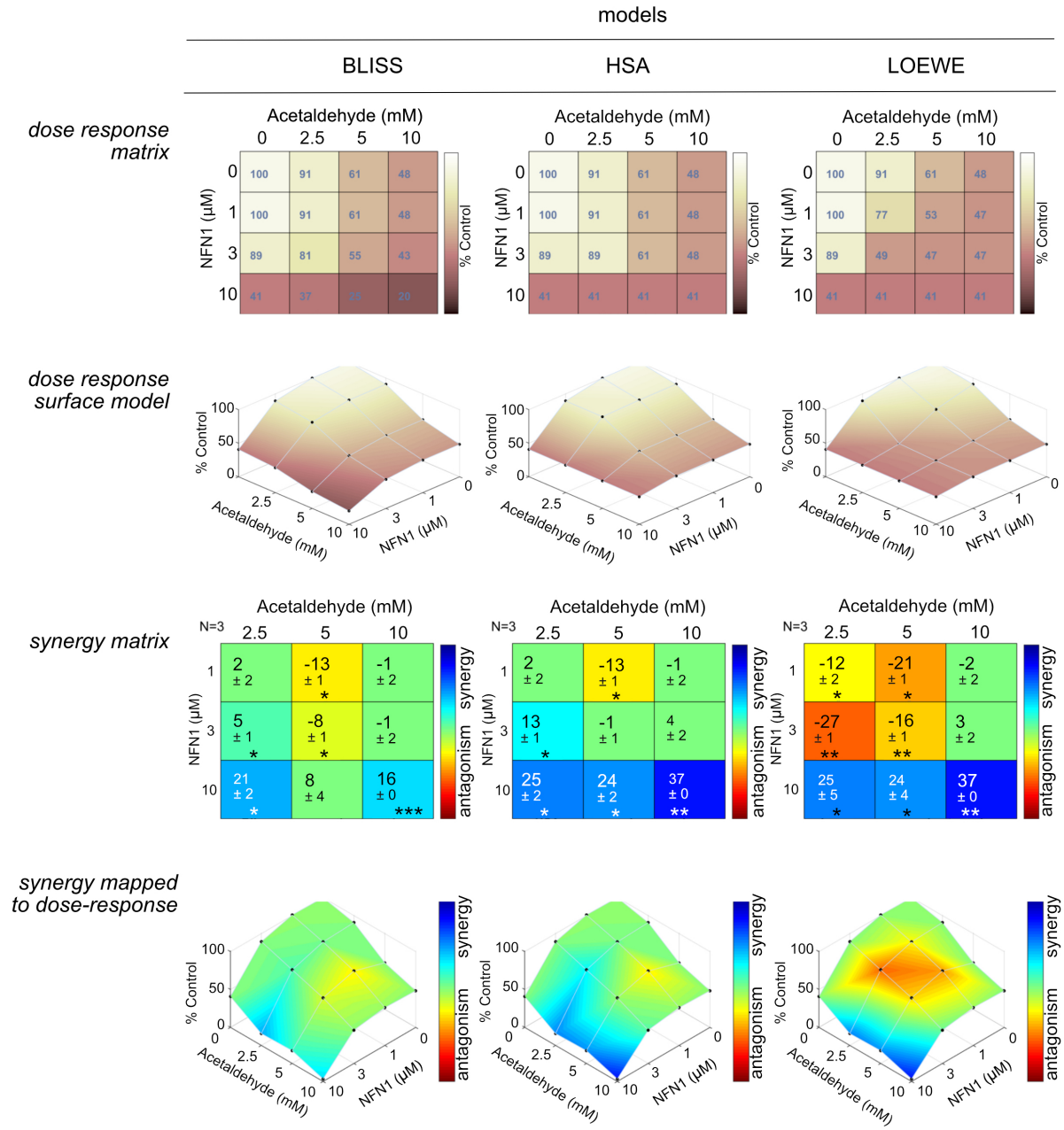

Figure 3.18: **Mapping Synergistic Interactions Between Acetaldehyde and NFN1 in HepG2 Cells**

BLISS, HSA and LOEWE dose-response models were used to determine whether synergistic or antagonistic interactions underlied the cytotoxicity of acetaldehyde and NFN1 in HepG2 cells. P<0.05 (*), P<0.01 (**), P<0.001(***).

3.2.8 The Effect of 5-Nitrofurans *In Vivo*

3.2.8.1 The Effect of 5-Nitrofurans on ALDH activity *In Vivo*

As an interaction between ALDH and 5-NFNs was observed *in vitro* and *ex vivo* in liver, it was hypothesised that delivery of 5-NFNs *in vivo* would alter ALDH activity. The potential for ALDH:5-NFN interaction *in vivo* was tested through combined treatment of C57BL/6 mice with ethanol and the 5-NFN, NAZ in mice heterozygote and homozygote for the*Aldh1b1*-null allele (Figure 3.19). Administration of NAZ at 150 mg/kg in presence or absense of 20% ethanol and subsequent measurement of ALDH activity with PicoProbe™assay did not reveal altered changes in overall liver ALDH activity in ALDH1B1 deficient or proficient mice (Figure 3.20).

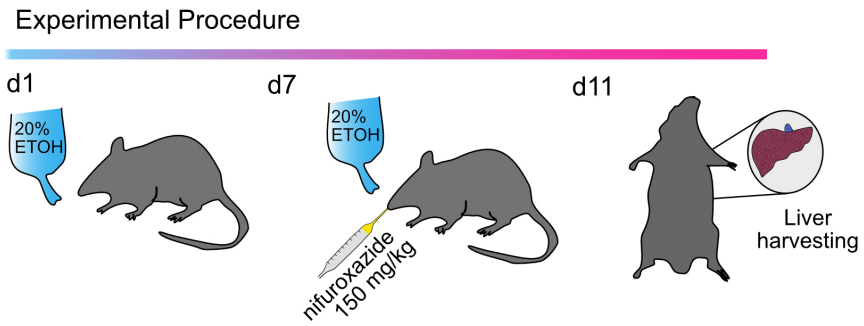

Figure 3.19: **Experimental Protocol for Testing ALDH:5-NFN Interaction *In Vivo***
C57BL/6 mice were administered 20% ethanol in drinking water for 7 days, followed by co-treatment with 20% ethanol and NAZ (150 mg/kg). After a total of 11 days, liver was harvested for analysis of ALDH activity and circulating blood was harvested by puncture of the inferior vena cava.

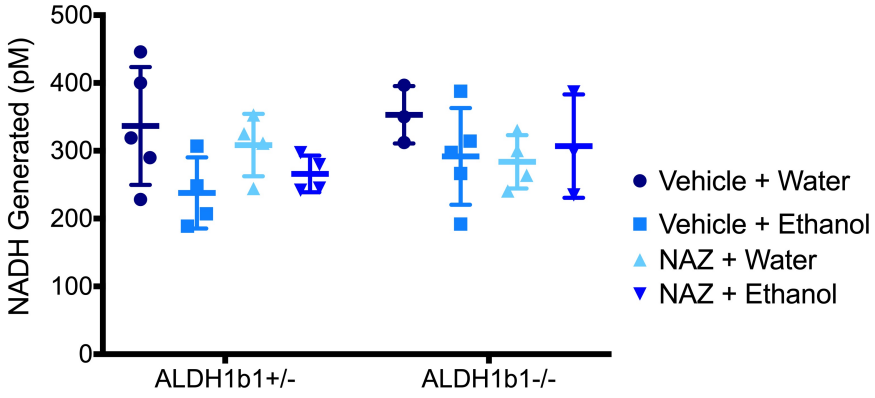

Figure 3.20: **Nifuroxazide Does Not Alter Overall Liver ALDH Activity *In Vivo* Upon Measurement with the ALDH PicoProbe™ Assay**
PCLS were prepared from the left lateral lobe of 6-8 week C57BL/6 mice and incubated with NFN compounds at 5 μM and 10 μM concentration for 24 h before analysis of ALDH activity via PicoProbe™assay (N = 3-5).

3.2.9 The Effect of 5-Nitrofurans on Endogenous ALDH Substrate Levels *In Vivo*

As an interaction between ALDH and 5-NFNs was observed *in vitro* and *ex vivo* in liver, it was hypothesised that delivery of 5-NFNs *in vivo* would alter metabolism of ALDH substrates in vivo. Moreover, it was speculated that inhibition of ALDH activity would result in accumulation of the ALDH1B1 and ALDH2 substrate, acetaldehyde. Acetaldehyde was focused on as a key substrate to be altered by 5-NFN exposure because: (i) Acetaldehyde is a common substrate for ALDH1B1 and ALDH2 enzymes and ALDH2 and ALDH1B1 are the two principal enzymes involved in acetaldehyde metabolism (ii) Patients treated with the 5-NFN, nifurtimox are intolerant to ethanol and acetaldehyde is a major ethanol metabolic product. To establish whether 5-NFNs perturb ALDH metabolic pathways *in vivo*, targeted analysis of the primary ALDH2 and ALDH1B1 substrate and ethanol metabolic product, acetaldehyde upon ethanol and 5-nitrofuran exposure was investigated. C57BL/6 mice homozygote or heterozygote for the acetaldehyde-metabolising enzyme, *Aldh1b1* were exposed to nifuroxazide and ethanol. After 11 days, at experimental end point, circulating blood samples were harvested (Figure 3.21).

As acetaldehyde is the primary major substrate of ALDH, plasma levels of acetaldehyde were measured using an ELISA-based assay. The ELISA-based assay for determination of aldehyde levels entailed incubation of 50 μL of freshly-harvested mouse plasma with a recombinant yeast ALDH in the presence of NAD for 20 min. The amount of acetaldehyde in the sample is indirectly determined by measuring the amount of NADH generated during the reaction time from the recombinant ALDH. Acetaldehyde levels are interpolated from an acetaldehyde ammonia trimer standard curve that was incubated alongside the samples. Treatment of *Aldh1b1*-null heterozygous

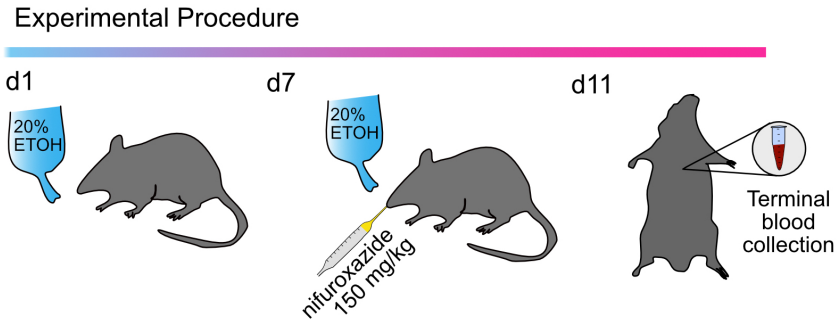

Figure 3.21: **Experimental Protocol for Assessing the Downstream Effects of the ALDH:5-NFN Interaction *In Vivo***
C57BL/6 mice were administered 20% ethanol in drinking water for 7 days, followed by co-treatment with 20% ethanol and nifuroxazide (150 mg/kg). After a total of 11 days, liver was harvested for analysis of ALDH activity and circulating blood was harvested by puncture of the inferior vena cava.

and homozygous mice with a co-administration of 20% ethanol and 150 mg/kg NAZ yielded elevated levels of circulating acetaldehyde (P = 0.0238) (Figure 3.22).

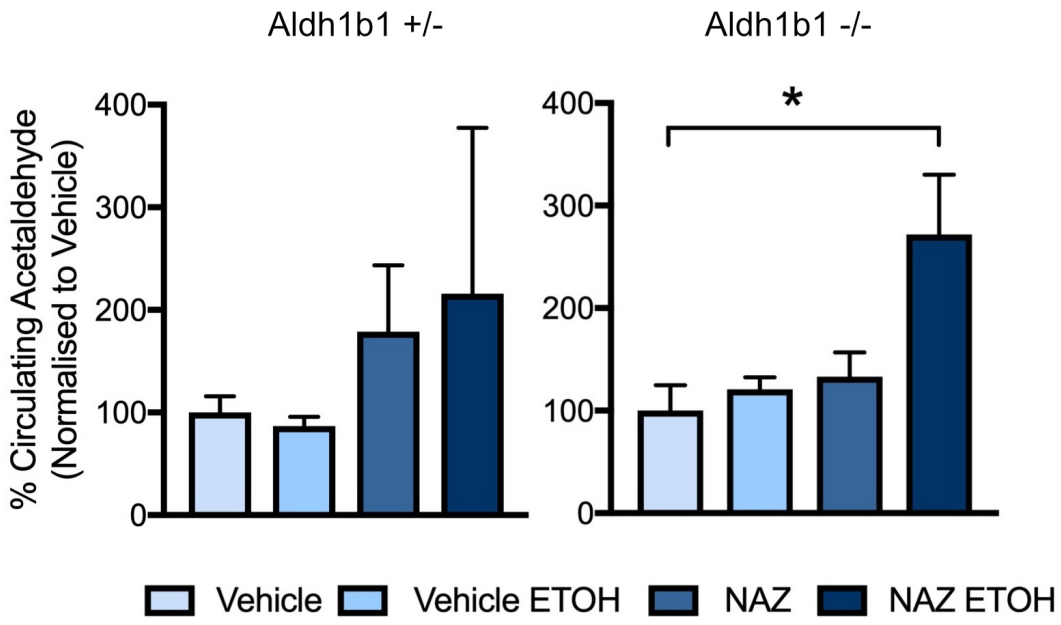

Figure 3.22: **5-Nitrofurans Alter Acetaldehyde Metabolism in *ALDH1b1* Mutant Mice**

Circulating blood was harvested at the experimental endpoint. Levels of the ALDH substrate, acetaldehyde were quantified through ELISA-based assay employing recombinant yeast ALDH and readout of NADH generation. Treatment of ALDH1b1-null mice with co-administrated ethanol and NAZ yielded elevated levels of circulating acetaldehyde. Statistical significance was tested by Mann-Whitney U test. Error bars represent standard error of the mean (N = 3-5) (P = 0.0238).

3.3 Summary

In this chapter the potential for ALDH:5-NFN interactions in mammalian systems was explored. I identified that 5-nitrofurans inhibit the dehydrogenase and esterase activity of ALDH enzymes toward aldehyde and ester substrates. I demonstrated that ALDH1B1 and ALDH2 enzymes are expressed in the liver at the transcript and protein level, are catalytically active and remain expressed in the *ex vivo* precision cut liver slice model during short-term culture. I utilised this tool to investigate the ALDH:5-NFN interaction *ex vivo* and critically observed that inhibition of the dehydrogenase activity of ALDHs by physiological levels of 5-NFNs is recapitulated in ALDH-expressing tissue models and is potent enough to be revealed after only 24 h of 5-NFN exposure. Not only did I find that the dehydrogenase capacity of ALDH1B1 is altered by 5-NFN exposure but that the activity of ALDH2 toward ester substrates is also inhibited *in vitro*. The inhibitory activity of 5-NFNs against ALDH enzymes was not recapitulated when the dehydrogenase activity of *in vivo* ALDH enzymes was tested by ELISA-based ALDH assays after exposure to the 5-NFN, nifuroxazide. When I tested the inhibitory effects of high concentrations of 5-NFNs toward ALDHs *in vitro*, nifuroxazide was discovered to be the least potent inhibitor. A lower concentration of nifuroxazide *in vivo* resulting from 150 mg/kg dose compared to 10 µL *ex vivo* dose coupled to a relatively short half-life of nifuroxazide might explain why these inhibitory effects were not seen *in vivo*. Potentially, ethanol exposure in the *ALDH1b1*-null mice could have led to a compensatory upregulation of the ALDH2 isoform that the *in vivo* dehydrogenase activity assay would not delineate. Treatment of *ALDH1b1* homozygous-null mice with a combination of ethanol and nifuroxazide was sufficient to elevate circulating concentrations of acetaldehyde in plasma. This indicates that nifuroxazide and ethanol coexposure in mice that are deficient for one of the

two major acetaldehyde-metabolising enzymes is a stressor to the acetaldehyde detoxification pathway. In *ALDH1b1* heterozygous mice, expression of ALDH1B1 reduces the impact of nitrofuran and ethanol coexposure on levels of acetaldehyde when compared to vehicle control, emphasising the importance of ALDH1B1 as a 5-nitrofuran target and for protection against 5-Nitrofuran-induced acetaldehyde accumulation. Reassuringly, given the hepatotoxic side effects of 5-NFNs, I show that 5-nitrofurans are cytotoxic to HepG2 cells of liver origin. Given that ALDH1B1 and 2 are expressed in this cell line and were shown to inhibit ALDH activity *in vitro* and *ex vivo*, I hypothesised that ALDH inhibition by 5-nitrofurans would make cells more sensitive to exogenous exposure to the toxic ALDH substrate, acetaldehyde. As there are fundamental differences in the three most popular classes of synergy reference models: HSA (Berenbaum, 1989), Loewe (Loewe, 1953) and Bliss (Bliss, 1939), data tested against all three models were reported. One commonality between these three reference models is that an assumption is made about the expected effect of two components in a combination matrix not interacting (Yadav et al., 2015). The HSA model takes the simple assumption that the expected effect of combination is one that is equal to or greater than the effect seen when a single drug is applied at a high concentration. From a synergy perspective, this model assumes that the effect of the drug combination is more than the sum of the effect of its parts. For example, that if a synergistic effect is apparent, the response to a combination of acetaldehyde and ethanol is greater than the sum of the response from a single administration of ethanol or acetaldehyde. The Loewe model presents the most compelling data to support a synergistic model of interaction between acetaldehyde and NFN1 and is reportedly a more stringent method of synergy modelling (Yadav et al., 2015). Loewe is based on an additivity approach that predicts what the effect

would be if a drug was combined with itself. The Bliss independence model is also regarded as more stringent and models the effects of individual drugs in a combination as independent yet competing events (Yadav et al., 2015). 5-NFN treatment enhanced the sensitivity of cells to the toxic effects of exogenously administered acetaldehyde in a synergistic manner. The synergistic effect between acetaldehyde and NFN1 is most notable at higher concentrations of each component (Figure 3.18). Collectively, this data supports a mechanism whereby exposure to 5-NFNs, particularly NFN1 and nifuroxazide inactivates the core ALDH1B1 and ALDH2 catalytic activity of enzymes expressed in the liver. I hypothesised that 5-NFNs would have the potential to invoke changes to acetaldehyde metabolism and that this is responsible for their *in vivo* toxicity. To address this, I quantified the levels of circulating acetaldehyde in the plasma of *Aldh1b1*-null homozygous and heterozygous mice upon nifuroxazide and ethanol exposure. In this *Aldh1b1*-deficient model, Aldh2 is the only key acetaldehyde-metabolising enzyme present. Upon ethanol challenge, acetaldehyde levels were not significantly altered, which could be due to a compensatory upregulation of Aldh enzyme in response to ethanol and therefore acetaldehyde exposure. In mice homozygous for the *Aldh1b1*-null allele, nifuroxazide and ethanol co-exposure resulted in significantly increased levels of circulating plasma acetaldehyde. These results provide evidence that 5-nitrofurans inactivate ALDH1B1 and ALDH2 catalytic activity in the liver and that this has a downstream impact upon the metabolism of DNA-damaging ALDH substrates *in vivo*.

Chapter 4

Development of LC-MS Methods to Quantify Aldehydes in Biological Samples

4.1 Introduction

4.1.1 Overview

Various methods can be used to evaluate the presence of aldehydes in biological systems. These include the use of flurorescent probes, enzyme assays and MS-based detection and quantification. In the previous chapter, I evaluated the relative abundance of acetaldehyde through use of an ELISA-based method. Whilst this method allows comparison of relative acetaldehyde amounts between samples, HPLC and MS-based techniques offer the opportunity to quantify absolute levels of aldehydes in biological matrices. Despite research toward understanding ALDH networks and the function of ALDH in aldehyde metabolism, 19 human isoforms of ALDH have been classified and the full repertoire of aldehydes that are metabolised by these enzymes has not yet been established. I chose to set up a workflow that would enable detection and quantification of acetaldehyde in plasma that could be readily adapted for the analysis of other aldehydes with a similar experimental approach in the future.

4.1.2 Aims

This second results chapter encompasses the aim to develop a method of aldehyde quantification that would enable high throughput analysis of aldehydes in low-volume plasma samples. To this end, the experiments in this chapter were performed under the following objective:

1. Establish an analytical method for aldehyde measurement in plasma samples.

   To achieve this objective, an experimental approach was developed whereby aldehydes were rapidly derivatised to ensure their minimal loss from samples, followed by chromatographic separation and MS-detection of derivatised aldehydes using Triple-Quadrupole-MS/MS and High-Resolution Accurate-Mass (Orbitrap) MS techniques.

4.2 Results

4.2.1 HPLC-MS Based Detection of Aldehydes

With the aim of establishing an LC-MS method for the analysis of derivatised acetaldehyde and other aldehyde ALDH1B1/2 substrates in plasma, the following stages of method development were performed:

1. Chromatographic separation of acetaldehyde-2,4-DNPH was optimised with different stationary and mobile phases.

2. Detection of parent ions for acetaldehyde-2,4-DNPH was achieved. This was performed on two systems:
   (i) UltiMate™3000 HPLC (Thermo) inline with the Q Exactive™Orbitrap system (Thermo)
   (ii) Acquity™Ultra Performance LC (Waters) inline with a QTrap 5500 (AB Sciex).

3. Derivatisation of acetaldehyde and deuterated acetaldehyde internal standard, d_4-acetaldehyde with 2,4-DNPH.

4. Product ions for acetaldehyde-2,4-DNPH and d_4-acetaldehyde-2,4-DNPH were generated and transitions selected for quantitation.

5. Standard curve was established for acetaldehyde-2,4-DNPH in aqueous solution.

6. Clean-up of derivatisations in aqueous and plasma matrix was tested.

7. Standard curve was established for acetaldehyde-2,4-DNPH in plasma matrix.

4.2.2 Orbitrap, High Resolution Accurate-Mass HPLC-MS Detection

4.2.2.1 Chromatographic Separation of Aldehyde-2,4-DNPHs in Water and Plasma Matrices

For concentration and targeted selection of acetaldehyde-2,4-DNPH, HPLC conditions were established using pre-synthesised aldehyde-2,4-DNPH reference standards. Carbon-18 was selected as a suitable stationary phase and the gradient in Table 4.1 was found to afford separation of aldehyde-2,4-dinitrophenylhydrazones using water and acetonitrile as the mobile phases.

Table 4.1: Chromatographic Gradient on Accucore™ C18

Retention (min)	Flow (mL/min)	% A	% B	Curve
0	0.05	98	2	5
0	0.3	80	20	5
0.3	0.3	80	20	5
0.5	0.3	80	20	5
4	0.3	70	30	5
7	0.3	10	90	5
9.5	0.3	10	90	5
10	0.3	80	20	5
12	0.3	80	20	5
12.1	0.02	80	20	5

Mobile Phase A, MS-grade water; Mobile Phase B, acetonitrile.

Gradient flow rate, 0.3 mL/min.

Column temp, 45°C.

Column Type, Accucore™ C18 LC Column 80Å, 2.6 μm, 2.1 mm X 30 mm.

Chromatograms of each aldehyde-2,4-dinitrophenylhydrazone were compared between simple and more complex biological mixtures, water and deproteinated plasma, respectively. Freshly collected mouse plasma and MS-grade water was spiked with acetaldehyde-2,4-dinitrophenylhydrazone to a final concentration of 10 μM (10% acetonitrile). Samples were deproteinated through addition of 1 volume acetonitrile and 2.5 volumes methanol. Supernatant was vacuum concentrated and resulting pellets were resuspended to initial volume in 2% acetonitrile before chromatographic analysis on Accucore™C18 HPLC column, injecting 20 μL volume (44.8 ng on column mass of acetaldehyde-2,4-DNPH). Peaks were selected for each aldehyde-2,4-dinitrophenylhydrazone (Figure 4.1A, Figure 4.2A, Figure 4.3A). Peak intensity was calculated for water and plasma-spiked samples (Figure 4.1B, Figure 4.2B, Figure 4.3B). These conditions enabled HPLC-MS detection of the parent ion of each aldehyde-2,4-dinitrophenylhydrazone. For these reasons, this chromatography set-up was chosen as the buffer system going forwards.

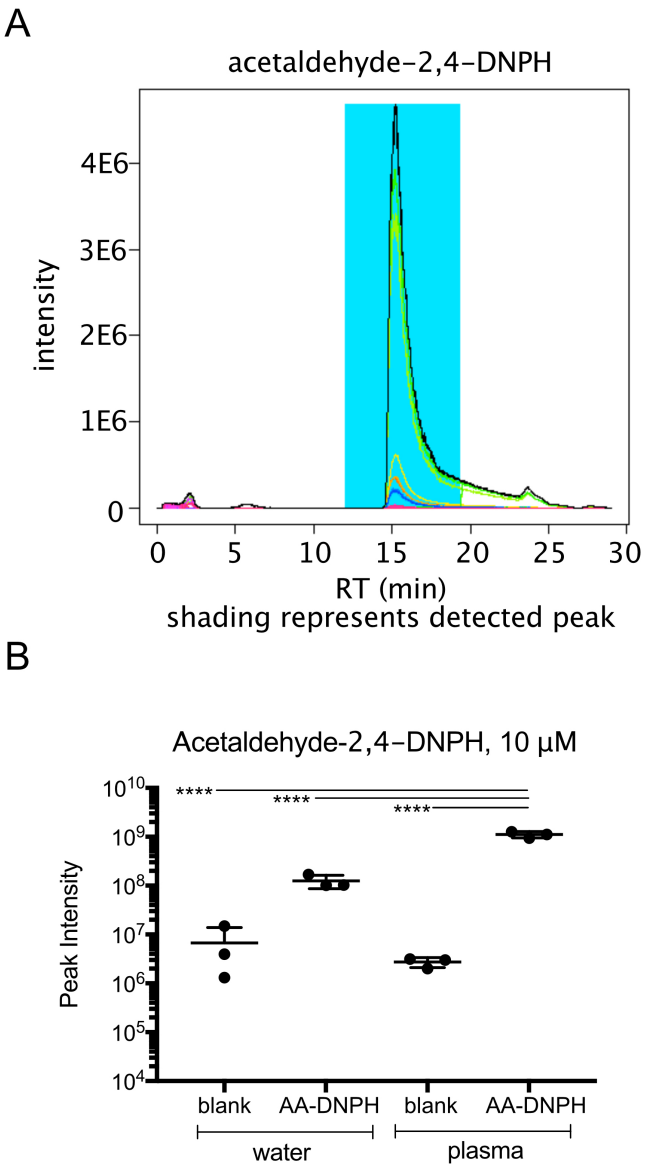

Figure 4.1: **HPLC-MS Analysis of Plasma and Water Matrices Fortified with Acetaldehyde-2,4-DNPH Standard**

2% acetonitrile loading conditions. Data points are the mean of 3 technical replicates. Error bars represent standard deviation. Statistical significance was tested by ANOVA.

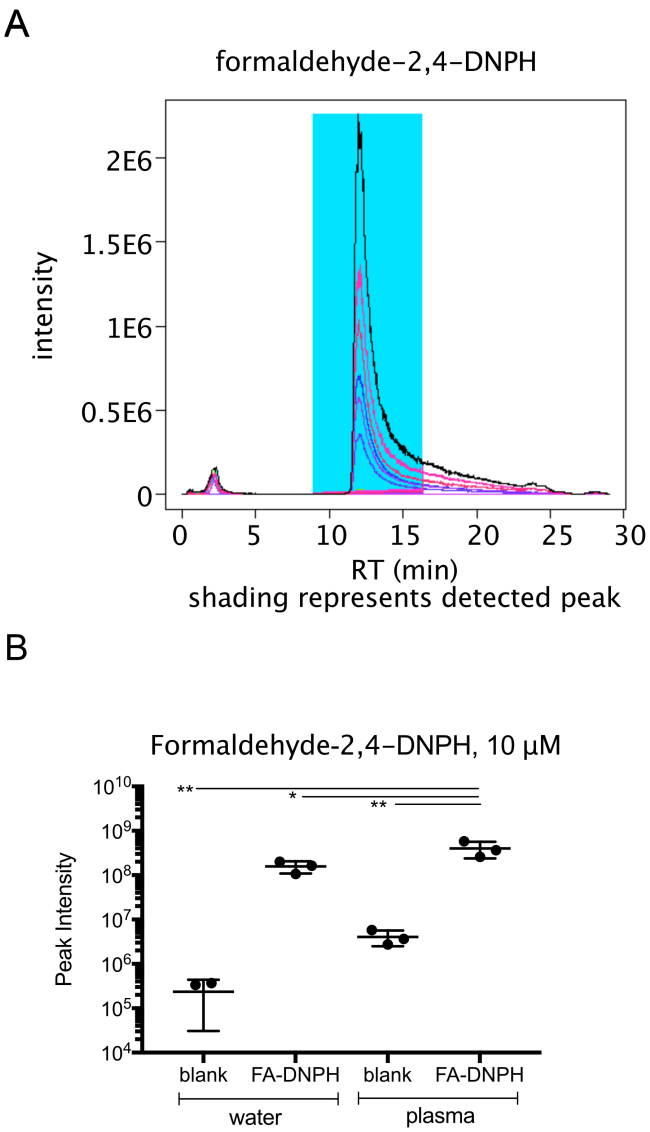

Figure 4.2: **HPLC-MS Analysis of Plasma and Water Matrices Fortified with Formaldehyde-2,4-DNPH Standard**

2% acetonitrile loading conditions. Data points are the mean of 3 technical replicates. Error bars represent standard deviation. Statistical significance was tested by ANOVA.

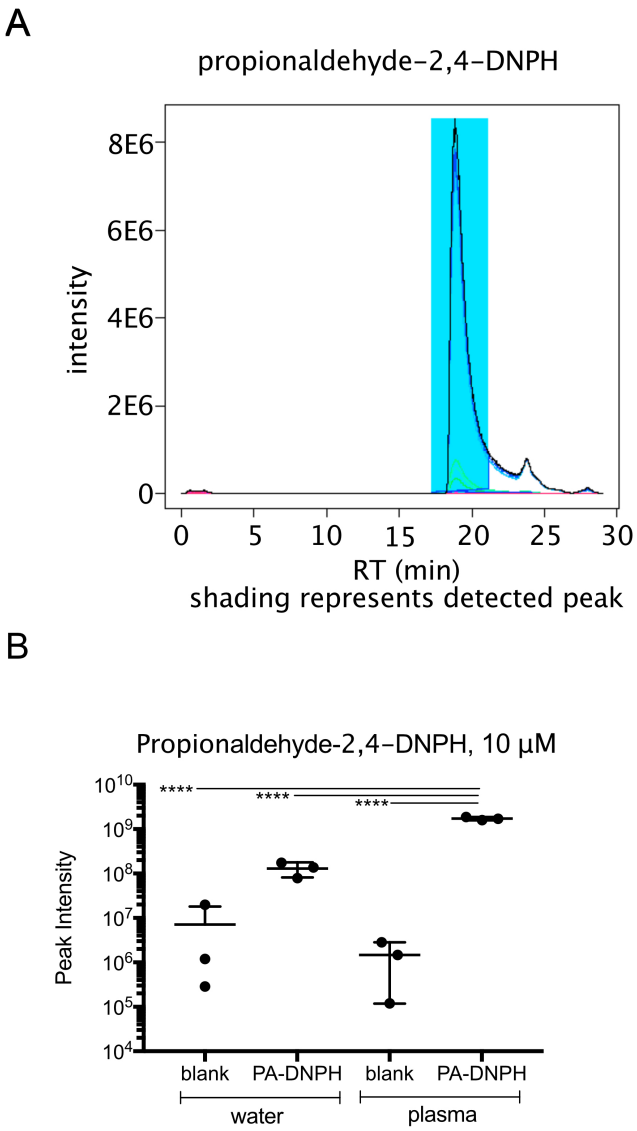

Figure 4.3: **HPLC-MS Analysis of Plasma and Water Matrices Fortified with Propionaldehyde-2,4-DNPH Standard**

2% acetonitrile loading conditions. Data points are the mean of 3 technical replicates. Error bars represent standard deviation. Statistical significance was tested by ANOVA.

4.2.3 Fortification of Plasma with Aldehyde-DNPH Standards Yields Quantifiable Increases in Corresponding Peak Intensity

Mouse plasma, 90 μL was spiked with serially diluted aldehyde-2,4-dinitrophenylhydrazones to final concentrations in the range 1 nM to 10 μM (10% acetonitrile). Samples, 100 μL were deproteinated through addition of 1 volume acetonitrile and 2.5 volumes methanol. Supernatant was vacuum concentrated and resulting pellets were resuspended to the initial plasma volume in 2% acetonitrile before chromatographic analysis on Accucore™ C18 HPLC column. The parent ion of each aldehyde-2,4-dinitrophenylhydrazone was monitored, eluting peaks were selected for each aldehyde-2,4-dinitrophenylhydrazone and peak area intensity quantified using AssayR (Figure 4.4, Figure 4.5, Figure 4.6).

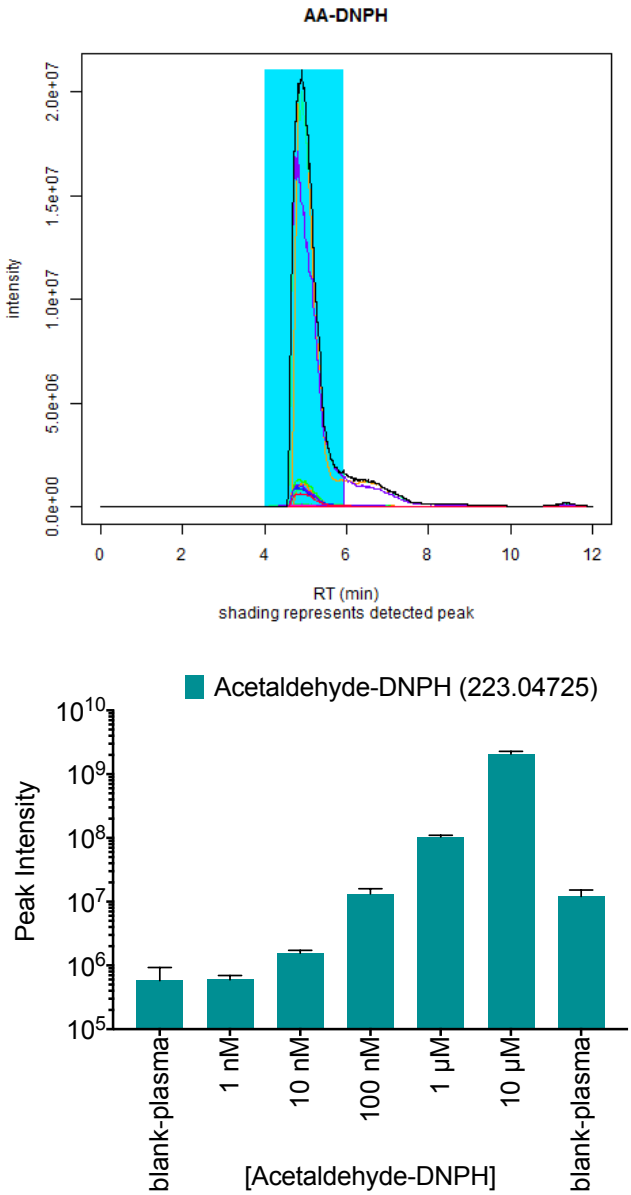

Figure 4.4: **HPLC-MS Analysis of Plasma Matrix Fortified with Acetaldehyde-2,4-DNPH Standard (1 nM - 10 μM)**
Acetaldehyde-2,4-DNPH standards were spiked into 90 μL of plasma at a final concentration of 1 nM - 10 μM. Final loading conditions were in 2% (*v/v*) acetonitrile.

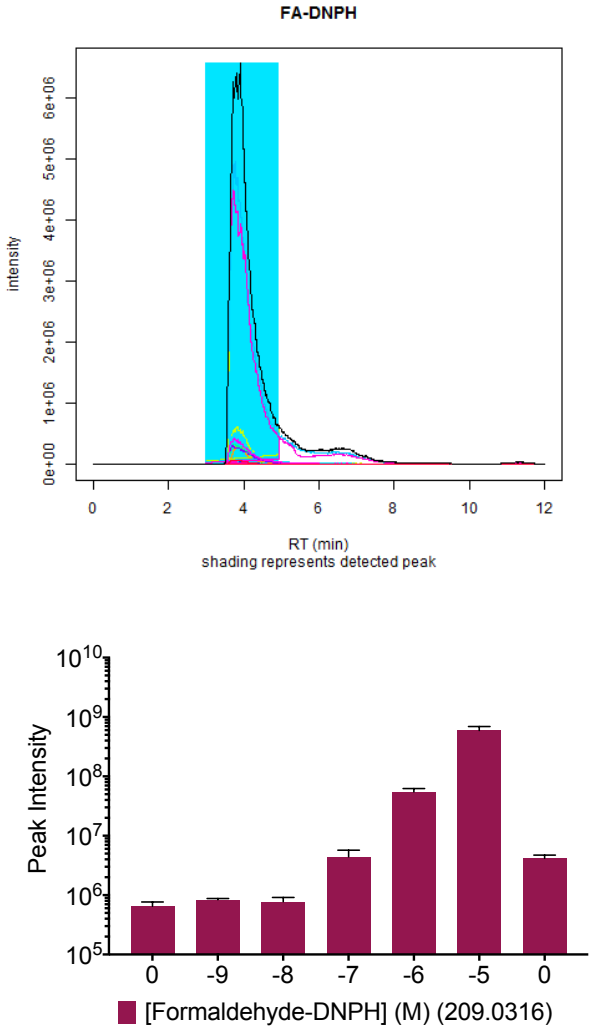

Figure 4.5: **HPLC-MS Analysis of Plasma Matrix Fortified with Formaldehyde-2,4-DNPH Standard (1 nM - 10 μM)**
2% acetonitrile loading conditions. Formaldehyde-2,4-DNPH standards were spiked into 90 μL of plasma at a final concentration of 1 nM - 10 μM. Final loading conditions were in 2% (*v/v*) acetonitrile.

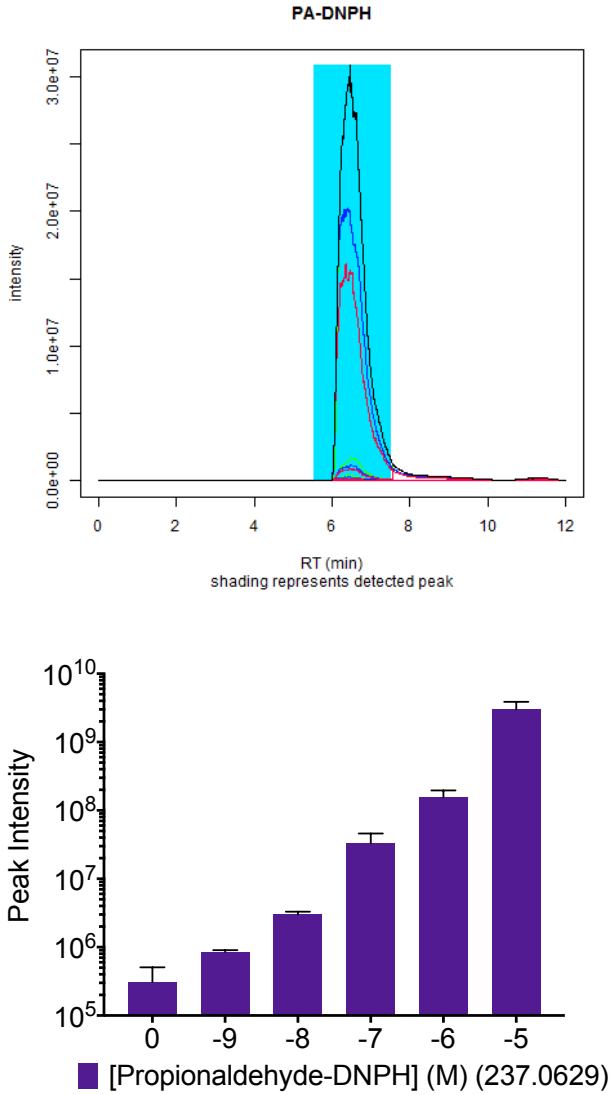

Figure 4.6: **HPLC-MS Analysis of Plasma Matrix Fortified with Propionaldehyde-2,4-DNPH Standard (1 nM - 10 μM)**
Propionaldehyde-2,4-DNPH standards were spiked into 90 μL of plasma at a final concentration of 1 nM - 10 μM. Final loading conditions were in 2% (*v/v*) acetonitrile.

Serial dilutions of each aldehyde-2,4-dinitrophenylhydrazone yielded corresponding changes in peak intensity. To observe whether standards were binding to the column between runs due to incomplete elution of adsorbed molecules or whether reference standards contained trace amounts of additional contaminating aldehyde, parent ions for all three aldehyde-2,4-DNPH were examined in each standard, scanning the three parent ions; acetaldehyde-2,4-DNPH, *m/z* 223.0473; propionaldehyde,2,4-DNPH, *m/z* 237.0629; formaldehyde-2,4-DNPH, *m/z* 209.0316 (Figure 4.7). Reassuringly, for each aldehyde-2,4-DNPH the highest intensity peak identified was for the parent ion of that molecule and peak intensities increased relative to analyte concentration. Next, lower concentrations of acetaldehyde-2,4-DNPH were tested on a replacement C18 column; increasing concentration of acetaldehyde-2,4-DNPH standard was correlated with relative increases in peak intensity of the parent ion, acetaldehyde-2,4-DNPH *m/z* 223.0473 (Figure 4.8).

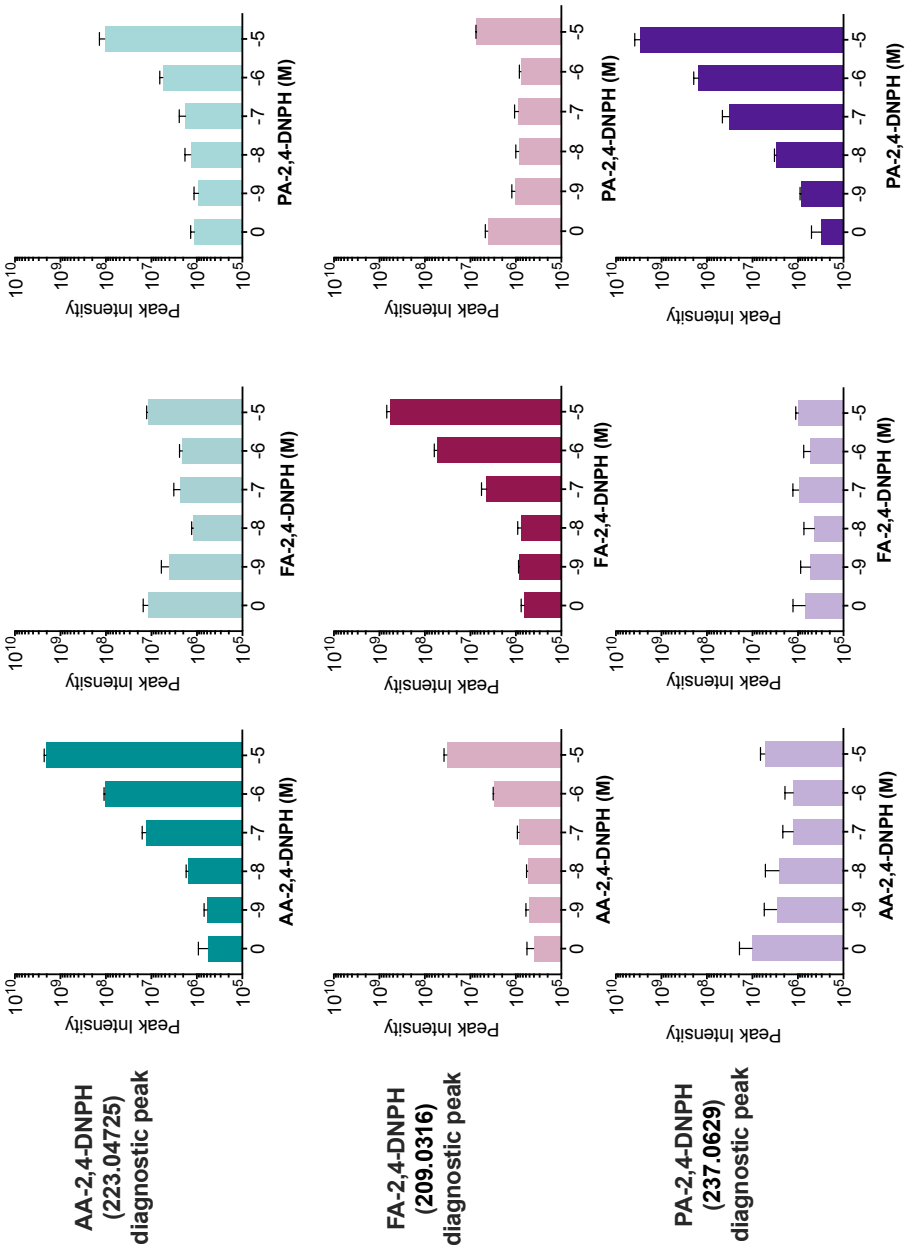

Figure 4.7: **HPLC-MS Analysis of Plasma Fortified with AA-DNPH, FA-DNPH and PA-DNPH to Establish Background Levels of Each Aldehyde-DNPH**

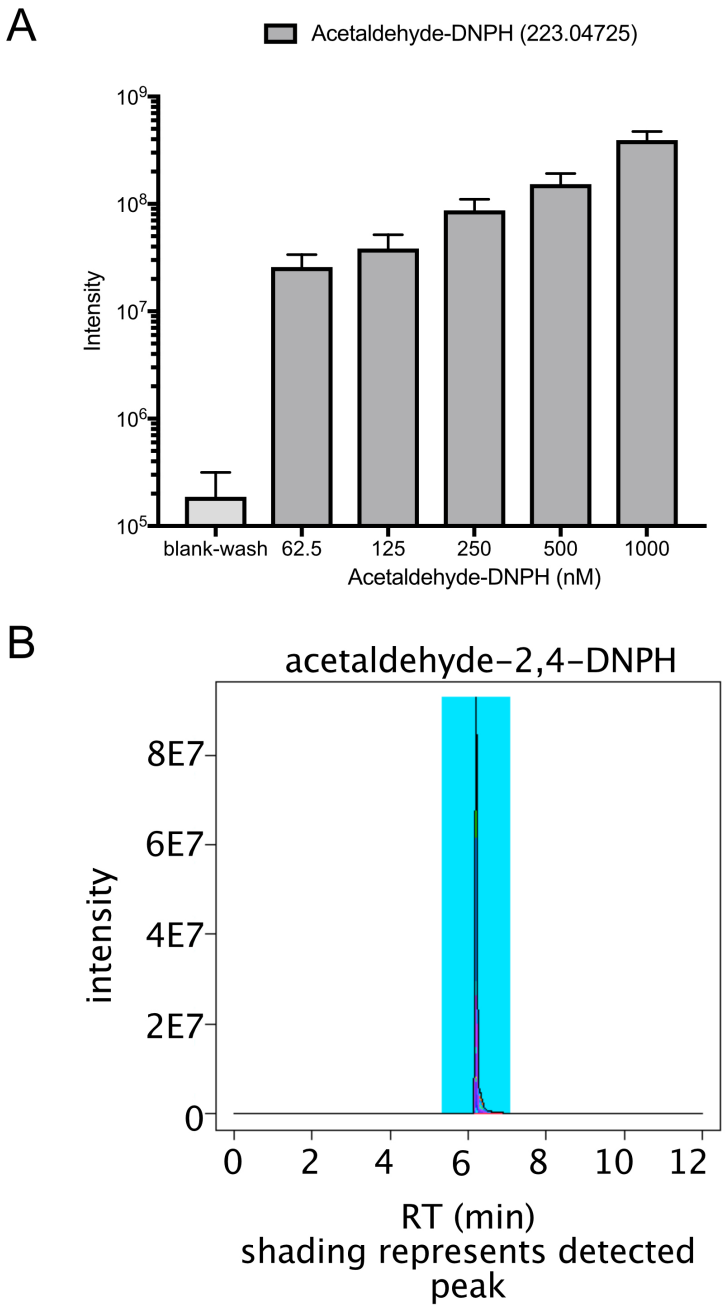

Figure 4.8: **HPLC-MS analysis of Plasma Fortified with Acetaldehyde-2,4-DNPH**

(2% acetonitrile loading conditions)

4.2.4 Triple-Quadrupole MS Based Detection

4.2.4.1 Chromatographic Detection of Acetaldehyde-2,4-DNPHs

Next, acetaldehyde-2,4-DNPH standard was analysed on a Triple-quadrupole system. It is standard for quantitative MS to be performed on a Triple-quadrupole due to their sensitivity and robustness. This is in contrast to discovery, where high-resolution accurate-mass Orbitrap mass spectrometers excel.

4.2.4.2 Tuning on Reference Standard and Synthesised Aldehyde-DNPH Standards

Identification of parent ion for reference standard

To verify the molecular weight of the reference standard for acetaldehyde-2,4-DNPH, a Q1 (survey) scan was performed on 10 ng/mL (45 nM) standard directly injected to the MS and analysed in negative mode (Figure 4.9A). Acetaldehyde-2,4-DNPH is displayed in the mass spectrum, *m/z* 223.2. The $[M-H]^-$ peak verified presence of the parent ion. Expansion of the *m/z* axis range to *m/z* 222.5-223.9 highlighted the peak apex of the parent ion at *m/z* 223.1 (Figure 4.9B).

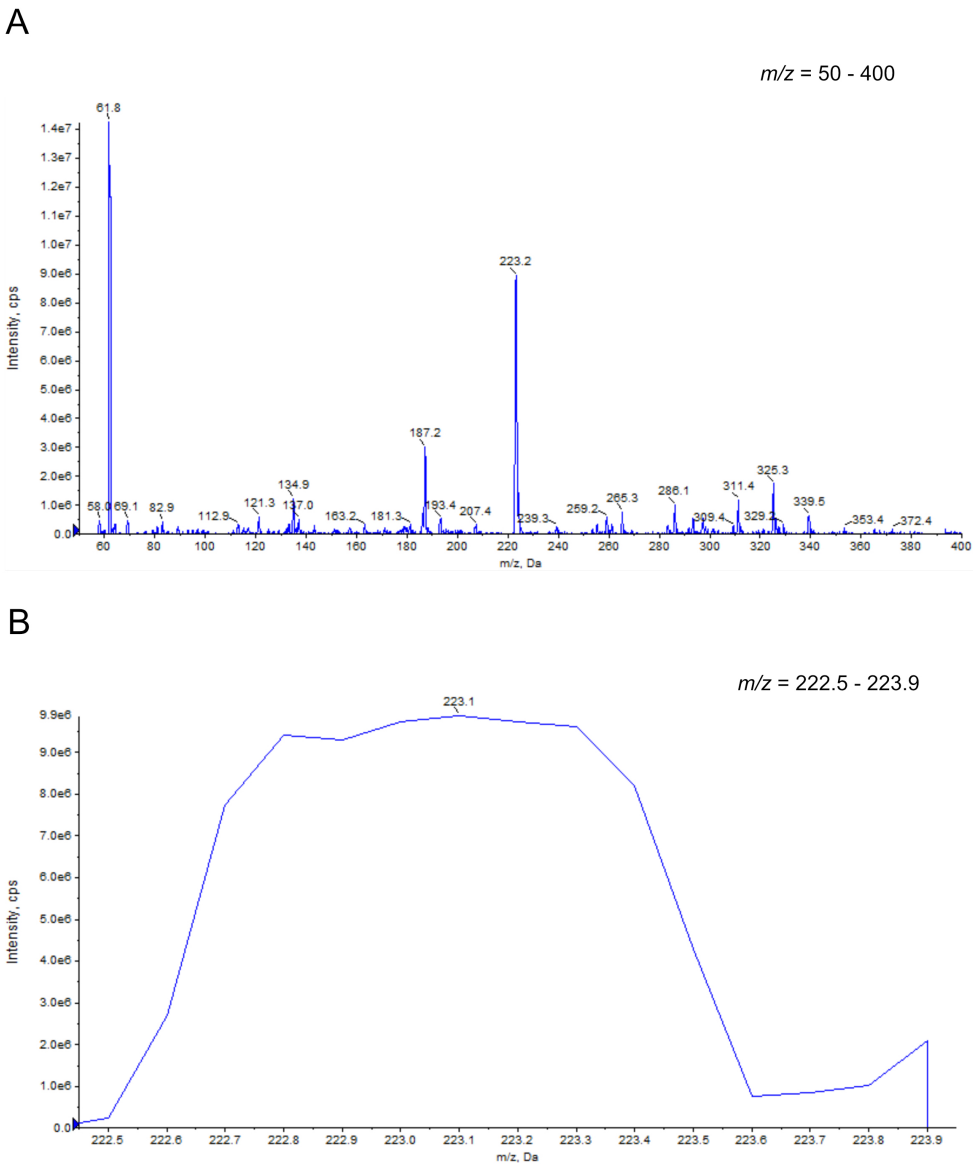

Figure 4.9: **Tuning on Acetaldehyde-2,4-DNPH Standard**

The acetaldehyde-2,4-DNPH reference standard was directly infused to the MS at a concentration of 10 ng/mL (45 nM) in H_2O. **A**. Full-scan mass chromatogram (*m/z* 50-400 amu) of acetaldehyde-2,4-DNPH. **B**. The $[M-H]^-$ parent ion of acetaldehyde-2,4-DNPH observed at *m/z* 223.1. Axis range *m/z* 222.5 - 223.9.

Identification of product ions for pre-synthesised reference standard

The top four product ions from $[M-H]^-$ parent ion *m/z* 223.1 that were identified during tuning are listed in Table 4.2.

Table 4.2: Product Ions from Acetaldehyde-2,4-DNPH Standard $[M-H]^-$ (precursor ion *m/z* 223.1

product ion	*m/z*	CE (*V*)	CXP (*V*)	intensity
1	151.00	-14	-13	62480
2	163.10	-16	-7	54120
3	121.9	-26	-11	52480
4	76.0	-20	-7	47060

collision energy (CE); cell exit potential (CXP).

4.2.5 Aldehyde Derivatisation

In the previous method development steps, optimisation of sample loading conditions and chromatography was performed with aldehyde-2,4-DNPH reference standards. This enabled:

1. establishing a diagnostic ion for each aldehyde derivative.
2. elucidation of optimal HPLC conditions for the derivatives of interest.

Because this method was to be applied to biological samples of blood origin and derivatisation was chosen to improve acetaldehyde detection, the acetaldehyde derivatisation reaction was performed in aldehyde-spiked plasma. This was important for method development because it enables:

1. establishment of the efficiency of derivatisation
2. optimisation of factors controlling the efficiency of derivatisation; temperature, pH, concentration of DNPH.
3. determination of the minimal and maximum limits of detection of aldehyde in plasma matrix.

Ultimately, initiating these method development studies into acetaldehyde derivatisation paves the way for derivatisation of aldehydes in the blood of mice, and specifically, the quantification of aldehydes including acetaldehyde-DNPH with high-resolution accurate-mass LC-MS.

4.2.5.1 Derivatisation of Aldehydes in Water and Plasma Matrices Fortified with Aldehydes

Firstly, the derivatisation reaction of aldehydes with DNPH was tested. Plasma was used as this was the intended sample matrix for acetaldehyde quantification. Water samples spiked with aldehyde were also derivatised in parallel, as a less complex control to address whether anything in the more complex biochemical matrix of deproteinated plasma interfered with the derivatisation reaction and consequent HPLC-MS analysis.

4.2.5.2 UV-Vis Detection of Aldehyde-2,4-DNPH Compounds

To test the success of the derivatisation reaction and address whether aldehyde derivatives were synthesised under the tested conditions, the absorbance of samples at 430 nm was monitored by UV-Vis. To test the suitability of this as an indicator of successful derivatisation, absorbance of serially diluted pre-synthesised acetaldehyde-2,4-DNPH reference standard was measured (Figure 4.10A). Standards were solubilised in acetonitrile but acetonitrile absorbs at a similar wavelength to the aldehyde-2,4-DNPH compounds. A solution to this was to incubate the aldehyde-2,4-DNPH compounds in alkaline conditions by addition of 2M NaOH to the reference standard or reaction mixture. Under alkaline conditions, the absorbance of racetaldehyde-2,4-DNPH reference standard shifted (Figure 4.10A). Increasing concentrations of acetaldehyde-2,4-DNPH were accompanied by relative increases in peak intensity at 430 nm (Figure 4.10B,C). Monitoring the absorbance of acetaldehyde-2,4-DNPH under alkaline conditions at 430 nm could therefore afford confirmation of its presence in derivatised standards and samples and would be utilised to address sample extraction efficiency with solid phase extraction methods.

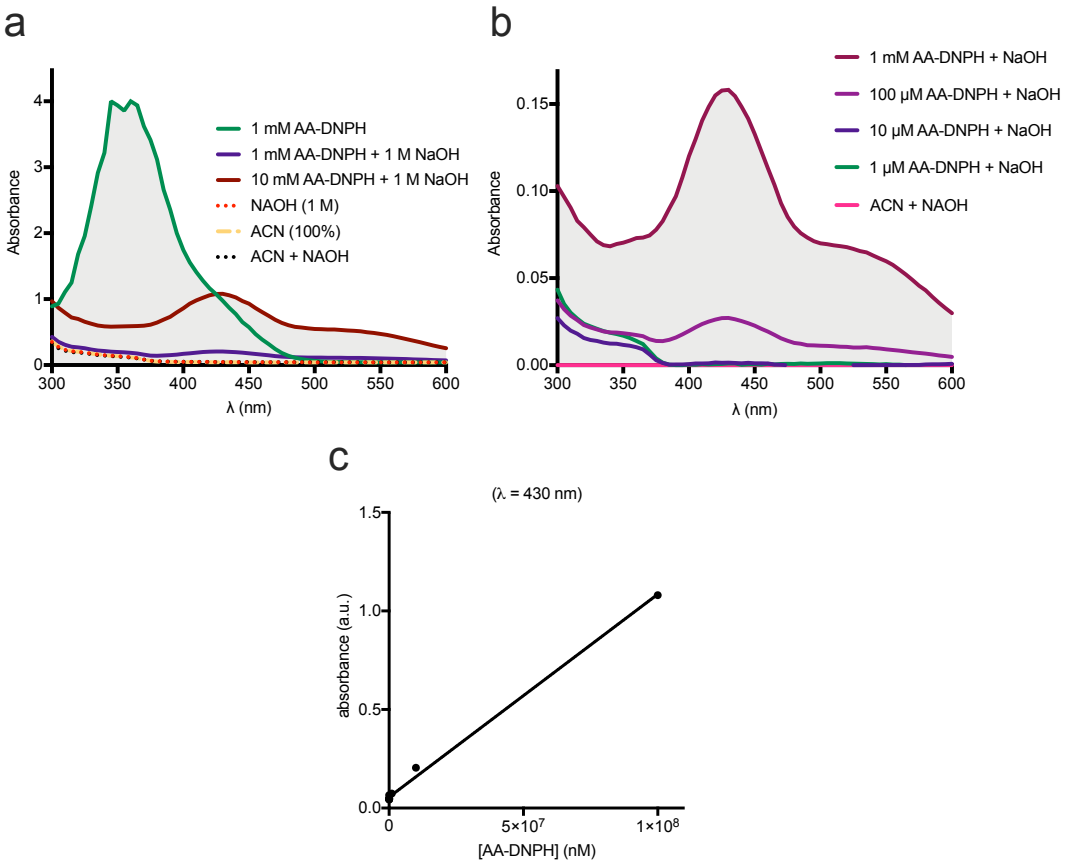

Figure 4.10: **UV-Vis Detection of Acetaldehyde-2,4-DNPH**

Reference standards solubilised in 100% acetonitrile (MeCN). **A**. Absorbance Spectra of acetaldehyde-2,4-DNPH (350-600 nm). **B**. Increasing concentrations of acetaldehyde-2,4-DNPH were accompanied by relative increases in peak intensity at 430 nm. **C**. Standard curve, Concentration of acetaldehyde-2,4-DNPH against absorbance at 430 nm (λ= 430 nm).

4.2.5.3 Extraction of Derivatised Aldehydes

Extraction method

Following the derivatisation reaction, the reaction mixture contained high salt concentrations that are incompatible with MS systems. Although it is possible to divert salt away from the Orbitrap source during loading onto the HPLC, solid phase extraction (SPE) was employed to separate the reaction product from the high-salt reaction mixture (Figure 4.11).

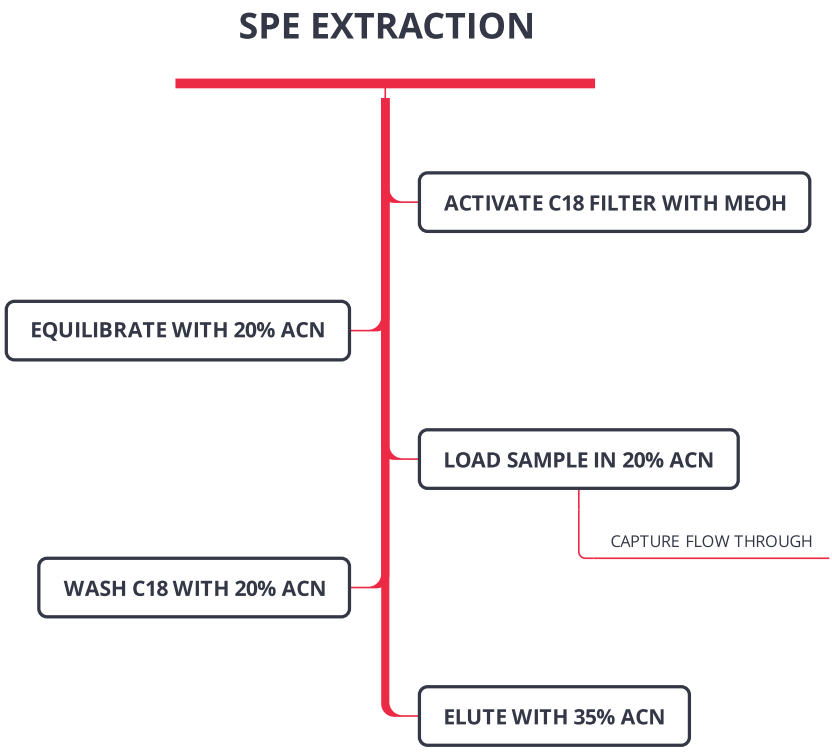

Figure 4.11: **Workflow for Solid Phase Extraction of Derivatised Aldehyde-2,4-DNPHs**

Extraction of acetaldehyde-2,4-DNPH

To test the suitability of SPE for reaction clean-up, reference standards were subjected to clean-up on StageTips containing C18 disks (Rappsilber et al., 2007). Standards were solubilised in different concentrations of acetonitrile (2% and 20%) to determine optimal binding conditions for the standards. Reference standards in both 2% and 20% acetonitrile exhibited good binding to the column and eluted well with 35% acetonitrile (Figure 4.12). The UV-Vis absorbance for reference aldehyde derivative standards was higher for samples dissolved in 20% acetonitrile than 2% acetonitrile. The difference in absorbance could be a result of better solubility and dissolution of aldehyde derivative reference standards in 20% acetonitrile than 2% acetonitrile. Deproteinated samples containing 1 mM acetaldehyde were derivatised in 80-fold molar excess DNPH and formation of the product monitored with UV-Vis (Figure 4.13).

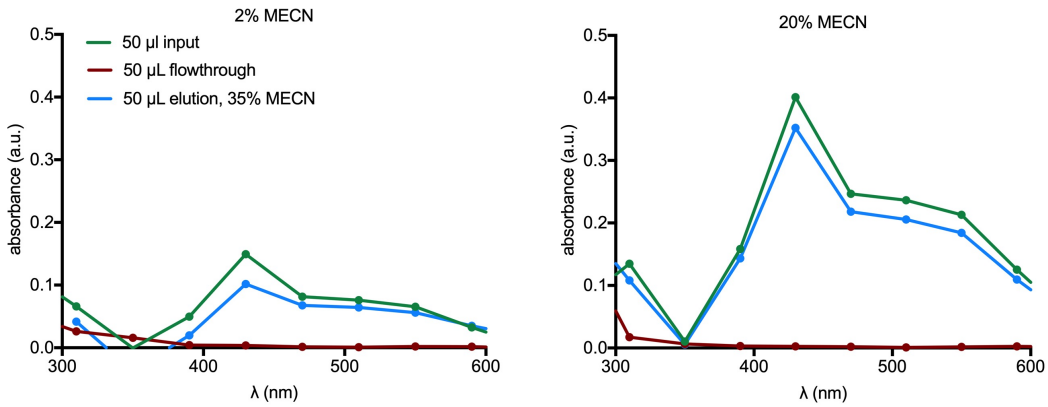

Figure 4.12: **Solid Phase Extraction of 1 mM acetaldehyde-2,4-DNPH Solution with StageTips**

Reference standards solubilised in 2% and 20% acetonitrile (MeCN) were subjected to SPE on C18.

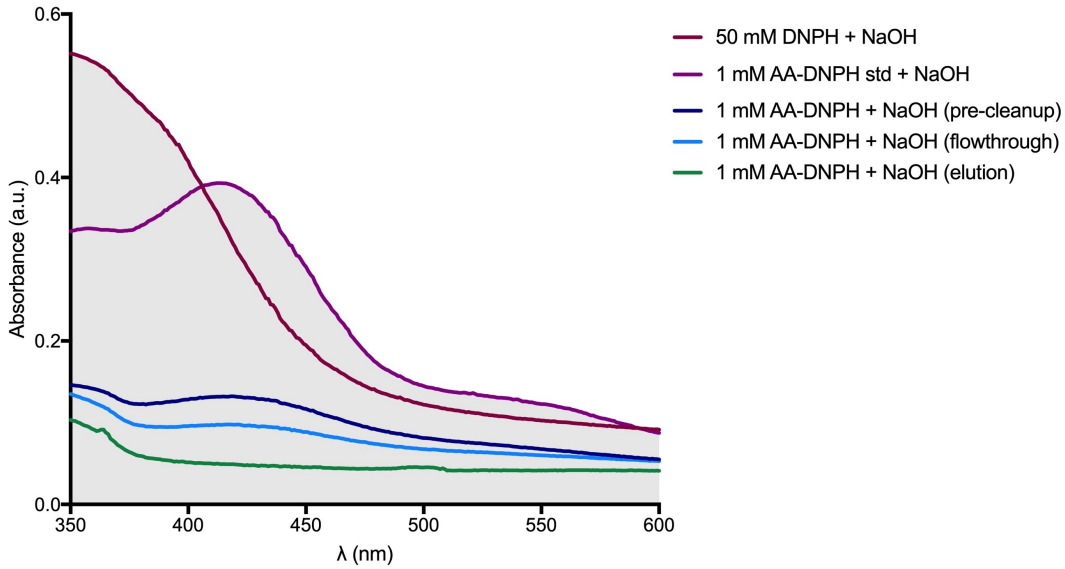

Figure 4.13: **Solid Phase Extraction of Derivatised Acetaldehyde with StageTips**

1 mM acetaldehyde was derivatised with 80-fold molar excess DNPH, reaction products were cleaned-up with SPE on C18 material and resulting product alongside reference standard was solubilised in 20% acetonitrile. Absorbance at 420 nm was assayed under alkaline conditions (2M NaOH, 50 μL: reaction product 50 μL).

4.2.5.4 Identification of Parent Ion for Synthesised Standard

To verify the molecular weight of the freshly synthesised acetaldehyde-2,4-DNPH standard, a Q1 (survey) scan was performed on infused standard using a QTrap 5500 mass spectrometer, operated in negative ion electrospray ionisation (ESI) mode. Acetaldehyde-2,4-DNPH was diluted in mobile phase (water:acetonitrile 4:1, *v/v*). Acetaldehyde-2,4-DNPH is displayed in the mass spectrum at *m/z* 223.1 (Figure 4.14). The presence of the $[M-H]^-$ peak verified the presence of the parent ion as a reporter of the presence of acetaldehyde-2,4-DNPH.

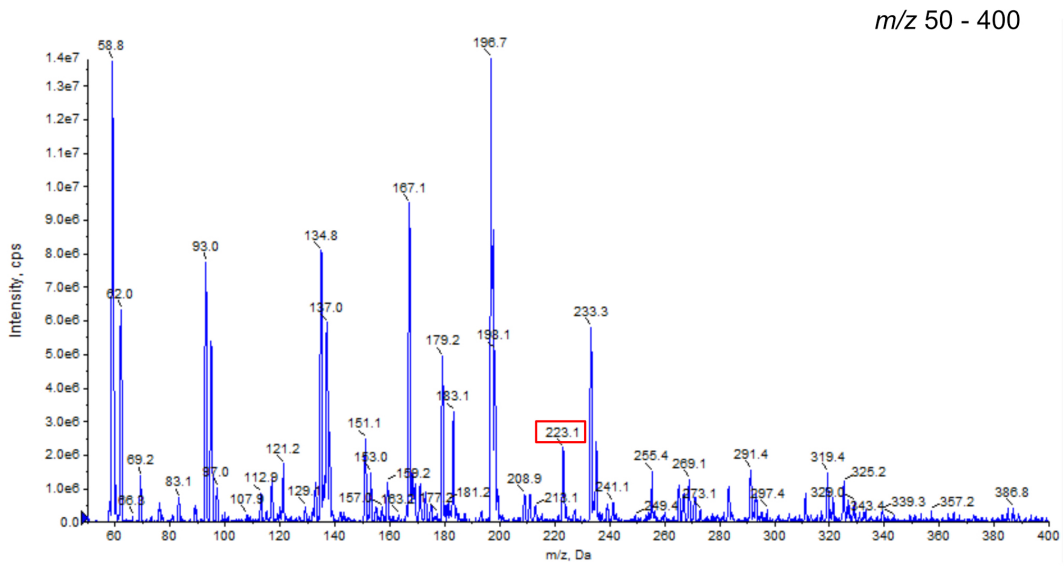

Figure 4.14: **Tuning On Derivatised Acetaldehyde-2,4-DNPH Standard** Derivatised acetaldehyde-2,4-DNPH was directly injected to the MS at a dilution of 1:1000000 in 100% acetonitrile. Full survey scan was performed (*m/z* 50.0-400.0).

4.2.5.5 Identification of Product Ions for Derivatised Acetaldehyde-2,4-DNPH

Acetaldehyde was derivatised through 1:1 (*v/v*) reaction with DNPH solublised in HCL and the reaction proceeded for 1 h at room temperature. The resulting reaction was diluted 1:10000 in H_2O and infused to isolate the $[M-H]^-$ parent ion of acetaldehyde-2,4-DNPH. The $[M-H]^-$ ion with *m/z* 223.1 was observed during full survey scan in the *m/z* range 50.0 - 400.0. The top four transitions from the $[M-H]^-$ parent ion *m/z* 223.1 identified during tuning are listed in Table 4.5.

Table 4.3: Product Ions from Derivatised Acetaldehyde-2,4-DNPH (precursor ion *m/z* 223.1)

product ion	*m/z*	CE (*V*)	CXP (*V*)	intensity
1	151.0	-14	-13	82680
2	122.0	-28	-11	70070
3	59.1	-26	-7	63860
4	76.0	-18	-7	49990

collision energy (CE); cell exit potential (CXP).

4.2.5.6 Tuning on d_4-Labelled Derivatised Acetaldehyde

4.2.5.7 Derivatisation

To evaluate the efficiency and success of derivatisation, it is imperative that derivatisation of an internal standard that is chemically distinct from the analyte of interest is performed. Deuterated acetaldehyde (d_4-acetaldehyde) was chosen as an appropriate internal standard and was subsequently derivatised. Reassuringly the $[M-H]^-$ ion, *m/z* = 227.1 was observed after direct injection of the reaction. Tuning of this for the top four product ions of the $[M-H]^-$ ion is presented in Table 4.4.

Table 4.4: Product Ions from Derivatised d_4-Acetaldehyde-2,4-DNPH (precursor ion *m/z* 227.1)

product ion	*m/z*	CE (*V*)	CXP (*V*)	intensity
1	167.0	-16	17	57100
2	137.0	-26	-15	21430
3	76.0	-20	-7	16210
4	123.0	-28	-9	15640

collision energy (CE); cell exit potential (CXP).

4.2.5.8 Standard Curve: Derivatised Standard

Acetaldehyde was spiked into plasma to a final concentration of 2 mg/mL, derivatised with DNPH in 6N HCL and serially diluted. Ten microlitres of 40, 5 and 2.5 ng/mL solutions were injected onto C18 (400, 50 and 25 pg on column masses, respectively) (Table 4.5). Chromatographic separation of acetaldehyde-2,4-DNPH was monitored with the *m/z* 223>122 transition (Figure 4.15A). Plotting of analyte relative concentration (2.5-40 ng/mL, $\approx$ 10-180 nM) against peak area counts for the transition *m/z* 223>122 to generate a standard curve demonstrated a linear relationship between concentration and peak intensity (Figure 4.15B).

Table 4.5: Detection of Acetaldehyde-2,4-DNPH Transition *m/z* 223>122 in Plasma Spiked with Acetaldehyde and Derivatised with DNPH

run order	type	DNPH	peak area	[acetaldehyde] (ng/mL)	retention time (min)
1	solvent blank		2480	0.00	3.49
2	double blank		25000	0.00	3.49
3	standard	✓	46800	0.00	3.49
4	standard	✓	61400	2.50	3.48
5	standard	✓	76400	5.00	3.48
6	standard	✓	376000	40.0	3.47
7	solvent blank		517	0.00	3.47

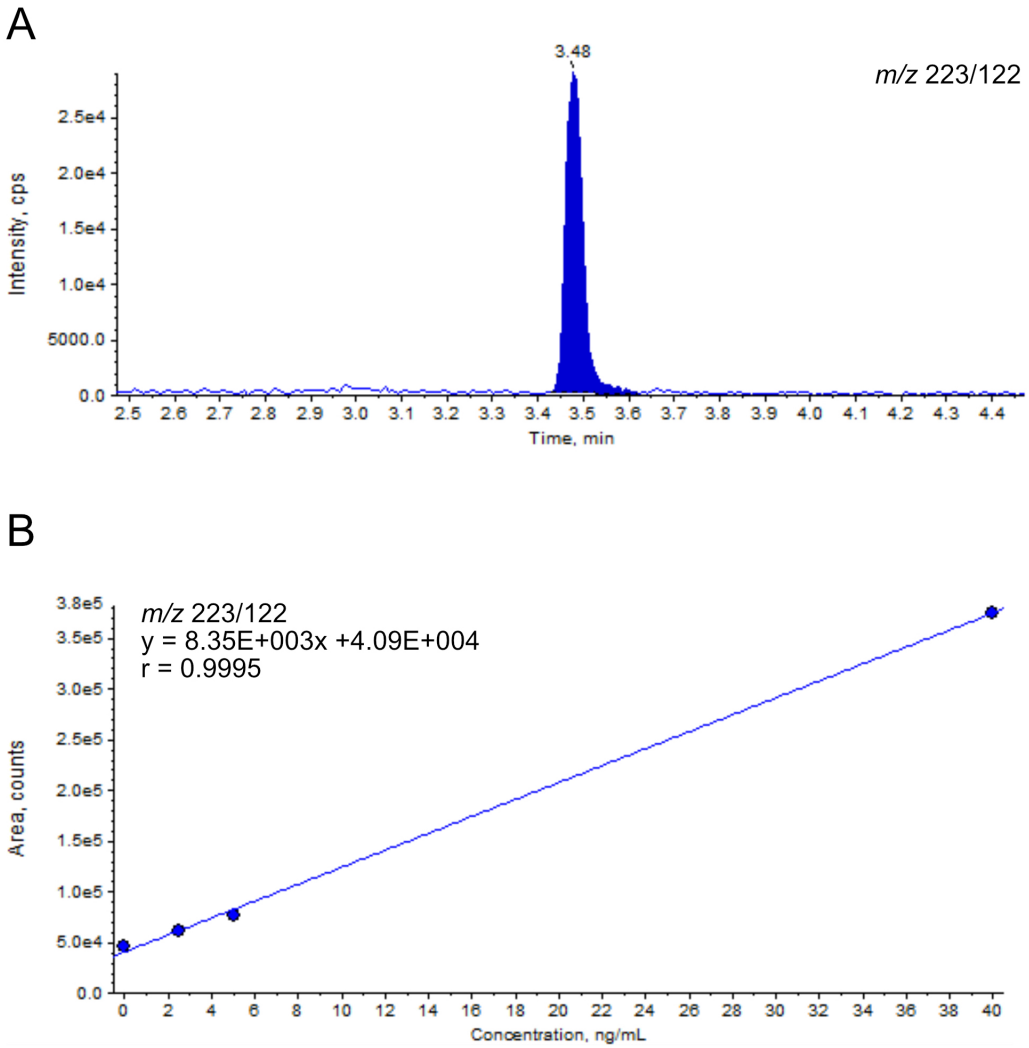

Figure 4.15: **Standard Curve for Derivatised Acetaldehyde-2,4-DNPH**

4.2.5.9 Derivatisation of Acetaldehyde and d_4-Acetaldehyde

Derivatisation

Next, derivatisation of acetaldehyde alongside a deuterated isotope was performed. Both acetaldehyde and the deuterated isotope, d_4-acetaldehyde (internal standard) at equal concentrations of 4 mg/mL were derivatised in a 1:1 (*v/v*) reaction with 20 mg/mL DNPH in 6N HCL at RT for 1 h at a final reaction volume of 200 μL.

Chromatography and MS Detection

The resulting reaction mixture was diluted 1:10000 in H_2O to reduce the peak intensity and was separated using column and gradient settings indicated in Table 4.6. Tuning conditions that were used for analysis of the acetaldehyde-2,4-DNPH and d_4-acetaldehyde-2,4-DNPH in these samples are displayed in Table 4.7. Samples, 10 μL were injected and Multiple Reaction Monitoring (MRM) for transitions of derivatised acetaldehyde (*m/z* 223.0>59.1, 223.0>76.0, 223.0>151.0, 223.0>122.0) and derivatised d_4-acetaldehyde (*m/z* 227.1>76.0, *m/z*227.1>123.0, *m/z*227.1>137.0, *m/z*227.1>167.0) was used to detect the derivatised aldehydes (Figure 4.16, Figure 4.17).

Derivatised acetaldehyde and d_4-acetaldehyde were analysed for the tuned transitions that correspond to acetaldehyde-2,4-DNPH (*m/z* 223.0) (Table 4.7, Figure 4.16). The resulting chromatograms indicate peaks for each ion transition, confirming their use as quantitative ions. Reassuringly, no peaks were observed in samples containing d_4-acetaldehyde and no acetaldehyde. Transition *m/z* 223.0>76.0 was chosen as the major quantitative ion to be taken forwards due to its high peak intensity and distinctive peak. When the same derivatised samples were analysed for the presence of the tuned transitions for d_4-acetaldehyde-2,4-DNPH (*m/z*227.1)

(Table 4.7, Figure 4.17), the transition *m/z* 227.1>76.0 was selected as this exhibited a high-intensity peak with no signs of ion suppression as with the other transitions, *m/z* 227.1>167.0 and *m/z* 227.1>137.0. Reassuringly, peaks for the transition *m/z* 227.1>76.0 that correspond to d_4-acetaldehyde-2,4-DNPH were not present in the acetaldehyde-only containing samples and were at minimal ($\approx$ 300) intensity in the mobile phase blank.

Table 4.6: Chromatographic Gradient on ACQUITY C18

Retention (min)	Flow (mL/min)	%A	%B	Curve
1.5	0.4	75	15	5
2.00	0.4	15	85	5
5.00	0.4	15	85	5
5.50	0.4	85	15	5
7.50	0.4	85	15	5

Buffer A, MS-grade water; Buffer B, acetonitrile.

Gradient flow rate = 0.4 mL/min

Column temp = 45°C

Column Type = Waters ACQUITY UPLC HSS T3 Column, 100Å, 1.8 μm, 2.1 mm X 150 mm.

Table 4.7: Tuning Conditions for Analysis of Hydrazone Derivatives of Acetaldehyde and d_4-Acetaldehyde

Analyte	Precursor ion (*m/z*)	Product ions (*m/z*)	Time (ms)	CE (*V*)	CXP (*V*)	DP (*V*)
AA-2,4-DNPH	223.000	223.000	50.0	-5.000	-6.000	-60.000
	223.000	151.000	50.0	-14.000	-13.000	-60.000
	223.000	122.000	50.00	-28.000	-11.000	-60.000
	223.000	59.100	50.0	-26.000	-7.000	-60.000
	223.000	76.000	50.0	-18.000	-7.000	-60.000
d_4-AA-2,4-DNPH	227.000	227.000	50.0	-5.000	-15.000	-90.000
	227.000	167.000	50.0	-16.000	-17.000	-90.000
	227.000	137.000	50.0	-26.000	-15.000	-90.000
	227.000	76.000	50.0	-20.000	-7.000	-90.000
	227.000	123.000	50.0	-28.000	-9.000	-90.000

Gradient flow rate = 0.4 mL/min, Column temp = 45°C, Column Type = Waters ACQUITY UPLC HSS T3 Column, 100Å, 1.8 μm, 2.1 mm X 150 mm. Ionisation Parameters; Turbo Spray. Curtain Gas, 40.00; Collision Gas, Medium; IonSpray Voltage (IS), -4500; Temperature, 500.0; Ion Source Gas 1, 40.00; Ion Source Gas 2, 60.00. Collision energy (CE); Voltage (V); A1 (acetaldehyde-2,4-DNPH); d_4-A1 (d_4-acetaldehyde-2,4-DNPH); Collision cell exit potential (CXP); De-clustering potential (DP).

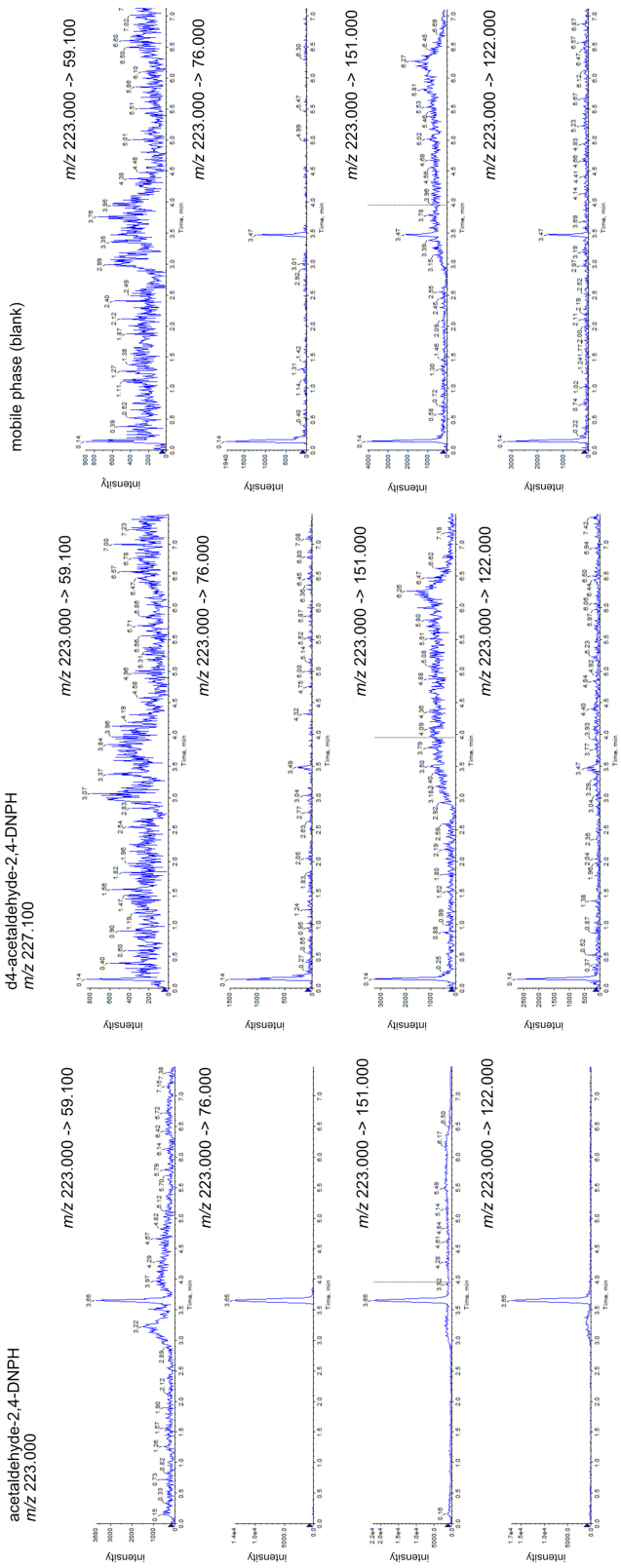

Figure 4.16: **Extracted Ion Chromatogram for *m/z* 223.0 in Derivatised Samples**

Acetaldehyde-2,4-DNPH, d_4-acetaldehyde-2,4-DNPH and blank (mobile phase). Multiple Reaction Monitoring (MRM) for transitions from the 223.0 $[M\text{-}H]^-$ parent ion of acetaldehyde-2,4-DNPH.

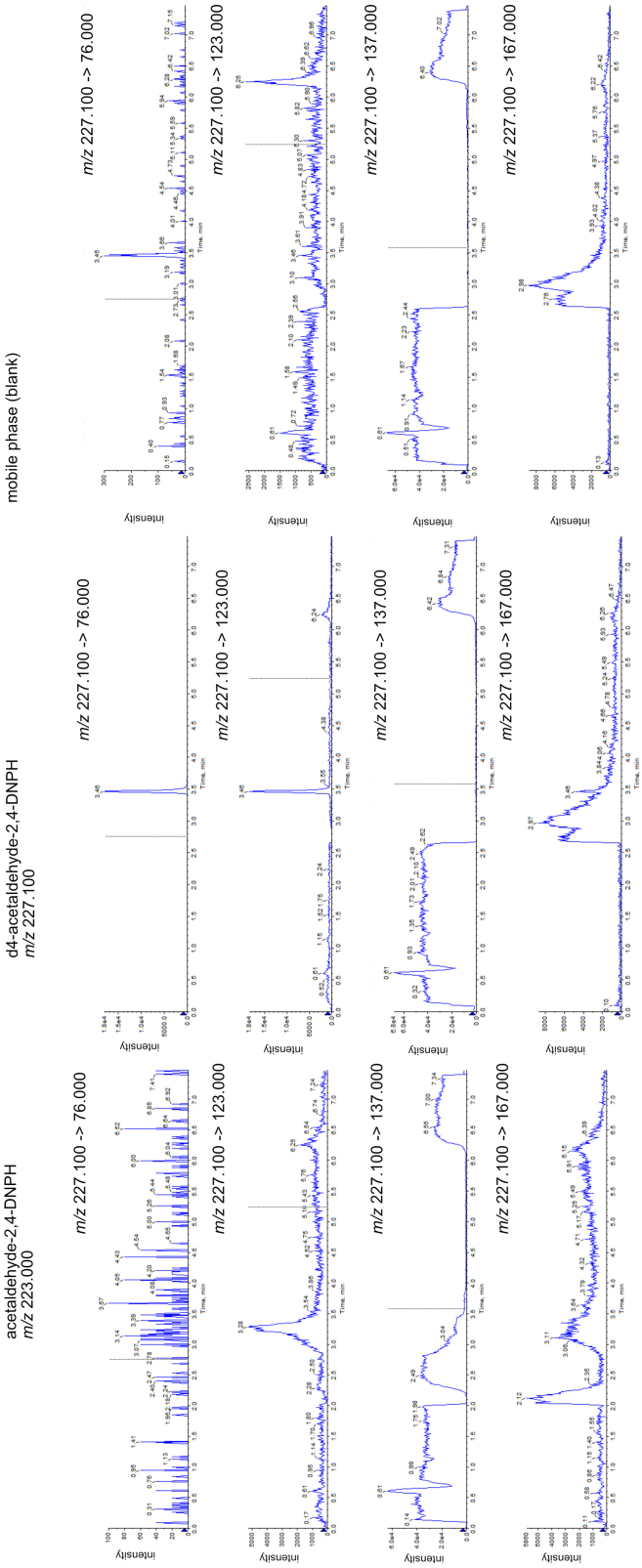

Figure 4.17: **Extracted Ion Chromatogram for *m/z* 227.1 in Derivatised Samples**

Acetaldehyde-2,4-DNPH, d_4-acetaldehyde-2,4-DNPH and blank (mobile phase). Multiple Reaction Monitoring (MRM) for transitions from the 223.0 $[M\text{-}H]^-$ parent ion of d_4-acetaldehyde-2,4-DNPH.)

4.2.5.10 Acetaldehyde-2,4-DNPH Standard Curve

To test the derivatisation of different concentrations of acetaldehyde, 100 μL serial dilutions of acetaldehyde starting at 4 mg/mL alongside 100 μL of 4 mg/mL internal standard, d_4-acetaldehyde were derivatised with 100 μL of 20 mg/mL DNPH in 6N HCL at room temperature for 1 h in a total reaction volume of 300 μL. Reactions were diluted 1:10000 in H_2O to a final volume of 200 μL and 10 μL injected on column, resulting in an on-column mass of 13 ng - 65 pg derivatised aldehyde and 13 ng mass of derivatised d_4-acetaldehyde analysed. Detection of the ion transitions *m/z* 223>76, *m/z* 227>76 (Figure 4.18) were used to generate a standard curve (Table 4.8, Figure 4.19).

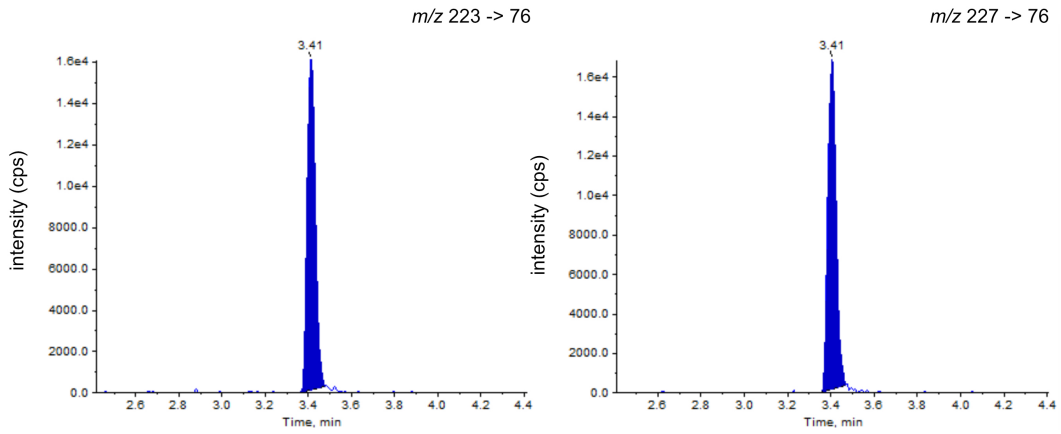

Figure 4.18: **Extracted Ion Chromatogram for Ion Transitions of Acetaldehyde-2,4-DNPH and d_4-Acetaldehyde-2,4-DNPH**
Extracted Ion Chromatogram for *m/z* 227>76 transition of d_4-acetaldehyde-2,4-DNPH.

Table 4.8: Derivatised Standard Curve

	AA			**d_4-AA**			
sample	amount (ng)	peak area (cts)	peak height (cps)	peak area (cts)	peak height (cps)	accuracy (%)	calc. amount (ng)
solvent blank (H_2O)	0	0	0	0	N/A	N/A	
standard d_4, 0.4 mg/mL	0	187	236	23800	9240	N/A	-
standard d_4, 4 mg/mL	0	0	0	63000	25400	N/A	No Peak
AA-DNPH, 1 mg/mL	3.25	15300	5580	64100	24800	94.3	-
AA-DNPH, 2 mg/mL	6.5	87700	34200	160000	60900	108	-
AA-DNPH, 4 mg/mL	13	42800	16000	43700	17000	97.2	-

Gradient flow rate = 0.4 mL/min, Column temp = 45°C

Column Type = Waters ACQUITY UPLC HSS T3 Column, 100Å, 1.8 μm, 2.1 mm X 150 mm.

Counts per second (cps), acetaldehyde (AA), counts (cts). calculated (calc.).

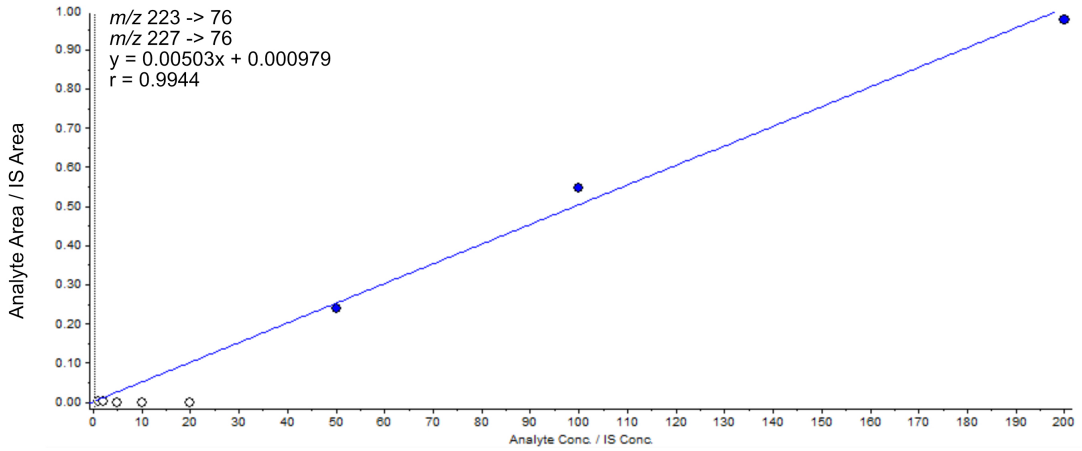

Figure 4.19: **Standard Curve for Transition *m/z* 227>*m/z* 76 of Derivatised Acetaldehyde**

Standard curve generated from normalised Peak Area of derivatised acetaldehyde and d_4-acetaldehyde. Transition *m/z* 227>*m/z* 76.

4.2.5.11 Effect of pH on Aldehyde Derivatisation

The composition of solvents used to solubilise DNPH were tested for their effect on aldehyde derivatisation. D_4-acetaldehyde was serially diluted and derivatised as detailed in Chapter 2. DNPH, 20 mg/mL was solubilised in four different solvents:

(i) 6N HCL

(ii) 0.1N HCL

(iii) acetonitrile:0.001N HCl (aq) (3:2 *v/v*), pH 3

(iv) acetonitrile:water (3:2 *v/v*), pH 6

The reaction, 300 μL was diluted 1:10000 in H_2O and 10 μL was injected onto column (Figure 4.20). Resulting chromatographs indicate that both 6N HCL and acetonitrile:0.001N HCl (aq) (3:2 *v/v*), pH 3 afforded efficient derivatisation and detection of d_4-acetaldehyde.

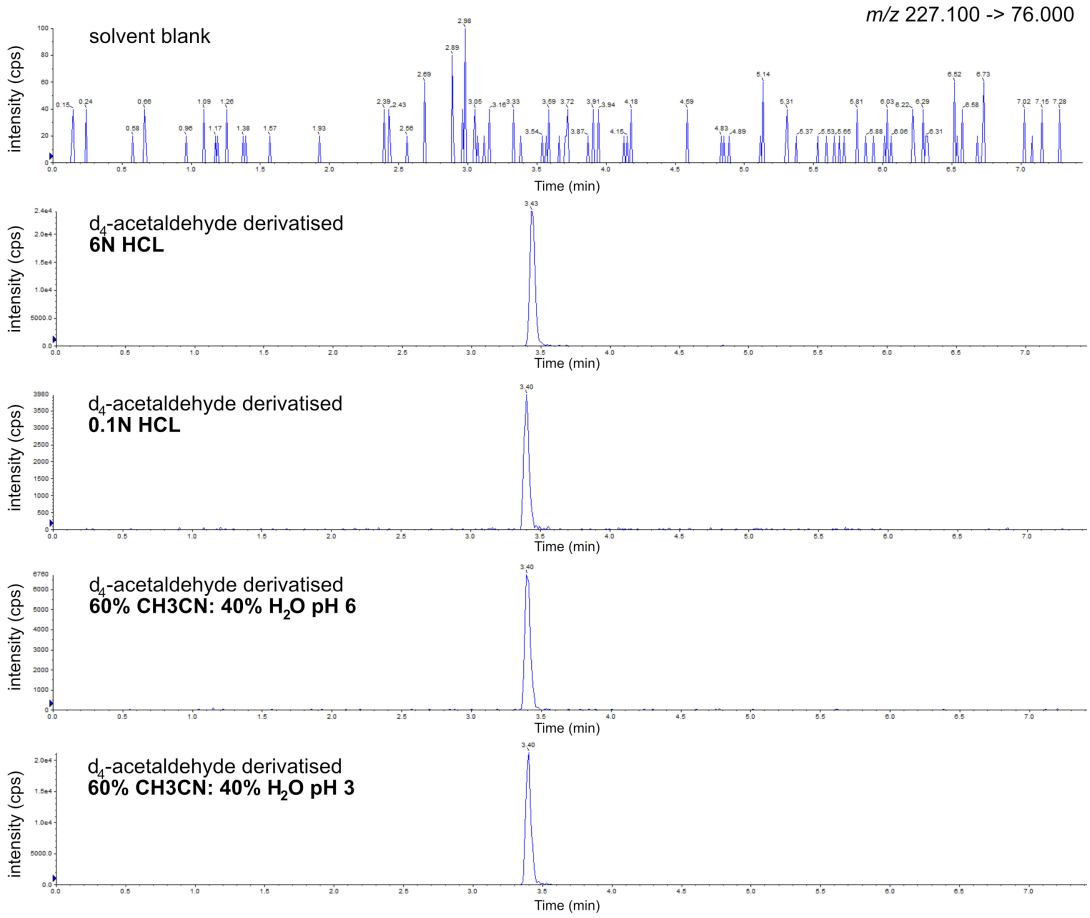

Figure 4.20: **Derivatisation of d_4-Acetaldehyde with varying pH**
Peak intensity of the *m/z* 227.100>76.000 transition was measured in samples derivatised with DNPH in 6N HCL; 0.1N HCL; 60% acetonitrile : 40% 0.001 N HCL, pH 3; or 60% acetonitrile : 40% water, pH 6.

4.3 Summary

This chapter initiated method development for the derivatisation and HPLC-MS analysis of aldehydes in plasma. To increase throughput and enable detection of multiple aldehydes in plasma matrices, improving on the selectivity of ELISA-based methods for acetaldehyde detection, a sample preparation and HPLC-MS method to derivatise and detect acetaldehyde in blood plasma was set up. Derivatisation with DNPH was employed to generate aldehyde-2,4-DNPHs with enhanced stability and molecular weight for HPLC-MS detection. I explored a broader approach to aldehyde quantitation with Orbitrap LC-MS that opened up potential to explore the metabolism of multiple aldehydes during a single MS run. This enabled me to follow three aldehydes during chromatographic set up and paired with the derivatisation approach, yields opportunity to address aldehyde biology in a broader context, focusing on quantification of several aldehydes in a biological sample, rather than targeted analysis of a single compound.

Chapter 5

ALDH-Mediated Signalling Determines an Extensive Gene Expression Network in Melanoma

5.1 Introduction

5.1.1 Overview

ALDH enzymes are experimental markers of cell populations with cancer-initiating ability and development of chemoresistance. Although ALDH activity is widely reported as a marker of these properties, it is clear that ALDH has a functional role in establishing cancer-initiation and development of chemoresistance. For example, subpopulations of ALDH1A3^{high} cells have been identified in melanoma (Boonyaratanakornkit et al., 2010; Luo et al., 2012), ALDH1A3 is upregulated in melanoma cells when compared to melanocytes (Pérez-Alea et al., 2017) and is also upregulated following treatment of melanoma with BRAF and MEK inhibitors (Sarvi et al., 2018). Considering that ALDH1A3 levels are elevated during tumorigenesis and upon development of resistance to current targeted chemotherapeutics, ALDH1A3 is an attractive candidate for the development of targeted inhibitors.

The 5-nitrofuran, nifuroxazide is an inhibitor of ALDH1A3 enzymatic activity *in vitro* and exposure of the A375 melanoma cell line to nifuroxazide or DIMATE selectively depletes cells that express high levels of ALDH (ALDH1A3^{high}), as demonstrated by ALDEFLUOR™ staining (Sarvi et al., 2018; Pérez-Alea et al., 2017). Although ALDH1A3 is an appealing target for the development of chemotherapeutics, the functional advantage to cells of ALDH1A3-expression in chemoresistance has not been determined.

5.1.2 Aims

The Patton laboratory has previously demonstrated that ALDH1A3 is targeted by nifuroxazide in melanoma, selectively targeting ALDH1A3^{high} melanoma populations. I hypothesised that the ALDH1A3^{high} population would possess a gene expression profile distinct from ALDH1A3^{low} and ALDH1A3^{null} populations and that gene expression would be dependent upon retinoic acid signalling. This results chapter explores the aim to understand the consequence of ALDH1A3 expression on cellular transcriptional profiles. To this end, the experiments in this chapter were performed under two objectives:

1. Identify key transcriptional programmes of ALDH1A3^{high}, ALDH1A3^{low} and ALDH1A3^{null} populations

   To achieve this objective, A375 melanoma cells were isolated on the basis of their ALDH-expression. ALDH1A3^{high} and ALDH1A3^{low} cells were analysed for transcriptional expression alongside an A375 cell line null for ALDH1A3, A375-ALDH1A3^{C21}.

2. Identify genes and transcriptional signatures that are dependent upon ALDH1A3 activity to (i) decipher the differences between Aldefluor™-sorted and ALDH1A3-null populations and (ii) establish whether ALDH1A3 expression is essential for retinaldehyde and retinoic acid transcriptional signalling in BRAFV600E melanoma.

5.2 Results

5.2.1 Preparation of ALDH Subpopulations for mRNA-Seq

To characterise functional advantages of ALDH1A3 expression in melanoma subpopulations, first I wanted to determine differences in the genetic landscape of ALDH1A3 high and ALDH1A3 low expressing cells. To do this, I analysed the ALDH-expression of A375 melanoma lines (Figure 5.1A) with the ALDEFLUOR™ assay and sorted the top and bottom 5% of cells with ALDH activity using flow cytometry.(Figure 5.1B). Upon flow cytometry analysis of the A375 population, a strong ALDEFLUOR™ signal was revealed, with successful inhibition of ALDEFLUOR™-staining in the ALDEFLUOR™- and DEAB (ALDH inhibitor)- treated control. Ablation of ALDH1A3 activity in ALDH1A3^{C21} resulted in a characteristic shift in ALDEFLUOR activity that has been previously reported (Sarvi et al., 2018). Total RNA was extracted from the sorted cell populations and prepared for RNA sequencing (Figure 5.1B).

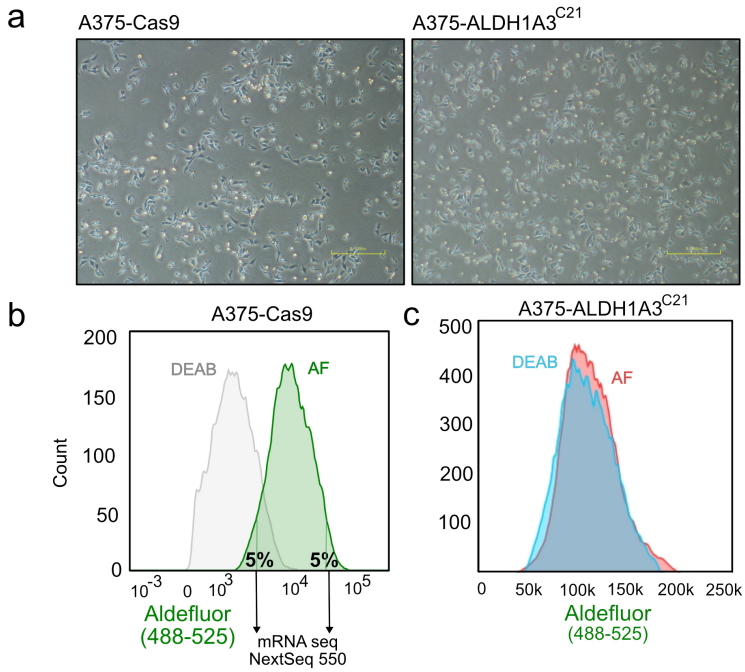

Figure 5.1: **A375 CRISPR Cell Lines**

A. Human melanoma (A375) cell lines, ALDH1A3-Cas9 and ALDH1A3-null CRISPR clone, A375-ALDH1A3^{C21}.

B. A375-Cas9 cell line stained with ALDEFLUOR™ with or without cotreatment with the ALDH inhibitor, DEAB. The top and bottom 5% of ALDEFLUOR™-stained cells were cell sorted. Messenger RNA was extracted from the top and bottom 5% and an unsorted sample control sequenced.

C. The A375-ALDH1A3^{C21} CRISPR clone has minimal uptake of ALDEFLUOR™ reagent. ALDEFLUOR™ staining of the ALDH1A3-null cellular population overlaps with DEAB-treated controls. Abbreviations; DEAB, N,N-diethylaminobenzaldehyde; AF, ALDEFLUOR™.

5.2.2 ALDH^{high} and ALDH^{low} Populations Exhibit Different Gene Expression Patterns

Once total mRNA NextSeq 550 sequencing was performed, reads were aligned to the genome and processed normalised counts were processed through analysis of differentially expressed genes (DEG) (Chapter 2). The DEG list was sorted according to p-value and false discovery rate (FDR) adjusted p-value (padj, q), using a 5% cut off threshold for each. Using both the p-value and adjusted p-value (padj, q), a total of 2,236 genes of the 57,914 total mapped RNAs had expression values that were statistically significant. These thresholds were applied because when measuring gene expression levels of thousands of genes in a small sample set (N=3), the q value takes into account the FDR and adds another level of stringency to the analyses. Resulting differentially expressed genes in the ALDH^{high} and ALDH^{low} populations are represented with a volcano plot (Figure 5.2). Gene plots highlighted in green represent those genes that are more highly expressed in ALDH1A3^{high} populations than ALDH1A3^{low}. Grey plots highlight genes that are more highly expressed in ALDH1A3^{low} populations than ALDH1A3^{high}. Gene labels indicate the most differentially expressed genes when using a highly stringent P value cut off below 1E-23.

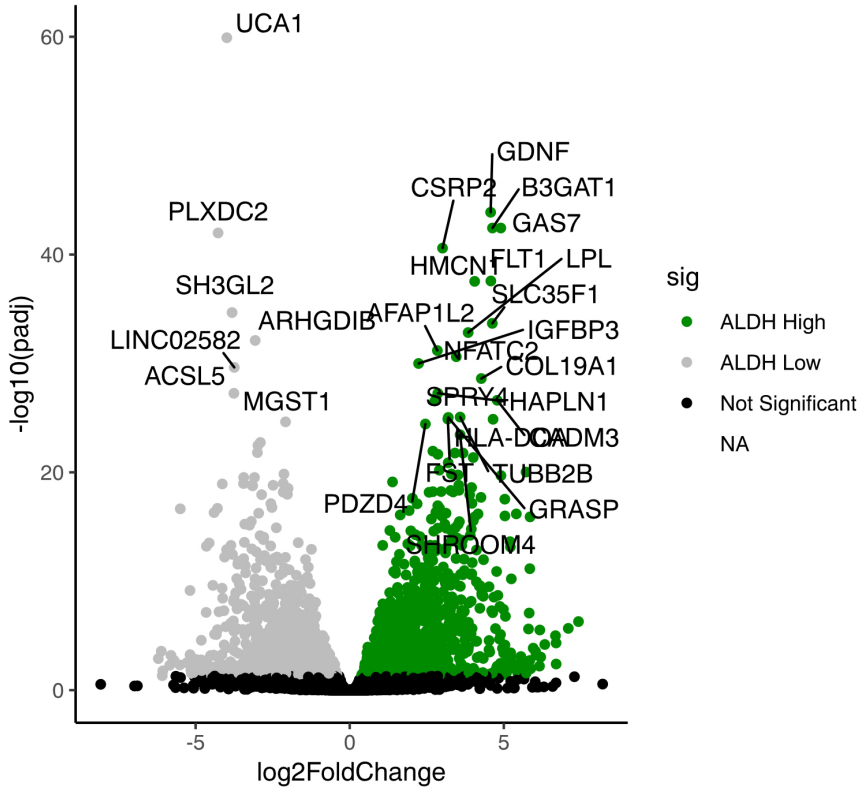

Figure 5.2: **Differential Expression Analysis of ALDH1A3^{high} and ALDH1A3^{low} Cells**

Volcano plot representation of DEG analysis. Gene plots highlighted in green represent those genes that are more highly expressed in ALDH1A3^{high} populations than ALDH1A3^{low}. Grey plots highlight genes more highly expressed in ALDH1A3^{low} populations than ALDH1A3^{high}. Gene labels indicate the most differentially expressed genes that have an adjusted P value < 1E-23. Non significant genes are labelled in black and have P>0.05.

5.2.3 ALDH^{high} and ALDH^{low} Populations Express Contrasting Networks of Genes

To investigate differential expression of pathways relevant in melanoma between ALDH1A3^{high} and ALDH1A3^{low} cells, performed gene set enrichment analysis (GSEA) was performed using gene lists that were curated from the literature and cancer genome databases, including The Cancer Genome Atlas (TCGA). This analysis revealed which pathways are differentially expressed in melanoma cells that exhibit high and low levels of ALDH activity. Eight out of twenty two gene sets passed thresholding (Figure 5.3). Given that these gene sets covered a wide range of cancer specific pathways, it was interesting to observe that clusters especially associated with *MITF*^{low} expression (*MITFlow* neurodevelopmental, development) and neural development (Rambow-NCSC Cluster, WIKIP Neural Crest Differentiation). Not only were these neural gene sets enriched in the ALDH high population, but complementary gene sets including GO: Peripheral Nervous System Development and GO: Glial Cell Differentiation gene sets were discovered in the top 10 differentially expressed gene sets when Gene Ontology (GO) Analysis was performed.

The Microphthalmia-associated transcription factor, *MITF* is a determining factor in melanocyte development and has been shown to be regulated by SOX10 which binds at the *Mitf* promoter to activate transcription (Goding, 2000). Expression of *Mitf* is essential for the commitment to the melanocyte lineage from neural crest precurors during development (Goding, 2000). MITF-low cells have elevated motile and invasive capacity, have a higher tumour-formation capacity in xenograft assays and arise spontaneously in MITF-high cell cultures (Cheli et al., 2011). Further analysis of *MITF* target genes in high and low ALDH populations revealed differential expression of *SLC16A6, MCOLN3, PSCA, CDKN2A, BCAN* and *ABCC2*. The A375 cell line is *MITF*-low and is resistant to *MITF* silencing (Wang et al., 2018),

never-the-less, *MITF* targets are differentially expressed between ALDH^{high} and ALDH ^{low} cells.

With a focus on genes involved during neural crest and melanocyte differentiation, *GAS7* was a promising candidate for follow up from differential expression of ALDH-high and ALDH-low cells 5.2. Although GAS7 is not prognostic in melanoma (Human Protein Atlas), *GAS7* is a key gene described by Rambow et al. (2018) is a key set of neural crest stem cell (NCSC) genes that comprise a deterministic signature for minimal residual disease. Minimal residual disease describes the cells which remain during chemotherapy and which eventually lead to tumour relapse. Analysis of this NCSC signature (Figure 5.5) revealed a stark contrast between ALDH high and low populations. Twenty one NCSC-determinant genes were expressed at higher levels in ALDH high cells (Figure 5.5). This is a critical finding that is highly relevant to uncovering the function of ALDH1A3 in the ALDH high, tumour-initiating and chemo-resistant population.

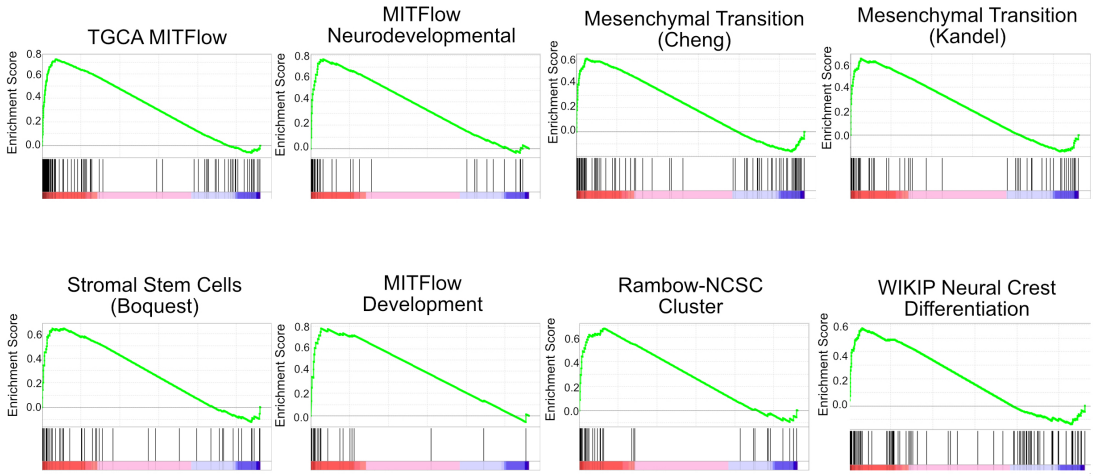

	Gene Set	SIZE	NES	FDR q-val
1	TCGA MITFLOW	107	2.1	0
2	MITFLOW NEURODEVELOPMENTAL	35	1.8	0
3	CHENG- MESENCHYMAL TRANSITION	91	1.7	0.012
4	KANDEL - MESENCHYMAL TRANSITION	61	1.7	0.012
5	BOQUEST-STROMAL STEM CELLS	53	1.7	0.01
6	MITFLOW DEVELOPMENT	21	1.7	0.009
7	RAMBOW-NCSC CLUSTER	36	1.6	0.01
8	WIKIP NEURAL CREST DIFFERENTIATION	100	1.6	0.009
9	TIROSH MITF	95	1.6	0.013
10	MITFLOW NEURONAL	42	1.5	0.038
11	LUO - MELANOMA CSC SUBSET	84	1.5	0.047
12	JONSSON-PROLIFERATIVE	36	1.4	0.062
13	PLOPER -LYSOSOMAL GENES WITH CLEAR ELEMENT	59	1.3	0.153
14	HOEK PROLIFERATIVE	50	1.3	0.165
15	MITF NOVEL TARGET GENES	64	1.2	0.187
16	TAUBE - EMT CORE	82	1.1	0.478
17	MITF TARGET GENES COMBINED	77	1	0.497
18	STAT3 TARGETS	40	1	0.512
19	TIROSH AXL	93	1	0.58
20	MITF TARGET GENES	21	0.9	0.644
21	TCGA IMMUNE	98	0.9	0.637
22	JONSSON-PIGMENTATION	83	0.9	0.611

Figure 5.3: **GSEA of Melanoma-Specific Transriptional Pathways**
Gene enrichment plots highlight pathways that are statistically differentially expressed between high and low ALDH-expressing melanoma. The table (below) reports gene set against the size of the gene set, normalised enrichment score (NES) and FDR q-value. Statistically enriched gene sets were stringently refined by using a FDR cut-off less than 0.01.

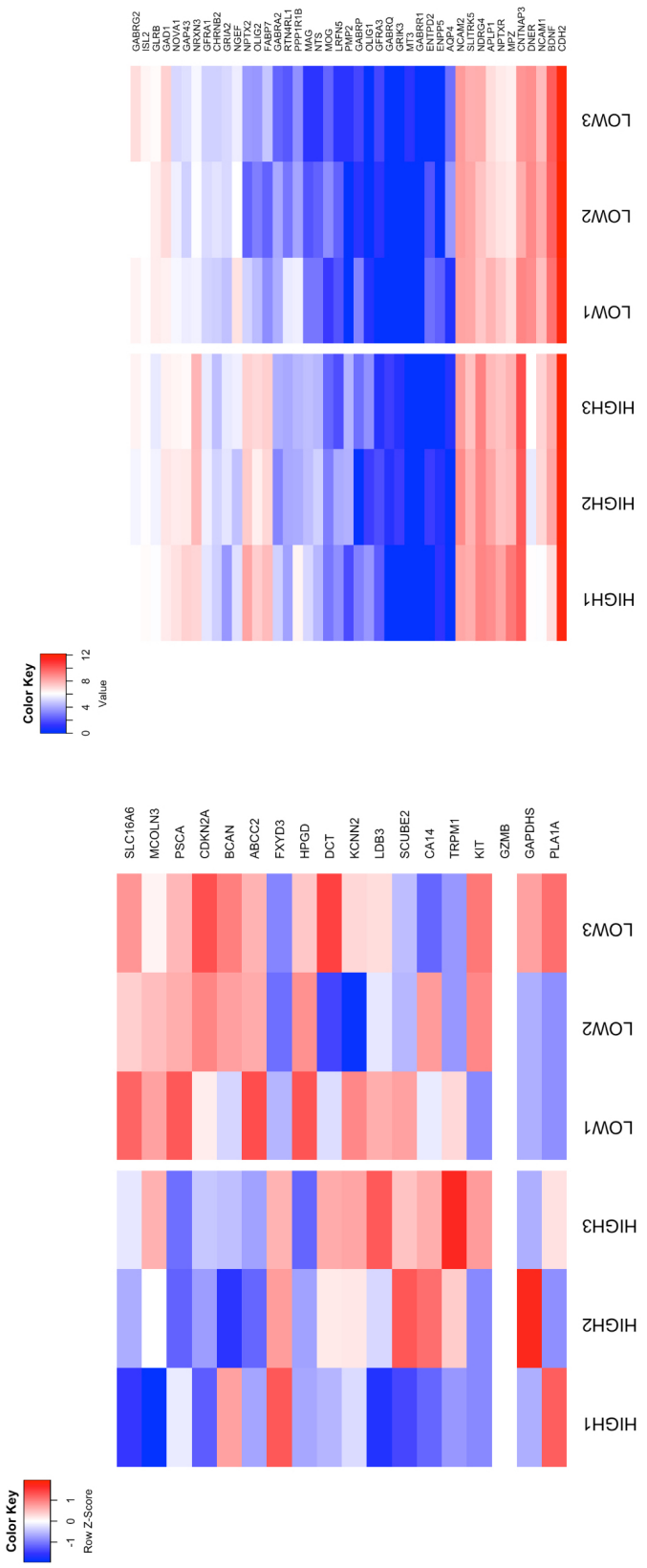

Figure 5.4: **MITF Targets are Differentially Expressed in ALDH1A3^{high} Compared to ALDH1A3^{low} Populations** The A375 cell line is an *MITF*-low expressing cell line. The *MITF*target genes *SLC16A6, MCOLN3, PSCA, CDKN2A, BCAN and ABCC2* were differentially expressed in ALDH1A3^{high} compared to ALDH1A3^{low} populations, with higher expression in ALDH1A3^{low} cells. The *MITF* target gene signature is as described by the The Cancer Genome Atlas (TGCA). Upregulated genes are highlighted in red and downregulated genes in blue cells of the heatmap.

Figure 5.5: **Neural Crest Stem Cell Gene Expression Signature in the ALDH1A3^{high} Population**

The A375 cell line expresses genes in the neural crest stem cell cluster differentially in ALDH1A3^{high} compared to ALDH1A3^{low} populations. The neural crest stem cell cluster is associated with minimal residual disease and the signature is as described by (Rambow et al., 2018). Upregulated genes are highlighted in red and downregulated genes in blue cells of the heatmap.

As the NCSC gene signature was highly expressed in the high ALDH-expressing population, analysis was focused to the expression of neural-associated genes and role of ALDH1A3 in governing the expression of these. This was decided as retinoic acid is generated by the activity of ALDH1A3 and is also heavily involved in the regulation of neural development. With this in mind, I explored the expression of *RXR* and *RAR* retinoic acid receptors in the ALDH high and low populations. *RXRG* was one of the most abundant genes in the ALDH high population (Figure 5.6). To elucidate whether this was under the control of ALDH1A3, I examined expression of *RXRG* in the ALDH1A3-null cell line compared to Cas9-expressing only cells. Interestingly, *RXRG* expression was not perturbed upon removal of ALDH1A3 (Figure 5.6). Investigation of other retinoic acid receptor genes revealed that *RARB* is expressed at lower levels in ALDH1A3-null cells than ALDH1A3-proficient cells (Figure 5.6).

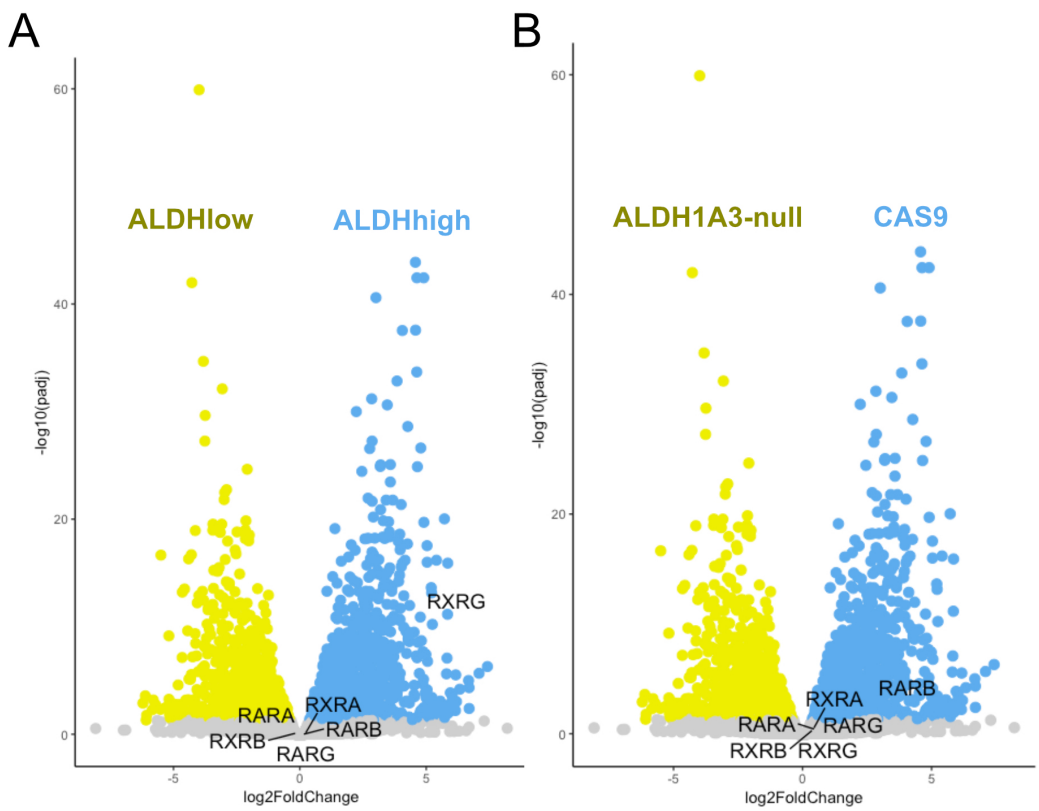

Figure 5.6: **Retinoic Acid Receptor Expression is Altered Under Different ALDH States**

Differential gene expression in ALDH high/low and ALDHcas9/1A3-null cell lines. RXRG was one of the most highly-abundant genes in the ALDH high population and expression of the RARB receptor is altered upon ALDH1A3 depletion. Non significant genes are labelled in grey and have P>0.05.

5.2.4 ALDH1A3 Expression Enhances Abundance of Retinoic Acid-Critical Transcripts

As ALDH1A3 protein is essential for ALDEFLUOR™ turnover and is the major transcript expressed at the transcriptomic level in A375 cells (Figure 5.7), it was hypothesised that the expression of retinoic acid genes would be under control of ALDH1A3 and the same population of genes in ALDHhigh vs ALDHlow and ALDH1A3 vs ALDH1A3-null populations would overlap. To explore the overlap between genes that are differentially expressed in $ALDH^{high}$ populations and upon removal of ALDH1A3 activity in the A375 cell line, I compared which genes were shared between these populations (Figure 5.8). 20.5% of genes differentially expressed in ALDH high and low populations are also differentially expressed in ALDH1A3-null A375 cells and conversely, 33.8% of genes differentially expressed between ALDH1A3 expressing and non-expressing cells are differentially expressed between the top and bottom 5% of ALDH-expressing cells. These 458 genes are enriched for synaptic and neurodevelopmental genes and some are involved in the retinoic acid response (*AQP1*, *DUSP1*, *WNT7B*, *SOX9*), this is also supported with GO:term analysis which indicates that the response to retinoic acid signalling is perturbed. This indicates that the retinoic acid gene expression profile in melanoma is dependent upon ALDH1A3.

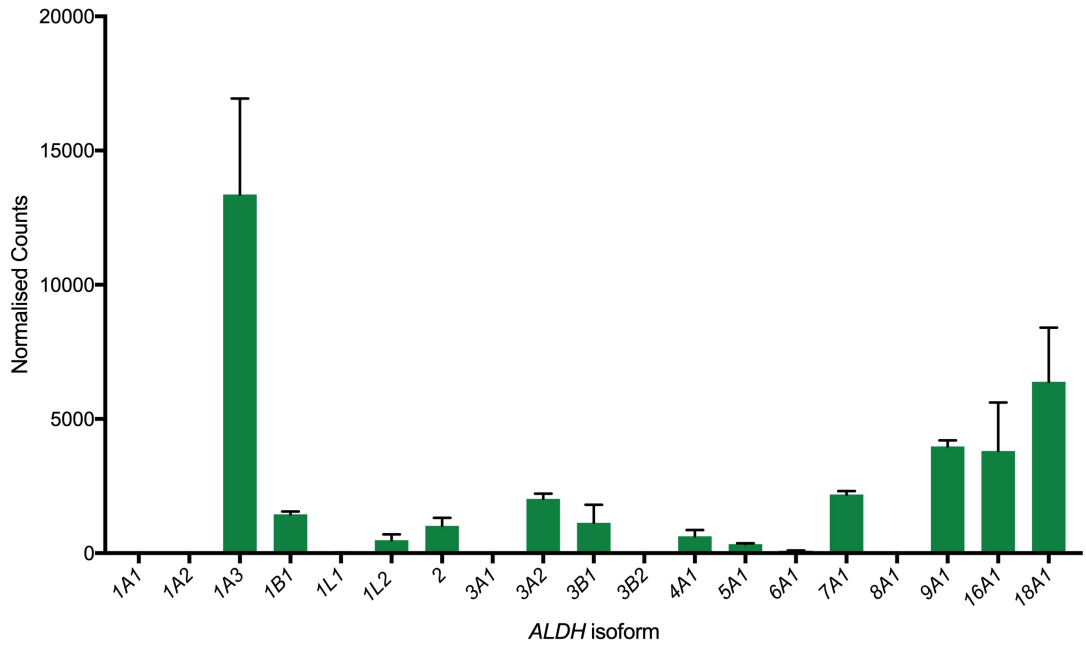

Figure 5.7: ***ALDH1A3* is the Predominant ALDH Transcript Expressed in the A375 Cell Line**

Aldh isoforms are expressed within the A375 cell line and *Aldh1a3* is the predominant of all 19 human isoforms. Error bars represent standard deviation.

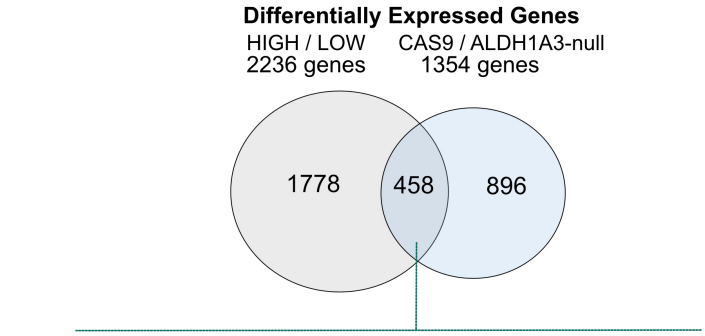

GO biological processes
regulation of postsynaptic specialization assembly (GO:0099150)
regulation of postsynapse assembly (GO:0150052)
regulation of postsynaptic density assembly (GO:0099151)
sympathetic nervous system development (GO:0048485)
positive regulation of excitatory postsynaptic potential (GO:2000463)
autonomic nervous system development (GO:0048483)
cochlea development (GO:0090102)
positive regulation of kidney development (GO:0090184)
modulation of excitatory postsynaptic potential (GO:0098815)
regulation of endothelial cell apoptotic process (GO:2000351)
regulation of smooth muscle cell migration (GO:0014910)
neuron projection extension (GO:1990138)
positive regulation of osteoblast differentiation (GO:0045669)
kidney morphogenesis (GO:0060993)
developmental growth involved in morphogenesis (GO:0060560)
response to retinoic acid (GO:0032526)
extracellular matrix organization (GO:0030198)
nerve development (GO:0021675)
developmental cell growth (GO:0048588)
glycosaminoglycan biosynthetic process (GO:0006024)

GO cellular component complete
inward rectifying potassium channel (GO:0008282)
filopodium membrane (GO:0031527)
integral component of postsynaptic density membrane (GO:0099061)
extracellular matrix component (GO:0044420)
intrinsic component of postsynaptic density membrane (GO:0099146)
basement membrane (GO:0005604)
chloride channel complex (GO:0034707)
integral component of postsynaptic specialization membrane (GO:0099060)
intrinsic component of postsynaptic specialization membrane (GO:0098948)
postsynaptic density membrane (GO:0098839)
Golgi lumen (GO:0005796)
collagen trimer (GO:0005581)
Schaffer collateral - CA1 synapse (GO:0098685)
collagen-containing extracellular matrix (GO:0062023)
postsynaptic specialization membrane (GO:0099634)
extracellular matrix (GO:0031012)
integral component of postsynaptic membrane (GO:0099055)
sarcolemma (GO:0042383)
intrinsic component of postsynaptic membrane (GO:0098936)
intrinsic component of synaptic membrane (GO:0099240)

Figure 5.8: **GO Expression of Genes Which Are Commonly Differentially Expressed in Both ALDH1A3^{high} and ALDH1A3^{low}cells and ALDH-Depleted Cell Lines**

Differentially expressed genes in ALDH1A3^{high}, ALDH1A3^{low} and ALDHcas9/1A3-null cell lines were compared to distinguish common links between four populations that either have ALDH1A3 expression or have low/no ALDH1A3 expression. Overlapping genes were analysed against GO GSEA terms. Gene categories are sorted by fold-change with FDR < 0.05 and raw p-value <0.001.

5.3 Summary

To decipher the contribution of ALDH1A3 expression to the characteristics of $ALDH^{high}$ cells with tumour-initiating and chemoresistant properties, transcriptional analysis of ALDH-proficient and ALDH-deficient cells was performed. GSEA was performed to elucidate associated gene sets and signaling pathways that were differentially expressed in different ALDH1A3 environments. A key transcriptional difference in melanoma cell populations that exhibit differential expression of ALDH1A3 was identified. I have shown that subpopulations differ in the expression of key genes responsible for retinoic acid signalling, neural cell development and control over *MITF*, a major melanocyte transcription factor.

I have found that ALDH-expressing cells, which have been shown to develop resistance to traditional chemotherapies express genes which underpin neural stem cell development and have been associated with minimal residual disease in melanoma. Recently, Rambow et al. (2018) investigated minimal residual disease which can be likened to the tumour-initiating cancer cells that persist during chemotherapy treatment (Figure 5.9. They found that expression of a core set of genes (NCSC Rambow gene set Cluster) is a predictor of melanoma chemotherapeutic resistance. This core set of genes is dependent upon *RXRG* expression and can be controlled by administration of RXRG inhibitors, which is one of the most statistically significant genes upregulated in the ALDHhigh subpopulation I have characterised. Although ALDH1A3 is notorious for its expression in the cancer-initiating cell and retinoic acid signalling through RXR is dependent upon ALDH, the link between ALDH1A3 and the minimal residual disease gene cluster identified by Rambow has not been made until now. I propose that retinoic acid synthesis by ALDH1A3 bridges the link between altered RXRG signalling to confer the NCSC state and the function

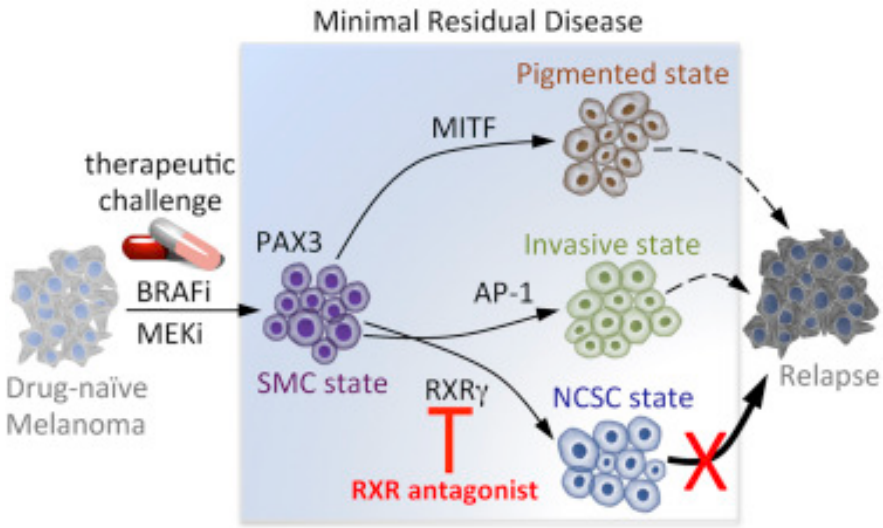

Figure 5.9: **RXRG induces the NCSC state following BRAF and MEK inhibitor therapy**

Exposure of melanoma to BRAF and MEK inhibitors causes cells to become nutrient-deprived ("starved"-like melanoma cells, SMC). Analysis of patient biopsies by Rambow et al. (2018) revealed the NCSC was a predominant drug-tolerant state in patients which were on therapy. Interrogation of the NCSC signature revealed its similarity to both quiescent neural stem cells and drug-persister signature in lung cancer. Image from Rambow et al. (2018).

of ALDH1A3 in promoting tumour-initiating and chemo-resistant properties in melanoma (Figure 5.10). This is supported through my experimental finding that the expression of genes involved in the Rambow NCSC minimal residual disease cluster are differentially expressed in ALDH1A3 subpopulations and that absence of ALDH activity alters the expression of key retinoic acid receptor genes, *RXRG* and *RARB*. RXRG is activated by 9-*cis*-retinoic acid which activates retinoic acid receptors (RAR) and retinoid X receptors (RXR) receptors (Kane and Napoli, 2010). RAR is also activated by all-*trans*-retinoic acid, which is a product of ALDH1A3 metabolism of All-*trans*-Retinaldehyde (Table 1.1) (Kane and Napoli, 2010). This is relevant to the repurposing of nifuroxazide as therapeutic option for melanoma treatment. It has been established that nifuroxazide is selectively bioactivated in cells that express high levels of ALDH (Sarvi et al., 2018) and so might have further potential for the selective targeting of the NCSC state.

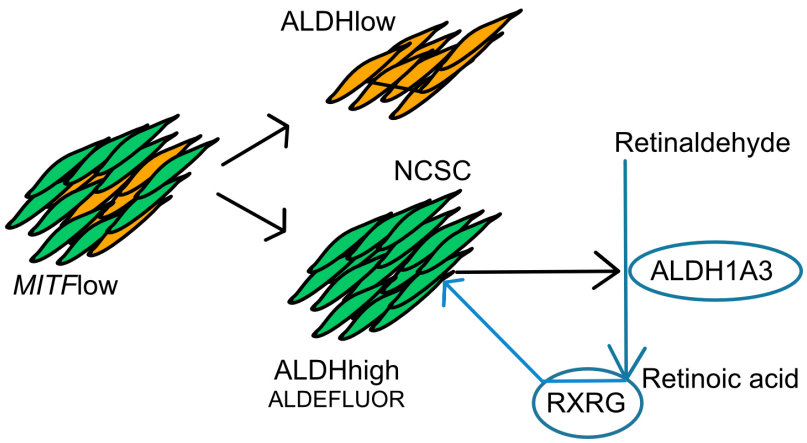

Figure 5.10: **ALDH1A3 as a Mediator of the NCSC State**
Exposure of melanoma to BRAF and MEK inhibitors causes cells to overexpress ALDH1A3 (Sarvi et al., 2018). Analysis of the ALDHhigh population revealed cell-type specific expression of NCSC genes, which is attributed to expression of the RXRgamma receptor, of which the ALDH1A3 substrate, retinaldehyde is a precursor.

Chapter 6

Conclusions and Future Directions

6.1 Conclusions

Throughout this thesis I have investigated the relevance of ALDH to two biological questions that relate to gene-drug interactions between ALDH and 5-NFNs and ALDH signalling in melanoma. With an array of methodological approaches, I have explored the downstream effects of 5-NFN exposure and expression of ALDH isoforms in both somatic tissue and cancer cell contexts. I have shown that mammalian ALDH enzymes are inhibited by 5-NFNs *in vitro* and that crucially, the inhibitory effect of 5-NFN exposure on ALDH activity is maintained in the PCLS *ex vivo* drug metabolism model. I demonstrate that 5-NFNs are cytotoxic in a liver-derived cell line and that 5-NFN and acetaldehyde exposure drives synergistic effects in HepG2 cells. Critically, through *in vivo* experiments in the *Aldh1b1*-deficient mouse line, I discovered that short-term exposure to 5-NFNs drive accumulation of circulating levels of acetaldehyde, indicating a novel route of 5-NFN toxicity. To enable future quantification of acetaldehyde, I instigated the set up of HPLC methods to quantify acetaldehyde concentrations in mouse plasma. I set up derivatisation and LC-MS sample preparation approaches to stabilise and extract aldehydes

from plasma matrices, identified diagnostic ions for acetaldehyde-DNPH with LC-Triple-Quadrupole-MS/MS. As ALDH enzymes metabolise various aldehydes, I followed three ALDH1B1/ALDH2 substrates (acetaldehyde, propionaldehyde and formaldehyde) through chromatographic set up coupled with high resolution accurate-mass Orbitrap-MS, to demonstrate the opportunity for pan-measurement of ALDH1B1 and ALDH2 substrates in plasma matrices. Finally, with an interest in identifying characteristics of ALDH populations that are sensitive to the effects of 5-NFNs in melanoma, I analysed the transcriptome of ALDH ^{high} and ALDH ^{low} populations in melanoma. I discovered that these populations differ in the expression of key genes that underlie retinoic acid metabolism but also that ALDH1A3-dependent and independently-curated minimal residual disease transcriptional profiles overlap. Collectively, these experiments demonstrate the importance of aldehydes in mediating the downstream effects of ALDH activity for both gene-drug interactions and cancer cell populations. However, some experiments could explore the dynamics of these interactions further, particularly when seeking to understand the contribution of genetic landscape and environmental effects to mediation of these signals.

6.2 Future Directions

6.2.1 Importance of Aldehydes in Mediating Cytotoxicity of 5-Nitrofurans and Minimal Residual Disease in Melanoma

6.2.1.1 Aldehydes

I propose that the synergistic effects of coexposure to nitrofurans and acetaldehyde are a result of dual targeting of the acetaldehyde-detoxification pathway via ALDH enzymes (Figure 6.1). I show that ALDH1B1 is required for detoxification of 5-NFN induced damage and propose that aldehydes arise as a result of inhibition of ALDH enzymes. Given that ALDH1B1 has a propensity for acetaldehyde metabolism, and shows preference for acetaldehyde as a substrate (Stagos et al., 2010), it is unlikely that ALDH1B1 exerts these protective functions through an additional mechanism. By initiating development of new mass spectrometry methods, in two mass spectrometry systems that allowed for robust detection but also pan-quantification of aldehydes. I would hope to be able to pin point the exact repertoire of aldehydes that accumulate during exposure to 5-nitrofurans. Such an approach is ambitious, considering that multiple research groups have studied aldehyde metabolism and usually report the analysis of a single aldehyde (Dator et al., 2017). The suitability of DNPH as a derivatisation agent for the study of aldehydes in plasma is subject to dispute due to background aldehydes which present a route of contamination during derivatisation. That said, data-dependent MS^n methods have been employed for MS^3 screening of DNPH derivatives to detect unknown or unexpected carbonyls in saliva (Dator et al., 2017). In addition, new tools employing quenched hydrazones have potential to enable fluorescent tagging of aldehyde load, albeit *in vitro*

(Yuen et al., 2016). Silva et al. (2018) have utilised a GC-high resolution MS method to measure 19 aldehydes but acetaldehyde had the highest LOD by more than 10X compared to the remaining 18 aldehydes measured, this is surprising as GC-MS is well-suited to the analysis of volatile aldehydes.

6.2.1.2 Bioactivation of Nitrofurans and DNA-damage

It still remains to be shown what the individual effect of 5-nitrofuran metabolites have on tissues *in vivo*. This would have an impact on the understanding of 5-nitrofuran side effects and delineation of additional underlying mechanisms but in terms of my experiments, would enable me to pinpoint exactly which ALDHs *in vivo* are responsible for ALDH-mediated bioactivation of 5-nitrofurans. I would test this through administration of stable isotope-labelled 5-nitrofurans with and without ethanol to *Aldh2*- and *Aldh1b1*-deficient mice. I would extract nitrofuran-metabolising tissues and circulating plasma to trace accumulated 5-nitrofuran species with high-resolution mass spectrometry that is well suited to discovery research. Incidentally, a recently identified nitrofuran metabolite, 5-Nitro-2-furaldehyde carries a carbonyl group and could itself be a potential substrate or inhibitor of ALDH enzymes (Zhang et al., 2017).

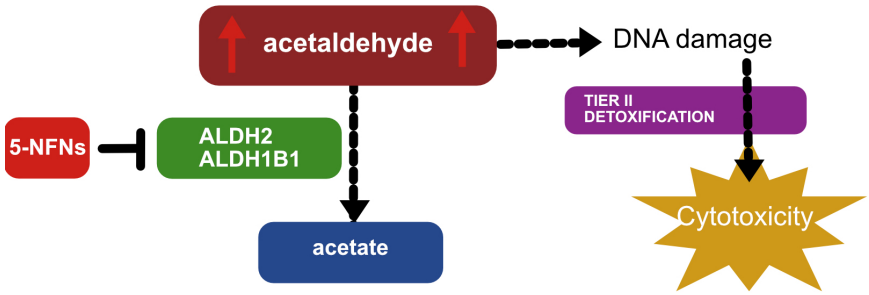

Figure 6.1: **Contribution of Acetaldehyde-Metabolism to 5-NFN Cytotoxicity**.
5-Nitrofuran-induced inhibition of acetaldehyde-metabolising ALDH enzymes promotes accumulation of DNA-damaging acetaldehyde and a reduction in acetate availability and promotes cellular toxicity.

I have shown that 5-NFNs depleted cell viability through the use of PrestoBlue reagent. This reagent is widely-used for the analysis of cell viability but is dependent on mitochondrial turnover of the substrate. As ALDH is a mitochondrially-expressed protein, it is possible that nitrofurans alter the mitochondrial capacity of the cell. I would test this further by using mitochondrial oxidation markers such as pMitoTimer to enable live-tracking of mitochondrial dynamics upon 5-nitrofuran exposure and delineation of the fine-interplay between ROS, lipid peroxidation and aldehyde biology.

The impact of 5-nitrofurans on circulating aldehydes is interesting. Recently, the important role of ALDH and components of DNA damage repair pathways in aldehyde detoxification have been brought to the forefront (Lu et al., 2017; Ray Chaudhuri and Nussenzweig, 2017). If protection through ALDH activity is insufficient or non-existent, resulting aldehyde adducts on DNA and proteins need to be resolved. DNA repair mechanisms can resolve metabolite inflicted DNA damage.

In the haematopoietic stem cell, it has been shown that formaldehyde-detoxifying *ADH5*, acetaldehyde- and formaldehyde-detoxifying *ALDH2* and Fanconi Anaemia component, *FANCD2* genes are key in preventing development of Fanconi Anaemia (Langevin et al., 2011). These aldehyde detoxifying and DNA repair mechanisms are not insurmountable, it has recently been demonstrated that homologous recombination(HR)-compromised cells are hypersensitive to acetaldehyde even with proficient FA pathway activity (Tacconi et al., 2017). Additionally, BRCA-mediated homology-directed DNA repair mechanisms are susceptible to the effects of formaldehyde. Aldehyde adducts on the DNA-repair enzyme, BRCA2 that arise from exposure to formaldehyde and acetaldehyde have been shown to target BRCA2 for proteasomal degradation (Lu et al., 2017). This means that aldehydes have the capacity to not only induce DNA damage

through destabilisation of DNA replication forks and resulting chromosomal abberations but actively prevent DNA-damage repair mechanisms from resolving aldehyde-induced damage. Acknowledging the importance of maintaining genetic stability and that aldehydes present a metabolic challenge to the cell, there is a need to further characterise chemical agents or cellular events that could lead aldehyde levels to rise in the cell and alter cellular homeostasis. To put a fresh stance on the effects of Aldh2 deficiency on alcohol-associated cancers, Seo et al. (2019) investigated an ethanol-induced propagation of oncogenic pathway signalling. As expected, administration of ethanol in the carbon tetra-chloride-induced liver fibrosis model elevated levels of MDA and 4-HNE in liver tumours in *ALDH2*-null mice, as well as elevated phosphorylated STAT3, p28 and pJNK markers of oxidative stress. Interestingly, they also demonstrated that oxidised mitochondrial DNA (8-OhDG) is sequestered into extracellular vesicles and exogenous administration of vesicles in HepG2 cell culture enhances the expression of the oxidative stress markers. They suggest that this effect is synergistic with acetaldehyde exposure, but in the absence of synergy analysis, whether these effects are truly additive or synergistic is to be established. This aside, these data comprise a signalling model where oncogenic pathways involving ethanol and acetaldehyde-induced damage can be communicated to neighbouring tumour cells. Given that acetaldehyde and 5-nitrofurans drive synergistic cytotoxic effects, it would be reasonable to hypothesise that carriers of the *ALDH2*2* mutation could be more susceptible to the acetaldehyde-inducing effects of 5-NFNs. Furthermore, 5-NFNs may be an attractive option for the treatment of chemoresistant populations in cancer. Chemoresistant cancer cell populations often exhibit impaired DNA-damage repair (Sitthi-Amorn et al., 2015). By enhancing aldehyde levels systemically with 5-NFNs, cells may be sensitised to the effects of chemotherapeutics. By

administering 5-NFNs to melanoma patients with tumours harbouring the NCSC signature, metabolism of the key retinoic acid drivers of RXRG signalling would be hindered. To understand the molecular mechanism underpinning the NCSC signature, delineation of retinoic acid receptors, their activation by retinoic acid (all-*trans*-retinal or 9-*cis*-retinal) and the contribution of ALDH1A3 to the metabolism of the retinaldehyde precursors needs to be addressed. The susceptibility of retinoids to isomerisation and oxidation presents a challenge for revealing the true substrates and products involved in the RXRG signalling response (Kane and Napoli, 2010).

6.2.1.3 Functions of ALDH in Cancer-Initiating Cells

It was shown that 5-NFNs inhibit the esterase activity of ALDH enzymes in a concentration-dependent manner. This is interesting because there are no known endogenous esterase substrates of ALDH enzymes. This enzymatic function could be evolutionarily redundant but there are no published screens that have looked to identify esterase substrates. Additionally, NFN1 had the most pronounced inhibitory effect on ALDH in cells and tissue and contains an ester group that could be susceptible to ester hydrolysis. If endogenous ester substrates of ALDH exist, this may have implications on metabolism of a wide range of biologically active compounds. Notably, Zhong et al. (2019) report that in the absense of ALDH2, cholesterol hydrolysis is impaired within lysosomes and contributes to increased foam cell formation. It is intriguing to hypothesise that ALDH contributes to metabolism of these compounds also through it's enzymatic ALDH activity.

6.3 Concluding Remarks

The work that I have undertaken in this thesis has identified the molecular and cellular consequences of a protein-drug interaction between ALDH and 5-NFNs. This work highlights mechanistically how ALDH:5-NFN interactions lead to acetaldehyde accumulation following 5-NFN exposure, offering a novel insight into the mechanism underpinning DNA-damage accumulation and development of side effects upon exposure to 5-NFNs. My development of derivatisation and HPLC-MS methods for aldehyde quantification sets the stage for the analysis of multiple aldehydes in biological matrices to decipher biological levels of aldehydes *in vivo* and the involvement of ALDH isoforms and envionmental or endogenous agents in mediating these levels. Finally, I have discovered that a critical chemotherapeutic-resistant population in melanoma is governed by ALDH1A3 expression. As a whole, these advances are important for understanding protein-drug and cell-specific-drug interactions between ALDH enzymes and 5-nitrofurans.

Bibliography

J. Abraham, S. Balbo, D. Crabb, and P. J. Brooks. Alcohol Metabolism in Human Cells Causes DNA Damage and Activates the Fanconi Anemia-Breast Cancer Susceptibility (FA-BRCA) DNA Damage Response Network. *Alcoholism: Clinical and Experimental Research*, 35(12): 2113–2120, 2011. ISSN 01456008. doi: 10.1111/j.1530-0277.2011.01563.x.

Y. Amanuma, S. Ohashi, Y. Itatani, M. Tsurumaki, S. Matsuda, O. Kikuchi, Y. Nakai, S. Miyamoto, T. Oyama, T. Kawamoto, K. A. Whelan, H. Nakagawa, T. Chiba, T. Matsuda, and M. Muto. Protective role of ALDH2 against acetaldehyde-derived DNA damage in oesophageal squamous epithelium. *Scientific Reports*, 5:14142, 2015. ISSN 2045-2322. doi: 10.1038/srep14142.

W. Ambroziak and R. Pietruszko. Metabolic Role of Aldehyde Dehydrogenase. *Advances in experimental medicine and biology*, 328:5–15, 1993. ISSN 0065-2598. doi: 10.1007/978-1-4615-2904-0_2.

S. Amir. Brain aldehyde dehydrogenase: Adaptive increase following prolonged ethanol administration in rats. *Neuropharmacology*, 17(7):463–467, 1978. ISSN 0028-3908. doi: 10.1016/0028-3908(78)90051-5.

S. Bae, J. Chon, M. S. Field, and P. J. Stover. Alcohol Dehydrogenase 5 Is a Source of Formate for De Novo Purine Biosynthesis in HepG2 Cells. *The Journal of Nutrition*, 147(4):499–505, 2017. ISSN 0022-3166. doi: 10.3945/jn.116.244467.

M. C. Berenbaum. What is synergy? *Pharmacological reviews*, 41(2):93–141, 1989. ISSN 0031-6997.

M. Beretta, K. Gruber, A. Kollau, M. Russwurm, D. Koesling, W. Goessler, W. M. Keung, K. Schmidt, and B. Mayer. Bioactivation of nitroglycerin by purified mitochondrial and

cytosolic aldehyde dehydrogenases. *The Journal of biological chemistry*, 283(26):17873–80, 2008. ISSN 0021-9258. doi: 10.1074/jbc.M801182200.

L. F. Blackwell, A. F. Bennett, K. E. Crow, P. D. Buckley, and L. W. Deady. A two-site model for the esterase and dehydrogenase activities of sheep liver aldehyde dehydrogenase. *Pharmacology Biochemistry and Behavior*, 18:83–87, 1983. ISSN 0091-3057. doi: 10.1016/0091-3057(83)90151-X.

C. I. Bliss. The Toxicity of Poisons Applied Jointly. *Annals of Applied Biology*, 26(3):585–615, 1939. ISSN 00034746. doi: 10.1111/j.1744-7348.1939.tb06990.x.

K. M. Bonney. Chagas disease in the 21st century: a public health success or an emerging threat? *Parasite*, 21:11, 2014. ISSN 1776-1042. doi: 10.1051/parasite/2014012.

J. B. Boonyaratanakornkit, L. Yue, L. R. Strachan, K. J. Scalapino, P. E. LeBoit, Y. Lu, S. P. Leong, J. E. Smith, and R. Ghadially. Selection of tumorigenic melanoma cells using ALDH. *The Journal of investigative dermatology*, 130(12):2799–808, 2010. ISSN 1523-1747. doi: 10.1038/jid.2010.237.

P. J. Brooks, M.-A. Enoch, D. Goldman, T.-K. Li, and A. Yokoyama. The alcohol flushing response: an unrecognized risk factor for esophageal cancer from alcohol consumption. *PLoS medicine*, 6(3):50, 2009. ISSN 1549-1676. doi: 10.1371/journal.pmed.1000050.

G. Burgos-Barragan, N. Wit, J. Meiser, F. A. Dingler, M. Pietzke, L. Mulderrig, L. B. Pontel, I. V. Rosado, T. F. Brewer, R. L. Cordell, P. S. Monks, C. J. Chang, A. Vazquez, and K. J. Patel. Mammals divert endogenous genotoxic formaldehyde into one-carbon metabolism. *Nature*, 548(7669):549–554, 2017. ISSN 0028-0836. doi: 10.1038/nature23481.

J. A. Castro, M. M. de Mecca, and L. C. Bartel. Toxic side effects of drugs used to treat Chagas' disease (American trypanosomiasis). *Human & Experimental Toxicology*, 25(8):471–479, 2006. ISSN 09603271. doi: 10.1191/0960327106het653oa.

K. Chandra Raj, L. Ingram, and J. Maupin-Furlow. Pyruvate decarboxylase: a key enzyme for the oxidative metabolism of lactic acid by Acetobacter pasteurianus. *Archives of Microbiology*, 176(6):443–451, 2001. ISSN 0302-8933. doi: 10.1007/s002030100348.

J. S. Chang, J.-R. Hsiao, and C.-H. Chen. ALDH2 polymorphism and alcohol-related cancers in Asians: a public health perspective. *Journal of Biomedical Science*, 24(1):19, 2017. ISSN 1423-0127. doi: 10.1186/s12929-017-0327-y.

S. Chawanthayatham, C. C. Valentine, B. I. Fedeles, E. J. Fox, L. A. Loeb, S. S. Levine, S. L. Slocum, G. N. Wogan, R. G. Croy, and J. M. Essigmann. Mutational spectra of aflatoxin B1 in vivo establish biomarkers of exposure for human hepatocellular carcinoma. *Proceedings of the National Academy of Sciences of the United States of America*, 114(15):E3101–E3109, 2017. ISSN 1091-6490. doi: 10.1073/pnas.1700759114.

Y. Cheli, S. Guiliano, T. Botton, S. Rocchi, V. Hofman, P. Hofman, P. Bahadoran, C. Bertolotto, R. Ballotti, and R. Ballotti. Mitf is the key molecular switch between mouse or human melanoma initiating cells and their differentiated progeny. *Oncogene*, 30(20):2307–2318, 2011. ISSN 0950-9232. doi: 10.1038/onc.2010.598.

D. Chen, L. Fang, H. Li, and C. Jin. The effects of acetaldehyde exposure on histone modifications and chromatin structure in human lung bronchial epithelial cells. *Environmental and Molecular Mutagenesis*, 59(5):375–385, 2018. ISSN 08936692. doi: 10.1002/em.22187.

Z. Chen, J. Zhang, and J. S. Stamler. Identification of the enzymatic mechanism of nitroglycerin bioactivation. *Proceedings of the National Academy of Sciences*, 99(12):8306–8311, 2002. ISSN 0027-8424. doi: 10.1073/pnas.122225199.

A. M. S. Cheung, T. S. K. Wan, J. C. K. Leung, L. Y. Y. Chan, H. Huang, Y. L. Kwong, R. Liang, and A. Y. H. Leung. Aldehyde dehydrogenase activity in leukemic blasts defines a subgroup of acute myeloid leukemia with adverse prognosis and superior NOD/SCID engrafting potential. *Leukemia*, 21(7):1423–1430, 2007. ISSN 0887-6924. doi: 10.1038/sj.leu.2404721.

R. Dator, A. Carrà, L. Maertens, V. Guidolin, P. W. Villalta, and S. Balbo. A High Resolution/Accurate Mass (HRAM) Data-Dependent MS3 Neutral Loss Screening, Classification, and Relative Quantitation Methodology for Carbonyl Compounds in Saliva. *Journal of The American Society for Mass Spectrometry*, 28(4):608–618, 2017. ISSN 1044-0305. doi: 10.1007/s13361-016-1521-y.

I. A. M. de Graaf, P. Olinga, M. H. de Jager, M. T. Merema, R. de Kanter, E. G. van de Kerkhof, and G. M. M. Groothuis. Preparation and incubation of precision-cut liver and intestinal slices for application in drug metabolism and toxicity studies. *Nature Protocols*, 5(9):1540–1551, 2010. ISSN 1754-2189. doi: 10.1038/nprot.2010.111.

G. Y. Di Veroli, C. Fornari, D. Wang, S. Mollard, J. L. Bramhall, F. M. Richards, and D. I. Jodrell. Combenefit: an interactive platform for the analysis and visualization of drug combinations. *Bioinformatics*, 32(18):2866–2868, 2016. ISSN 1367-4803. doi: 10.1093/bioinformatics/btw230.

Y. D'Souza, S. Dowlatshahi, and B. M. Bennett. Changes in aldehyde dehydrogenase 2 expression in rat blood vessels during glyceryl trinitrate tolerance development and reversal. *British journal of pharmacology*, 164(2b):632–43, 2011. ISSN 1476-5381. doi: 10.1111/j.1476-5381.2011.01448.x.

J.-J. Duan, J. Cai, Y.-F. Guo, X.-W. Bian, and S.-C. Yu. ALDH1A3, a metabolic target for cancer diagnosis and therapy. *International Journal of Cancer*, 139(5):965–975, 2016. ISSN 00207136. doi: 10.1002/ijc.30091.

G. Duester, F. A. Mic, and A. Molotkov. Cytosolic retinoid dehydrogenases govern ubiquitous metabolism of retinol to retinaldehyde followed by tissue-specific metabolism to retinoic acid. *Chemico-Biological Interactions*, 143-144:201–210, 2003. ISSN 0009-2797. doi: 10.1016/S0009-2797(02)00204-1.

M. Eggink, M. Wijtmans, A. Kretschmer, J. Kool, H. Lingeman, I. J. P. De Esch, W. M. A. Niessen, and H. Irth. Targeted LC-MS derivatization for aldehydes and carboxylic acids with a new derivatization agent 4-APEBA. *Analytical and Bioanalytical Chemistry*, 397(2): 665–675, 2010. ISSN 16182642. doi: 10.1007/s00216-010-3575-1.

J. Farres, T. T. Y. Wang, S. J. Cunningham, and H. Weiner. Investigation of the Active Site Cysteine Residue of Rat Liver Mitochondrial Aldehyde Dehydrogenase by Site-Directed Mutagenesis'. *Biochemistry*, 34:2592–2598, 1995.

I. Gagnon, G. Duester, and P. V. Bhat. Kinetic analysis of mouse retinal dehydrogenase type-2 (RALDH2) for retinal substrates. *Biochimica et biophysica acta*, 1596(1):156–62, 2002. ISSN 0006-3002. doi: 10.1016/s0167-4838(02)00213-3.

I. Gagnon, G. Duester, and P. V. Bhat. Enzymatic characterization of recombinant mouse retinal dehydrogenase type 1. *Biochemical Pharmacology*, 65(10):1685–1690, 2003. ISSN 00062952. doi: 10.1016/S0006-2952(03)00150-3.

J. I. Garaycoechea, G. P. Crossan, F. Langevin, L. Mulderrig, S. Louzada, F. Yang, G. Guilbaud, N. Park, S. Roerink, S. Nik-Zainal, M. R. Stratton, and K. J. Patel. Alcohol

and endogenous aldehydes damage chromosomes and mutate stem cells. *Nature*, 553 (7687):171–177, 2018. ISSN 1476-4687. doi: 10.1038/nature25154.

J. Gascon, C. Bern, and M.-J. Pinazo. Chagas disease in Spain, the United States and other non-endemic countries. *Acta Tropica*, 115(1-2):22–27, 2010. ISSN 0001706X. doi: 10.1016/j.actatropica.2009.07.019.

C. Ginestier, M. H. Hur, E. Charafe-Jauffret, F. Monville, J. Dutcher, M. Brown, J. Jacquemier, P. Viens, C. G. Kleer, S. Liu, A. Schott, D. Hayes, D. Birnbaum, M. S. Wicha, and G. Dontu. ALDH1 Is a Marker of Normal and Malignant Human Mammary Stem Cells and a Predictor of Poor Clinical Outcome. *Cell Stem Cell*, 1(5):555–567, 2007. ISSN 19345909. doi: 10.1016/j.stem.2007.08.014.

C. R. Goding. Mitf from neural crest to melanoma: signal transduction and transcription in the melanocyte lineage. *Genes & Development*, 14(14):1712–1728, 2000. ISSN 0890-9369. doi: 10.1101/GAD.14.14.1712.

C. E. Graham, K. Brocklehurst, R. W. Pickersgill, and M. J. Warren. Characterization of retinaldehyde dehydrogenase 3. *The Biochemical journal*, 394(Pt 1):67–75, 2006. ISSN 1470-8728. doi: 10.1042/BJ20050918.

E. R. Gross, V. O. Zambelli, B. A. Small, J. C. B. Ferreira, C.-H. Chen, and D. Mochly-Rosen. A personalized medicine approach for Asian Americans with the aldehyde dehydrogenase 2*2 variant. *Annual review of pharmacology and toxicology*, 55:107–27, 2015. ISSN 1545-4304. doi: 10.1146/annurev-pharmtox-010814-124915.

B. S. Hall, C. Bot, and S. R. Wilkinson. Nifurtimox activation by trypanosomal type I nitroreductases generates cytotoxic nitrile metabolites. *The Journal of biological chemistry*, 286(15):13088–95, 2011. ISSN 1083-351X. doi: 10.1074/jbc.M111.230847.

J. Hempel, J. Perozich, T. Chapman, J. Rose, J. S. Boesch, Z.-J. Liu, R. Lindahl, and B.-C. Wang. *Aldehyde Dehydrogenase Catalytic Mechanism*. Springer, Boston, MA, Boston, MA, 1999. doi: 10.1007/978-1-4615-4735-8_7.

J. S. Herrington, Z.-H. T. Fan, P. J. Lioy, and J. J. Zhang. Low acetaldehyde collection efficiencies for 24-hour sampling with 2,4-dinitrophenylhydrazine (DNPH)-coated solid sorbents. *Environmental science & technology*, 41(2):580–5, 2007. ISSN 0013-936X.

A. A. Horton. Mitochondrial metabolism of aldehydes. *The Biochemical journal*, 116(4):19P–20P, 1970. ISSN 0264-6021. doi: 10.1042/bj1160019pb.

B. C. Jackson, P. Reigan, B. Miller, D. C. Thompson, and V. Vasiliou. Human ALDH1B1 Polymorphisms may Affect the Metabolism of Acetaldehyde and All-trans retinaldehyde—In Vitro Studies and Computational Modeling. *Pharmaceutical Research*, 32(5):1648–1662, 2015. ISSN 0724-8741. doi: 10.1007/s11095-014-1564-3.

M. A. Kane and J. L. Napoli. Quantification of endogenous retinoids. *Methods in molecular biology (Clifton, N.J.)*, 652:1–54, 2010. ISSN 1940-6029. doi: 10.1007/978-1-60327-325-1_1.

J. Kim, C.-H. Chen, J. Yang, and D. Mochly-Rosen. Aldehyde dehydrogenase 2*2 knock-in mice show increased reactive oxygen species production in response to cisplatin treatment. *Journal of Biomedical Science*, 24(1):33, 2017. ISSN 1423-0127. doi: 10.1186/s12929-017-0338-8.

A. A. Klyosov. Kinetics and Specificity of Human Liver Aldehyde Dehydrogenases toward Aliphatic, Aromatic, and Fused Polycyclic Aldehydes. *Biochemistry*, 35(14):4457–4467, 1996. doi: 10.1021/bi9521102.

A. A. Klyosov, L. G. Rashkovetsky, M. K. Tahir, and W.-M. Keung. Possible Role of Liver Cytosolic and Mitochondrial Aldehyde Dehydrogenases in Acetaldehyde Metabolism †. *Biochemistry*, 1996.

V. Koppaka, D. C. Thompson, Y. Chen, M. Ellermann, K. C. Nicolaou, R. O. Juvonen, D. Petersen, R. A. Deitrich, T. D. Hurley, and V. Vasiliou. Aldehyde dehydrogenase inhibitors: a comprehensive review of the pharmacology, mechanism of action, substrate specificity, and clinical application. *Pharmacological reviews*, 64(3):520–39, 2012. ISSN 1521-0081. doi: 10.1124/pr.111.005538.

F. Langevin, G. P. Crossan, I. V. Rosado, M. J. Arends, and K. J. Patel. Fancd2 counteracts the toxic effects of naturally produced aldehydes in mice. *Nature*, 475(7354):53–58, 2011. ISSN 0028-0836. doi: 10.1038/nature10192.

T. Lapidot, C. Sirard, J. Vormoor, B. Murdoch, T. Hoang, J. Caceres-Cortes, M. Minden, B. Paterson, M. A. Caligiuri, and J. E. Dick. A cell initiating human acute myeloid leukaemia

after transplantation into SCID mice. *Nature*, 367(6464):645–648, 1994. ISSN 0028-0836. doi: 10.1038/367645a0.

H. N. Larson, J. Zhou, Z. Chen, J. S. Stamler, H. Weiner, and T. D. Hurley. Structural and functional consequences of coenzyme binding to the inactive asian variant of mitochondrial aldehyde dehydrogenase: roles of residues 475 and 487. *The Journal of biological chemistry*, 282(17):12940–50, 2007. ISSN 0021-9258. doi: 10.1074/jbc.M607959200.

J. Lin, M. C. Haffner, Y. Zhang, B. H. Lee, W. N. Brennen, J. Britton, S. K. Kachhap, J. S. Shim, J. O. Liu, W. G. Nelson, S. Yegnasubramanian, and M. A. Carducci. Disulfiram is a DNA demethylating agent and inhibits prostate cancer cell growth. *Prostate*, 71(4):333–343, 2011. ISSN 0270-4137. doi: 10.1002/PROS.21247.

M. Lin and J. L. Napoli. cDNA Cloning and Expression of a Human Aldehyde Dehydrogenase (ALDH) Active with 9-cis-Retinal and Identification of a Rat Ortholog, ALDH12. *Journal of Biological Chemistry*, 275(51):40106–40112, 2000. doi: 10.1074/jbc.M008027200.

J. J. Lipsky, M. L. Shen, and S. Naylor. In vivo inhibition of aldehyde dehydrogenase by disulfiram. *Chemico-biological interactions*, 130-132(1-3):93–102, 2001. ISSN 0009-2797.

S. Loewe. The problem of synergism and antagonism of combined drugs. *Arzneimittel-Forschung*, 3(6):285–90, 1953. ISSN 0004-4172.

M. I. Love, W. Huber, and S. Anders. Moderated estimation of fold change and dispersion for RNA-seq data with DESeq2. *Genome Biology*, 15(12):550, 2014. ISSN 1474-760X. doi: 10.1186/s13059-014-0550-8.

E. D. Lowe, G.-Y. Gao, L. N. Johnson, and W. M. Keung. Structure of Daidzin, a Naturally Occurring Anti-Alcohol-Addiction Agent, in Complex with Human Mitochondrial Aldehyde Dehydrogenase §. *Journal of Medicinal Chemistry*, 51(15):4482–4487, 2008. ISSN 0022-2623. doi: 10.1021/jm800488j.

S. Lu, W. Tan, S. Chadha, Y. Liu, M. Lee, R. Aebersold, A. R. Venkitaraman, E. Gabasova, D. Perera, K. Ahmed, S. Constantinou, and X. Renaudin. A Class of Environmental and Endogenous Toxins Induces BRCA2 Haploinsufficiency and Genome Instability Correspondence In Brief Environmental and endogenous aldehydes contribute to genome instability and potentially tumorigenesis through selective degradat. *Cell*, 169:1105–1118, 2017. doi: 10.1016/j.cell.2017.05.010.

Y. Luo, K. Dallaglio, Y. Chen, W. A. Robinson, S. E. Robinson, M. D. McCarter, J. Wang, R. Gonzalez, D. C. Thompson, D. A. Norris, D. R. Roop, V. Vasiliou, and M. Fujita. ALDH1A isozymes are markers of human melanoma stem cells and potential therapeutic targets. *Stem cells (Dayton, Ohio)*, 30(10):2100–13, 2012. ISSN 1549-4918. doi: 10.1002/stem.1193.

G. Lutfullah, N. Qaisar Khan, F. Amin, L. Kakakhel, and N. Azhar. Structural Modeling Studies of Aldehyde Dehydrogenase X: Insights into Key Interactions in the Tetrameric Assembly of the Isoenzyme. *Protein & Peptide Letters*, 18(1):41–57, 2011. ISSN 09298665. doi: 10.2174/092986611794328645.

S. A. Marchitti, C. Brocker, D. Stagos, and V. Vasiliou. Non-P450 aldehyde oxidizing enzymes: the aldehyde dehydrogenase superfamily. *Expert Opinion on Drug Metabolism & Toxicology*, 4(6):697–720, 2008. ISSN 1742-5255. doi: 10.1517/17425255.4.6.697.

T. Matsuda, A. Matsumoto, M. Uchida, R. A. Kanaly, K. Misaki, S. Shibutani, T. Kawamoto, K. Kitagawa, K. I. Nakayama, K. Tomokuni, and M. Ichiba. Increased formation of hepatic N2-ethylidene-2'-deoxyguanosine DNA adducts in aldehyde dehydrogenase 2-knockout mice treated with ethanol. *Carcinogenesis*, 28(11):2363–2366, 2007. ISSN 0143-3334. doi: 10.1093/carcin/bgm057.

A. Matsumoto, D. C. Thompson, Y. Chen, K. Kitagawa, and V. Vasiliou. Roles of defective ALDH2 polymorphism on liver protection and cancer development. *Environmental Health and Preventive Medicine*, 21(6):395–402, 2016. ISSN 1342-078X. doi: 10.1007/s12199-016-0579-2.

J. D. Maya, B. K. Cassels, P. Iturriaga-Vásquez, J. Ferreira, M. Faúndez, N. Galanti, A. Ferreira, and A. Morello. Mode of action of natural and synthetic drugs against Trypanosoma cruzi and their interaction with the mammalian host. *Comparative Biochemistry and Physiology - A Molecular and Integrative Physiology*, 146(4):601–620, 2007. ISSN 10956433. doi: 10.1016/j.cbpa.2006.03.004.

C. A. Morgan and T. D. Hurley. Development of a high-throughput in vitro assay to identify selective inhibitors for human ALDH1A1. *Chemico-biological interactions*, 234:29–37, 2015. ISSN 1872-7786. doi: 10.1016/j.cbi.2014.10.028.

C. A. Morgan, B. Parajuli, C. D. Buchman, K. Dria, and T. D. Hurley. N,N-diethylaminobenzaldehyde (DEAB) as a substrate and mechanism-based inhibitor for

human ALDH isoenzymes. *Chemico-Biological Interactions*, 234:18–28, 2015. ISSN 00092797. doi: 10.1016/j.cbi.2014.12.008.

M. F. Müller, Y. Zhou, D. J. Adams, and M. J. Arends. Effects of long-term ethanol consumption and Aldh1b1 depletion on intestinal tumourigenesis in mice. *The Journal of Pathology*, 2016. ISSN 00223417. doi: 10.1002/path.4869.

M. F. Müller, T. J. Kendall, D. J. Adams, Y. Zhou, and M. J. Arends. The murine hepatic sequelae of long-term ethanol consumption are sex-specific and exacerbated by Aldh1b1 loss. *Experimental and Molecular Pathology*, 105(1):63–70, 2018. ISSN 0014-4800. doi: 10.1016/J.YEXMP.2018.05.008.

M. Pérez-Alea, K. McGrail, S. Sánchez-Redondo, B. Ferrer, G. Fournet, J. Cortés, E. Muñoz, J. Hernandez-Losa, S. Tenbaum, G. Martin, R. Costello, I. Ceylan, V. Garcia-Patos, and J. A. Recio. ALDH1A3 is epigenetically regulated during melanocyte transformation and is a target for melanoma treatment. *Oncogene*, 36(41):5695–5708, 2017. ISSN 0950-9232. doi: 10.1038/onc.2017.160.

J. Perozich, H. Nicholas, B.-C. Wang, R. Lindahl, and J. Hempel. Relationships within the aldehyde dehydrogenase extended family. *Protein Science*, 8(1):137–146, 2008. ISSN 09618368. doi: 10.1110/ps.8.1.137.

F. Pietrocola, L. Galluzzi, J. Manuel, B.-S. Pedro, F. Madeo, and G. Kroemer. Cell Metabolism Review Acetyl Coenzyme A: A Central Metabolite and Second Messenger. *Cell Metabolism*, 21:805–821, 2015. doi: 10.1016/j.cmet.2015.05.014.

F. Rambow, A. Rogiers, O. Marin-Bejar, S. Aibar, J. Femel, M. Dewaele, P. Karras, D. Brown, Y. H. Chang, M. Debiec-Rychter, C. Adriaens, E. Radaelli, P. Wolter, O. Bechter, R. Dummer, M. Levesque, A. Piris, D. T. Frederick, G. Boland, K. T. Flaherty, J. van den Oord, T. Voet, S. Aerts, A. W. Lund, and J.-C. Marine. Toward Minimal Residual Disease-Directed Therapy in Melanoma. *Cell*, 174(4):843–855.e19, 2018. ISSN 00928674. doi: 10.1016/j.cell.2018.06.025.

J. Rappsilber, M. Mann, and Y. Ishihama. Protocol for micro-purification, enrichment, pre-fractionation and storage of peptides for proteomics using StageTips. *Nature Protocols*, 2 (8):1896–1906, 2007. ISSN 1754-2189. doi: 10.1038/nprot.2007.261.

A. Ray Chaudhuri and A. Nussenzweig. Thwarting endogenous stress: BRCA protects against aldehyde toxicity. *EMBO molecular medicine*, 9(10):1331–1333, 2017. ISSN 1757-4684. doi: 10.15252/emmm.201708194.

J. Rodriguez-Zavala and H. Weiner. Structural Aspects of Aldehyde Dehydrogenase that Influence Dimer–Tetramer Formation†. *Biochemistry*, 2002. doi: 10.1021/BI012081X.

S. Sarvi, R. Crispin, Y. Lu, L. Zeng, T. D. Hurley, D. R. Houston, A. von Kriegsheim, C.-H. Chen, D. Mochly-Rosen, M. Ranzani, M. E. Mathers, X. Xu, W. Xu, D. J. Adams, N. O. Carragher, M. Fujita, L. Schuchter, A. Unciti-Broceta, V. G. Brunton, and E. E. Patton. ALDH1 Bio-activates Nifuroxazide to Eradicate ALDHHigh Melanoma-Initiating Cells. *Cell Chemical Biology*, 25(12):1456–1469.e6, 2018. ISSN 24519456. doi: 10.1016/j.chembiol.2018.09.005.

G. L. Saulnier Sholler, S. Kalkunte, C. Greenlaw, K. McCarten, and E. Forman. Antitumor Activity of Nifurtimox Observed in a Patient With Neuroblastoma. *Journal of Pediatric Hematology/Oncology*, 28(10):693–695, 2006. ISSN 1077-4114. doi: 10.1097/01.mph.0000212994.56812.f2.

G. L. Saulnier Sholler, L. Brard, J. A. Straub, L. Dorf, S. Illyene, K. Koto, S. Kalkunte, M. Bosenberg, T. Ashikaga, R. Nishi, and G. Saulnier Sholler. Nifurtimox Induces Apoptosis of Neuroblastoma Cells in vitro and in vivo. *J Pediatr Hematol Oncol*, 31(3):187–193, 2009. doi: 10.1097/MPH.0b013e3181984d91.

G. L. Saulnier Sholler, G. M. Bergendahl, L. Brard, A. P. Singh, B. W. Heath, P. M. Bingham, T. Ashikaga, B. A. Kamen, A. C. Homans, M. A. Slavik, S. R. Lenox, T. J. Higgins, and W. S. Ferguson. A Phase 1 Study of Nifurtimox in Patients With Relapsed/Refractory Neuroblastoma. *Journal of Pediatric Hematology/Oncology*, 33(1):25–30, 2011a. ISSN 1077-4114. doi: 10.1097/MPH.0b013e3181f47061.

K. S. Saulnier Sholler, P. Lescault, L. Brard, K. Kim, R. K. Singh, J. Bond, S. Illenye, M. A. Slavik, T. Ashikaga, and G. L. Saulnier Sholler. Antitumor activity of nifurtimox is enhanced with tetrathiomolybdate in medulloblastoma. *International Journal of Oncology*, 38(5):1329–41, 2011b. ISSN 1019-6439. doi: 10.3892/ijo.2011.971.

W. Seo, Y. Gao, Y. He, J. Sun, H. Xu, D. Feng, S. H. Park, Y.-E. Cho, A. Guillot, T. Ren, R. Wu, J. Wang, S.-J. Kim, S. Hwang, S. Liangpunsakul, Y. Yang, J. Niu, and B. Gao. ALDH2 deficiency promotes alcohol-associated liver cancer by activating oncogenic pathways via

oxidized DNA-enriched extracellular vesicles. *Journal of Hepatology*, 2019. ISSN 0168-8278. doi: 10.1016/J.JHEP.2019.06.018.

L. Shi and B. P. Tu. Acetyl-CoA and the regulation of metabolism: mechanisms and consequences. *Current opinion in cell biology*, 33:125–31, 2015. ISSN 1879-0410. doi: 10.1016/j.ceb.2015.02.003.

S. D. Shukla, Y. J. Lee, P.-h. Park, and A. R. Aroor. Acetaldehyde alters MAP kinase signalling and epigenetic histone modifications in hepatocytes. *Novartis Foundation symposium*, 285: 217–24; discussion 224–8, 2007. ISSN 1528-2511.

R. S. Sidhu and A. H. Blair. Human liver aldehyde dehydrogenase. Esterase activity. *The Journal of biological chemistry*, 250(19):7894–8, 1975. ISSN 0021-9258.

L. K. Silva, G. A. Hile, K. M. Capella, M. F. Espenship, M. M. Smith, V. R. De Jesús, and B. C. Blount. Quantification of 19 Aldehydes in Human Serum by Headspace SPME/GC/High-Resolution Mass Spectrometry. *Environmental Science & Technology*, 52(18):10571–10579, 2018. ISSN 0013-936X. doi: 10.1021/acs.est.8b02745.

S. Singh, J. Arcaroli, D. C. Thompson, W. Messersmith, and V. Vasiliou. Acetaldehyde and retinaldehyde-metabolizing enzymes in colon and pancreatic cancers. *Advances in experimental medicine and biology*, 815:281–94, 2015. ISSN 0065-2598. doi: 10.1007/978-3-319-09614-8_16.

J. Sitthi-Amorn, B. Herrington, G. Megason, J. Pullen, C. Gordon, S. Hogan, T. Koganti, and C. Hicks. Transcriptome Analysis of Minimal Residual Disease in Subtypes of Pediatric B Cell Acute Lymphoblastic Leukemia. *Clinical Medicine Insights. Oncology*, 9:51–60, 2015. ISSN 1179-5549. doi: 10.4137/CMO.S17049.

W. C. Skarnes, B. Rosen, A. P. West, M. Koutsourakis, W. Bushell, V. Iyer, A. O. Mujica, M. Thomas, J. Harrow, T. Cox, D. Jackson, J. Severin, P. Biggs, J. Fu, M. Nefedov, P. J. de Jong, A. F. Stewart, and A. Bradley. A conditional knockout resource for the genome-wide study of mouse gene function. *Nature*, 474(7351):337–342, 2011. ISSN 0028-0836. doi: 10.1038/nature10163.

Y. Sonohara, J. Yamamoto, K. Tohashi, R. Takatsuka, T. Matsuda, S. Iwai, and I. Kuraoka. Acetaldehyde forms covalent GG intrastrand crosslinks in DNA. *Scientific Reports*, 9(1): 660, 2019. ISSN 2045-2322. doi: 10.1038/s41598-018-37239-6.

D. Stagos, Y. Chen, C. Brocker, E. Donald, B. C. Jackson, D. J. Orlicky, D. C. Thompson, and V. Vasiliou. Aldehyde dehydrogenase 1B1: molecular cloning and characterization of a novel mitochondrial acetaldehyde-metabolizing enzyme. *Drug metabolism and disposition: the biological fate of chemicals*, 38(10):1679–87, 2010. ISSN 1521-009X. doi: 10.1124/dmd.110.034678.

C. G. Steinmetz, P. Xie, H. Weiner, and T. D. Hurley. Structure of mitochondrial aldehyde dehydrogenase: the genetic component of ethanol aversion. *Structure*, 5(5):701–711, 1997. ISSN 0969-2126. doi: 10.1016/S0969-2126(97)00224-4.

M. Stewart, K. Malek, Q. Xiao, K. Dipple, and D. Crabb. The Novel Aldehyde Dehydrogenase Gene, ALDH5, Encodes an Active Aldehyde Dehydrogenase Enzyme. *Biochemical and Biophysical Research Communications*, 211(1):144–151, 1995. ISSN 0006-291X. doi: 10.1006/BBRC.1995.1789.

R. W. Storms, A. P. Trujillo, J. B. Springer, L. Shah, O. M. Colvin, S. M. Ludeman, and C. Smith. Isolation of primitive human hematopoietic progenitors on the basis of aldehyde dehydrogenase activity. *Proceedings of the National Academy of Sciences*, 96(16):9118–9123, 1999. ISSN 0027-8424. doi: 10.1073/pnas.96.16.9118.

C.-K. Sung, S.-M. Kim, C.-J. Oh, S.-A. Yang, B.-H. Han, and E.-K. Mo. Taraxerone enhances alcohol oxidation via increases of alcohol dehyderogenase (ADH) and acetaldehyde dehydrogenase (ALDH) activities and gene expressions. *Food and Chemical Toxicology*, 50(7):2508–2514, 2012. ISSN 0278-6915. doi: 10.1016/J.FCT.2012.04.031.

E. M. Tacconi, X. Lai, C. Folio, M. Porru, G. Zonderland, S. Badie, J. Michl, I. Sechi, M. Rogier, V. Matía García, A. S. Batra, O. M. Rueda, P. Bouwman, J. Jonkers, A. Ryan, B. Reina-San-Martin, J. Hui, N. Tang, A. Bruna, A. Biroccio, and M. Tarsounas. BRCA1 and BRCA2 tumor suppressors protect against endogenous acetaldehyde toxicity. *EMBO molecular medicine*, 9(10):1398–1414, 2017. ISSN 1757-4684. doi: 10.15252/emmm.201607446.

C. B. Ueta, J. C. Campos, R. P. e. Albuquerque, V. M. Lima, M.-H. Disatnik, A. B. Sanchez, C.-H. Chen, M. H. G. de Medeiros, W. Yang, D. Mochly-Rosen, and J. C. B. Ferreira. Cardioprotection induced by a brief exposure to acetaldehyde: role of aldehyde dehydrogenase 2. *Cardiovascular Research*, 114(7):1006–1015, 2018. ISSN 0008-6363. doi: 10.1093/cvr/cvy070.

M. Wang, N. Yu, L. Chen, P. W. Villalta, J. B. Hochalter, and S. S. Hecht. Identification of an Acetaldehyde Adduct in Human Liver DNA and Quantitation as N 2 -Ethyldeoxyguanosine. *Chemical Research in Toxicology*, 19(2):319–324, 2006. ISSN 0893-228X. doi: 10.1021/tx0502948.

M.-F. Wang, C.-L. Han, and S.-J. Yin. Substrate specificity of human and yeast aldehyde dehydrogenases. *Chemico-Biological Interactions*, 178(1-3):36–39, 2009. ISSN 00092797. doi: 10.1016/j.cbi.2008.10.002.

R. Wang, Y. He, V. Robinson, Z. Yang, P. Hessler, L. M. Lasko, X. Lu, A. Bhathena, A. Lai, T. Uziel, and L. T. Lam. Targeting Lineage-specific MITF Pathway in Human Melanoma Cell Lines by A-485, the Selective Small-molecule Inhibitor of p300/CBP. *Molecular Cancer Therapeutics*, 2018. doi: 10.1158/1535-7163.MCT-18-0511.

X. Wang, P. Penzes, and J. L. Napoli. Cloning of a cDNA encoding an aldehyde dehydrogenase and its expression in Escherichia coli. Recognition of retinal as substrate. *The Journal of biological chemistry*, 271(27):16288–93, 1996. ISSN 0021-9258. doi: 10.1074/jbc.271.27.16288.

H. Weiner, B. Wei, and J. Zhou. Subunit communication in tetrameric class 2 human liver aldehyde dehydrogenase as the basis for half-of-the-site reactivity and the dominance of the oriental subunit in a heterotetramer. *Chemico-biological interactions*, 130-132(1-3):47–56, 2001. ISSN 0009-2797. doi: 10.1016/s0009-2797(00)00221-0.

WHO. Weekly Epidemiological Record, 25 March 2011. *WHO*, 86(13):113–128, 2011.

WHO. Chagas Disease (American Trypanosomiasis) - factsheet. *Weekly epidemiological record*, 87(51):519–522, 2012. ISSN 0049-8114.

WHO. WHO Model List of Essential Medicines 20th List WHO Model List of Essential Medicines (March 2017) Explanatory notes. *WHO*, 2017.

S. R. Wilkinson, M. C. Taylor, D. Horn, J. M. Kelly, and I. Cheeseman. A mechanism for cross-resistance to nifurtimox and benznidazole in trypanosomes. *Proceedings of the National Academy of Sciences of the United States of America*, 105(13):5022–7, 2008. ISSN 1091-6490. doi: 10.1073/pnas.0711014105.

J. Wills, J. Edwards-Hicks, and A. J. Finch. AssayR: A Simple Mass Spectrometry Software Tool for Targeted Metabolic and Stable Isotope Tracer Analyses. *Analytical chemistry*, 89 (18):9616–9619, 2017. ISSN 1520-6882. doi: 10.1021/acs.analchem.7b02401.

B. Yadav, K. Wennerberg, T. Aittokallio, and J. Tang. Searching for Drug Synergy in Complex Dose-Response Landscapes Using an Interaction Potency Model. *Computational and structural biotechnology journal*, 13:504–13, 2015. ISSN 2001-0370. doi: 10.1016/j.csbj.2015.09.001.

Q. Yang, Y. Yao, K. Li, L. Jiao, J. Zhu, C. Ni, M. Li, Q. P. Dou, and H. Yang. An Updated Review of Disulfiram: Molecular Targets and Strategies for Cancer Treatment. *Current Pharmaceutical Design*, 25(30):3248–3256, 2019. ISSN 13816128. doi: 10.2174/1381612825666190816233755.

A. Yoshida, I. Y. Huang, and M. Ikawa. Molecular abnormality of an inactive aldehyde dehydrogenase variant commonly found in Orientals. *Proceedings of the National Academy of Sciences of the United States of America*, 81(1):258–61, jan 1984. ISSN 0027-8424.

A. Yoshida, L. C. Hsu, and V. Davé. Retinal oxidation activity and biological role of human cytosolic aldehyde dehydrogenase. *Enzyme*, 46(4-5):239–44, 1992. ISSN 0013-9432.

L. H. Yuen, N. S. Saxena, H. S. Park, K. Weinberg, and E. T. Kool. Dark Hydrazone Fluorescence Labeling Agents Enable Imaging of Cellular Aldehydic Load. *ACS Chemical Biology*, 11(8):2312–2319, 2016. ISSN 1554-8929. doi: 10.1021/acschembio.6b00269.

S. Zhang, P. Li, Z. Yan, J. Long, and X. Zhang. Identification and quantification of nitrofurazone metabolites by ultraperformance liquid chromatography–quadrupole time-of-flight high-resolution mass spectrometry with precolumn derivatization. *Analytical and Bioanalytical Chemistry*, 409(9):2255–2260, 2017. ISSN 1618-2642. doi: 10.1007/s00216-017-0191-3.

Y. Zhang, C. Wang, B. Yu, J.-D. Jiang, and W.-J. Kong. Gastrodin Protects against Ethanol-Induced Liver Injury and Apoptosis in HepG2 Cells and Animal Models of Alcoholic Liver Disease. *Biological and Pharmaceutical Bulletin*, 41(5):670–679, 2018. ISSN 0918-6158. doi: 10.1248/bpb.b17-00825.

D. Zhao, P. McCaffery, K. J. Ivins, R. L. Neve, P. Hogan, W. W. Chin, and U. C. Dräger. Molecular Identification of a Major Retinoic-Acid-Synthesizing Enzyme, a Retinaldehyde-Specific Dehydrogenase. *European Journal of Biochemistry*, 240(1):15–22, 1996. ISSN 00142956. doi: 10.1111/j.1432-1033.1996.0015h.x.

S. Zhong, L. Li, Y.-L. Zhang, L. Zhang, J. Lu, S. Guo, N. Liang, J. Ge, M. Zhu, Y. Tao, Y.-C. Wu, and H. Yin. Acetaldehyde dehydrogenase 2 interactions with LDLR and AMPK regulate foam cell formation. *The Journal of Clinical Investigation*, 129(1):252–267, 2019. ISSN 0021-9738. doi: 10.1172/JCI122064.

L. Zhou, H. Ishizaki, M. Spitzer, K. L. Taylor, N. D. Temperley, S. L. Johnson, P. Brear, P. Gautier, Z. Zeng, A. Mitchell, V. Narayan, E. M. McNeil, D. W. Melton, T. K. Smith, M. Tyers, N. J. Westwood, and E. E. Patton. ALDH2 Mediates 5-Nitrofuran Activity in Multiple Species. *Chemistry & Biology*, 19(7):883–892, 2012. ISSN 10745521. doi: 10.1016/j.chembiol.2012.05.017.

L. Zhou, D. Sheng, D. Wang, W. Ma, Q. Deng, L. Deng, and S. Liu. Identification of cancer-type specific expression patterns for active aldehyde dehydrogenase (ALDH) isoforms in ALDEFLUOR assay. *Cell Biology and Toxicology*, 35(2):161–177, 2019. ISSN 0742-2091. doi: 10.1007/s10565-018-9444-y.